Am J Cancer Res 2020;10(8):2649-2676
www.ajcr.us /ISSN:2156-6976/ajcr0117897

Original Article

AMXI-5001, a novel dual parp1/2 and microtubule polymerization inhibitor for the treatment of human cancers

Hassan Lemjabbar-Alaoui, Csaba J Peto, Yi-Wei Yang, David M Jablons

Department of Surgery, Thoracic Oncology Program, University of California, San Francisco 94143, USA

Received July 9, 2020; Accepted July 23, 2020; Epub August 1, 2020; Published August 15, 2020

Abstract: Poly (ADP-ribose) polymerase (PARP) has recently emerged as a central mediator in cancer resistance against numerous anticancer agents to include chemotherapeutic agents such as microtubule targeting agents and DNA damaging agents. Here, we describe AMXI-5001, a novel, highly potent dual PARP1/2 and microtubule polymerization inhibitor with favorable metabolic stability, oral bioavailability, and pharmacokinetic properties. The potency and selectivity of AMXI-5001 were determined by biochemical assays. Anticancer activity either as a single-agent or in combination with other antitumor agents was evaluated in vitro. In vivo antitumor activity as a single-agent was assessed in a triple-negative breast cancer (TNBC) model. AMXI-5001 demonstrates comparable IC50 inhibition against PARP and microtubule polymerization as clinical PARP inhibitors (Olaparib, Rucaparib, Niraparib, and Talazoparib) and the potent polymerization inhibitor (Vinblastine), respectively. In vitro, AMXI-5001 exhibited selective antitumor cytotoxicity across a wide variety of human cancer cells with much lower IC50s than existing clinical PARP1/2 inhibitors. AMXI-5001 is highly active in both BRCA mutated and wild type cancers. AMXI-5001 is orally bioavailable. AMXI-5001 elicited a remarkable In vivo preclinical anti-tumor activity in a BRCA mutated TNBC model. Oral administration of AMXI-5001 induced complete regression of established tumors, including exceedingly large tumors. AMXI-5001 resulted in superior anti-tumor effects compared to either single agent (PARP or microtubule) inhibitor or combination with both agents. AMXI-5001 will enter clinical trial testing soon and represents a promising, novel first in class dual PARP1/2 and microtubule polymerization inhibitor that delivers continuous and synchronous one-two punch cancer therapy with one molecule.

Keywords: PARP inhibitor, microtubule inhibitor, BRCA, homologous recombination, cancer therapy, synthetic lethality, breast cancer, malignancy, AMXI-5001

Introduction

According to American Cancer Society Cancer Facts and Figures from 2019, cancer is the second leading cause of death in the United States [1]. Despite the introduction of many novel therapeutics including immunotherapy, biologic, and targeted therapies, most patients with metastatic cancer benefit from any given therapy for a limited time only. This limited benefit is primarily due to intolerable side effects and resistance (primary or acquired) to standard therapies used in treating advanced cancers. Causes underlying the resistance include tumor mediated factors, interference from the tumor or immune environment, and epigenetic factors. Thus, advanced cancers continue to be serious, life-threatening, and incurable. Developing more effective and tolerable therapies to treat most cancers remains an unmet medical need.

Synthetic lethality is an emerging strategy in cancer treatment that seeks to exploit the oncogenic features of tumor cells rather than overcome them. Synthetic lethality occurs when essential and overlapping molecular pathways that control cellular functions are simultaneously inhibited [2-4]. Exploiting synthetic lethality may result in greater effects than inhibiting each pathway alone.

PARP and microtubules are attractive targets for many anti-cancer drugs. Microtubules play critical roles in cell structure, function, and processes including transport, migration and mito-

sis. Microtubule targeting agents (MTAs) inhibit the function of cellular microtubules by promoting polymerization and depolymerization. PARP1 and PARP2 proteins are involved with repairing single-strand DNA breaks that lead to toxic double-stranded breaks if not repaired prior to replication [2, 5-7]. Drugs that inhibit the PARP proteins cause multiple double-stranded breaks that lead to cell death.

A synergistic role of PARP and microtubule targeting agents is emerging in cancer therapy. Simultaneous targeting of PARP and microtubule polymerization may result in an amplified and prolonged DNA damage, an enhanced sensitization of cancers, and a broad anti-tumor efficacy with reduced risk for both cancer drug resistance and dose limiting peripheral neuropathy associated with microtubule targeting agents [8-13].

Emerging evidence suggests that microtubule targeting agents may exert a potentiating effect on PARP inhibitor-induced DNA damage [13]. Recent studies demonstrate that MTAs interfere with the trafficking of proteins critical for the double-strand DNA damage repair to include ATM, ATR, DNA-PK, Rad50, Mre11, p95/NBS1, p53, 53BP1, and p63 [13]. By impairing the trafficking of these critical double-stranded DNA damage repair proteins, MTAs may synergize with DNA damaging agents and the PARP inhibitors, which inhibit the alternative DNA repair pathway (base excision or single-strand repair), thereby resulting in prolonged DNA damage and enhanced cytotoxicity.

PARP inhibitors may enhance the anti-tumor activity of MTAs. In keeping, following microtubule inhibition by MTAs, PARP1 is auto-ribosylated and thus stimulated. Subsequently, the stimulated PARP interacts with and stabilizes important mitotic checkpoint proteins such as E3 ubiquitin ligase (CHFR), and thus leads to inhibition of cell cycle progression to M phase in replicating cancer cells [10, 12]. Consequently, cancer cell avoidance of mitotic catastrophe induced by MTAs implicates an important role of PARP activity in cancer cell resistance to these drugs. There are currently at least seven PARP inhibitors at various stages of clinical development [2, 14]. In addition to blocking PARP catalytic action, certain PARP inhibitors induce trapping of PARP proteins on DNA, thus generating toxic DNA-adducts [2]. These toxic DNA-adducts interfere with replication, causing cell death preferentially in cancer cells, which grow faster than non-cancerous cells.

Recent studies show that sustained DNA damage occurs with the combination of MTAs with either DNA damaging agents or radiation [15, 16]. This finding provides a likely explanation for why combinations involving a MTA and a DNA damaging agent have emerged “empirically” as active combinations in the majority of cancers. Moreover, The DNA damage repair inhibitors, such as PARP inhibitors, may sensitize cancers to MTAs as significantly increased apoptosis has been shown in cancer cells resistant to MTAs with combination treatment of a PARP inhibitor and a MTA.

These combined results suggest that MTAs may synergize with PARP inhibition in both DNA-double-strand break repair proficient and defective cancers, owing to their exacerbation of the DNA damage phenotype [13]. Given this supportive evidence, PARP inhibitors have been proposed to kill cancer cells resistant to MTAs in combinatorial regimens with MTAs [10, 12].

MTA-induced peripheral neuropathy is a major dose limiting toxicity for which no therapy is approved. A role for PARP inhibition in sensory neurotransmission has been established [8]. Recent reports demonstrate that PARP inhibition protects against microtubule targeting agent-induced painful neuropathy in rats [9], and thus supports that PARP inhibition may represent a novel therapeutic approach for this dose limiting toxicity associated with microtubule targeting agents.

Collectively, these findings suggest that simultaneous inhibition of PARP and microtubules may confer a broad and potent anti-tumor efficacy with reduced risk for MTA-induced dose limiting toxicity and cancer drug resistance. Accordingly, synchronous inhibition of PARP and microtubules may result in a synthetically lethal anti-cancer therapeutic strategy by ensuring a synchronous ‘one-two punch’ cancer therapy.

Here, we report the characteristics of a novel dual PARP1/2 and Microtubule Polymerization inhibitor, AMXI-5001. AMXI-5001 exhibits many of the biochemical and cytotoxic profiles found

with either or both the clinically approved PARP1/2 inhibitors such as Olaparib, Rucaparib, and Niraparib, and Talazoparib, and the microtubule inhibitors polymerization inhibitors such as Vinblastine, Vincristine and Colchicine. However, AMXI-5001 is able to achieve antitumor cell responses and elicit DNA repair biomarkers at much lower concentrations than all current clinical PARP1/2 inhibitors, an effect consistent with its dual target inhibition and enhanced biochemical potency. Moreover, the favorable metabolic stability, oral bioavailability, and pharmacokinetic properties of AMXI-5001 suggest that it is a useful addition to existing targeted agents in oncology.

Results

AMXI-5001 potently and selectively inhibits PARP1 and PARP2

AMXI-5001 was engineered using a medicinal chemistry approach, to generate novel bifunctional drug-like small molecules that synchronously inhibit the catalytic activity of PARP1 and microtubule polymerization (**Figure 1A**) *(manuscript in preparation).*

The inhibitory effect of the AMXI-5001 compound towards PARP1 was determined using a commercially available microplate assay kit (Universal Colorimetric PARP Assay from Trevigen, Inc., Gaithersburg, MD). Clinically approved PAPR inhibitors (Olaparib, Talazoparib, Niraparib, or Rucaparib) were used as a positive control for PARP inhibition. Since AMXI-5001 structure also comprises a microtubule targeting moiety, Paclitaxel was used as a negative control for PARP inhibition. As shown in **Figure 1A** and **1B**, AMXI-5001 inhibited PARP1 enzymatic activity with a very low IC50 of ~5 nmol/L. In a side-by-side comparison, we found that AMXI-5001 has comparable IC50 inhibition profile against PARP1 to other clinically approved PARP inhibitors to include Olaparib, Talazoparib, Rucaparib, and Niraparib (**Figure 1B**, **1C** and Table S1). In contrast, Paclitaxel did not affect PARP1 enzymatic activity (**Figure 1C**). AMXI-5001 was originally synthesized as a free base form. Subsequently and in an attempt to improve AMXI-5001 solubility, its hydrochloride salt form was identified and selected. As shown in **Figure 1B**, both the free base and HCL salt forms of the compound have equivalent effect against PARP1 enzymatic activity.

Most PARP1 inhibitors are known to also inhibit the homologous enzyme PARP2 due to the sequence similarity of PARP1 and -2 catalytic domains [17]. We found that AMXI-5001 inhibited PARP2 to a similar extent than the clinically approved PARP inhibitors Olaparib and Talazoparib, with IC50 of 0.05, 0.03, and 0.09 nmol/L, respectively (**Figure 1D**; Table S2).

PARP1 and 2 are nuclear enzymes that synthesize PAR chains on target proteins as a form of posttranslational modification. To assess the ability of AMXI-5001 to inhibit intracellular PARP activity, we exposed MDA-MB-436 breast cancer cells to the alkylating agent methyl methanesulfonate (MMS) to induce PAR synthesis and examined the ability of AMXI-5001 to inhibit PAR formation both by the validated HT PARP in vivo Pharmacodynamic ELISA Assay (Trevigen, Inc., Gaithersburg, MD), and by western blotting analysis. The clinically approved PARP inhibitors Olaparib and Talazoparib were used as positive controls for cellular PAR synthesis inhibition.

Using the HT PARP In Vivo Pharmacodynamic Assay, we found that AMXI-5001 inhibited intracellular PAR formation with an IC50 of 7 nmol/L (**Figure 1E**; Table S3). AMXI-5001 was comparable to Olaparib and modestly less potent than Talazoparib, which inhibited the cellular PAR formation with IC50s of 8, and 3 nmol/L, respectively (**Figure 1E** and Table S3). The effect of AMXI-5001 on the cellular PAR levels, and thus PARP activity, was also assessed by standard western blotting procedures (as described in the experimental section). As shown in **Figure 1F**, AMXI-5001 profoundly inhibited cellular PAR levels in an equivalent manner as the clinically approved PARPi (Olaparib and Talazoparib) (**Figure 1F**). In contrast treatment with MTA (Paclitaxel and Vinblastine) had no effect on the cellular PAR levels (Not shown).

In agreement with our HT PARP in vivo pharmacodynamic assay results, quantification of the PAR protein bands densities also showed that AMXI-5001 inhibited intracellular PAR formation with a very low IC50 of 10 nmol/L (Figure S1 and Table S4). In the western blot analysis, Talazoparib, inhibited the cellular PAR formation with IC50s 3 nmol/L (Figure S1 and Table S4).

The main mechanisms by which PARP inhibitors exert their cytotoxicity are accumulation of

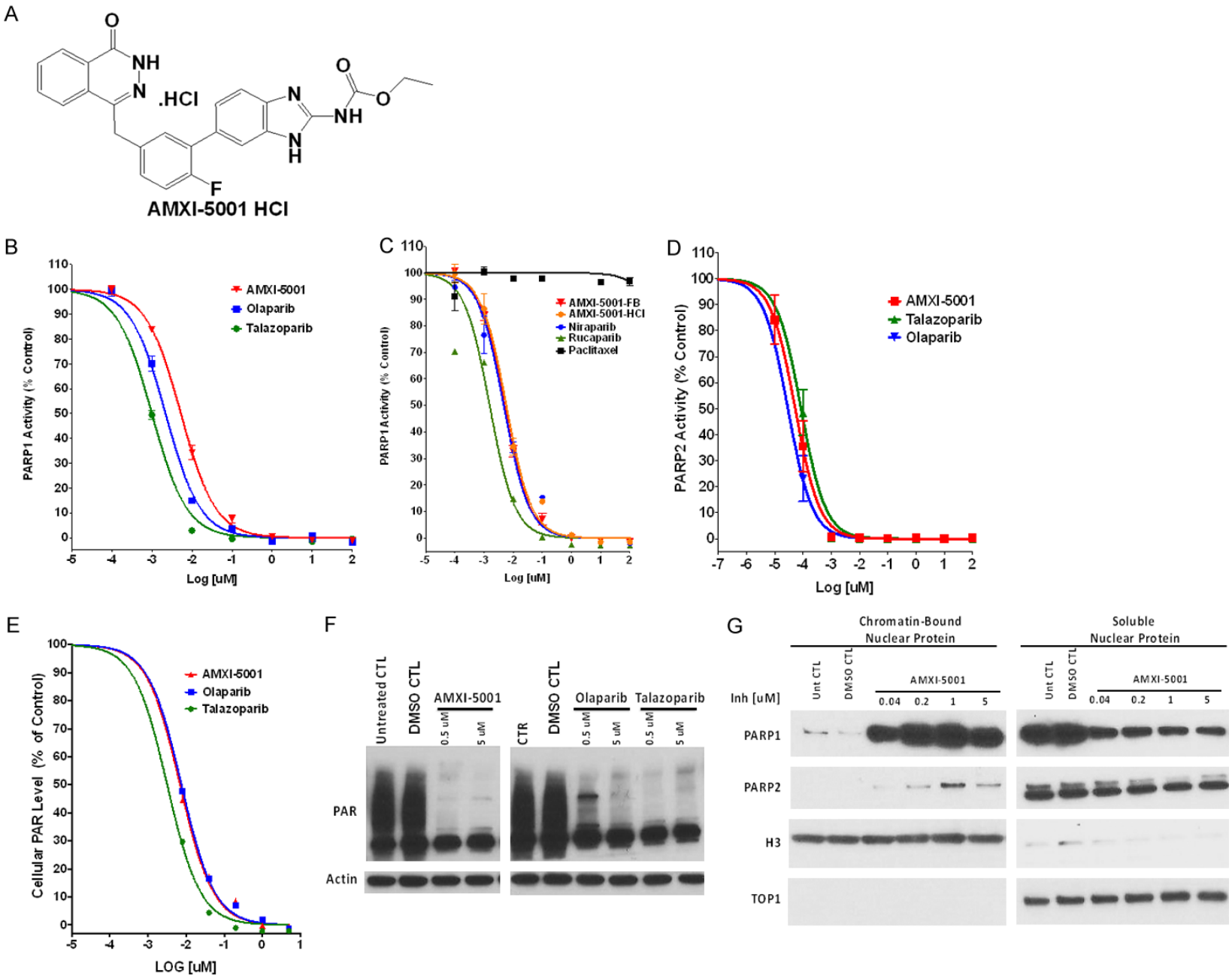
A
AMXI-5001 HCl
B
PARP1 Activity (% Control)
Log [uM]
AMXI-5001
Olaparib
Talazoparib
C
PARP1 Activity (% Control)
Log [uM]
AMXI-5001-FB
AMXI-5001-HCl
Niraparib
Rucaparib
Paclitaxel
D
PARP2 Activity (% Control)
Log [uM]
AMXI-5001
Talazoparib
Olaparib
E
Cellular PAR Level (% of Control)
LOG [uM]
AMXI-5001
Olaparib
Talazoparib
F
Untreated CTL
DMSO CTL
AMXI-5001
0.5 uM
5 uM
CTR
DMSO CTL
Olaparib
Talazoparib
PAR
Actin
G
Chromatin-Bound Nuclear Protein
Soluble Nuclear Protein
Inh [uM]
Unt CTL
DMSO CTL
AMXI-5001
0.04
0.2
1
5
PARP1
PARP2
H3
TOP1

Figure 1. AMXI-5001 is a potent PARP1/2 inhibitor. (A) Structure of AMXI-5001 HCl. (B-D) The inhibitory action of the test compounds towards PARP1 (B, C) and PARP2 (D) was determined using a commercially available microplate assay (Universal Colorimetric PARP Assay from Trevigen, Inc) for PARP1 and (BPS BIOSCIENCE INC) for PARP2. To determine the IC50 value for the inhibitors, the compounds were tested using increasing concentrations of the test compounds and the average absorbance of each inhibitor concentration was plotted against the log of the concentration of inhibitor using the GraphPad Prism 6 program. Subsequently, the IC50s for the PARP1 or PARP2 inhibition were determined after non-linear fit using GraphPad Prism. The inhibitory effects of both the free base form (AMXI-5001-FB) and the HCl salt form (AMXI-5001-HCl) of AMXI-5001 were evaluated. DMSO was used as a negative control. Clinically approved PARP inhibitors Olaparib, Talazoparib, Niraparib, or Rucaparib were used as a positive control for PARP1 inhibition. Paclitaxel was also used as a negative control. (E) AMXI-5001 reduced PAR levels in situ in MDA-MB-436 human breast cancer cells: Cells were grown for 24 hr in media with or without varying concentrations of AMXI-5001, Olaparib, or Talazoparib. Cell lysates were prepared and the PAR levels were assessed by HT PARP In Vivo Pharmacodynamic Assay. The normalized ratio of pg PAR/ug total protein for cells treated with increasing doses of test compounds (AMXI-5001, Olaparib, or Talazoparib) over normalized ratio for DMSO Control-treated cells, were plotted against the compound concentrations using non-linear fit using GraphPad Prism. (F) AMXI-5001 profoundly inhibited the PAR levels in situ in MDA-MB-436 human breast cancer cells. Cells were grown for 4 hr in media with or without varying concentrations of AMXI-5001, Olaparib, or Talazoparib. Cell lysates were analyzed by western blot with an anti-PAR or anti-actin antibodies. AMXI-5001 inhibited cellular PAR expression in a comparable manner as the clinically approved PARPi. DMSO-treated (DMSO CTL) or untreated cells (Untreated CTL) cells were used as negative controls. (G) AMXI-5001 treatment induced a strong and dose dependent chromatin binding of both PARP1, and to a lesser extent PARP2: MDA-MB-436 cell lines were co-treated for 3 hr with 0.01% MMS and vehicle controls or increasing doses of AMXI-5001. Subsequently, cell lysates were prepared and fractionated into nuclear-soluble and chromatin-bound fractions then analyzed by western blot with an anti-PARP1 or anti-PARP2. Anti-H3 and anti TOP1 antibodies were used as control loading for chromatin- bound or soluble nuclear fractions, respectively.

unrepaired single-strand breaks (SSBs) resulting from catalytic PARP inhibition, and PARP trapping at the replication fork. Most PARPis trap PARP1- and PARP2-DNA complexes at DNA damage sites that arise spontaneously and/or are produced by DNA damaging agents [18]. Different PARPis may vary in their specificity for PARP enzymes and PARP trapping activity.

To examine whether AMXI-5001 induces trapping of PARP-DNA complexes at DNA damage sites, we fractionated cell lysates into nuclear-soluble and chromatin-bound fractions. Cell lysates were prepared from human cancer cells (MDA-MB-436 or Ovcar-8) treated with vehicle controls or increasing doses of AMXI-5001 or PARPis. Clinically approved PAPRis, (Olaparib, Talazoparib, Niraparib, and Rucaparib) were used as positive controls for PARP-DNA complexes trapping. To increase base damage, we co-treated the cultured cells with low dose of the classic alkylating agent MMS (0.01%). Under drug-free conditions, most PARP1 was in the nuclear-soluble fraction (**Figures 1F** and S2, S3, S4 and S5). AMXI-5001 increased PARP1- and PARP2-chromatin binding (**Figures 1F** and S2, S3, S4 and S5). Notably, increasing the concentration of AMXI-5001 greatly induced PARP1 accumulation in the chromatin-bound fraction both in the breast cancer cells (MDA-MB-436) (**Figure 1G**) and in the ovarian cancer cells (Ovcar-8) (Figure S2). Similar results were also obtained in other cancer cells of various origins (Not shown). Under these conditions, PAR levels were also reduced by AMXI-5001 with similar potency as the clinical PARPis (Olaparib and Talazoparib) (Figures S3A and S3B). Moreover, In human cancer cells, AMXI-5001 induced chromatin binding of both PARP1 and PARP2 in the presence of the DNA damaging agent MMS (0.01%) (**Figures 1G** and S3 and S4). In a side-by-side comparison, we found that AMXI-5001 induces a dose dependent cellular PARP1 and PARP-2 trapping to DNA to a similar extent than Talazoparib in cells treated with MMS (Figures S4 and S5). However, AMXI-5001 produced substantially more potent PARP1 trapping than all the other clinical PARPis (Olaparib, Niraparib and Rucaparib) (Figures S4 and S5). At concentrations greater than 0.01 mM, both AMXI-5001 and Talazoparib resulted in a strong PARP1-DNA complex trapping with an approximatively 10 fold greater potency than Olaparib, albeit, AMXI-5001 was slightly more effective than Talazoparib (Figures S4, S5 and S6). In contrast, Niraparib and Rucaparib were only slightly more or less effective, respectively, in PARP1-DNA complex trapping when compared to Olaparib (Figures S5 and S6A). In keeping with our results in the PARP catalytic activity inhibition studies, both

the free base and HCl salt forms of AMXI-5001 exhibited equipotent cellular PARP1-DNA complex trapping (Figure S7).

AMXI-5001 binds to the catalytic domain of human PARP1: Co-crystal structure of AMXI-5001 in complex with human PARP1

PARP1 is a polypeptide whose activation requires binding as a homodimeric protein to a nicked DNA. This polypeptide possesses a highly conserved organization consisting of three main domains: a N-terminal DNA-binding domain which acts a DNA nick sensor, a central portion designated as the automodification domain (AMD) and which contains regions for dimerization and for modulating interactions with DNA and with proteins, and a C-terminal region, representing the most conserved part of the enzyme, and capable of catalyzing poly ADP-ribose (PAR) synthesis and of binding to target proteins [19]. In turn, this active site, also known as cat PARP, can be divided into an acceptor (adenosine) site and a donor (NIC) site. The acceptor site is occupied by the ADP moiety of PAR and the donor by NAD+. In the donor site, three subsites are described: a NIC-ribose (NI) binding site, a phosphate (PH) binding site and an adenine-ribose (AD) site [19].

To shed some light on the molecular mechanism of action of AMXI-5001, we performed co-crystal structure studies of AMXI-5001 in complex with Human PARP1 protein using Charles River's structural biology platform support Charles River's structural biology platform. Briefly, Screening for crystallization conditions was carried out with AMXI-5001 compound to obtain crystals suitable for X-ray data collection. Subsequently X-ray data was collected and structure solved and refined to 2.5 Å. AMXI-5001 was clearly bound in the active site with the interactions of the Human PARP1 active site residues with the ligand highlighted in Figure S8. Of particular note were the interactions of Asp 770 and Arg 878 with the amide tail and the stacking interactions of Tyr907 and Tyr896 with the aromatic moieties of the ligand. It should be noted that The Structure Solution had 2 molecules in the asymmetric unit. The solution clearly showed one copy of ligand for each molecule of PARP1 in the asymmetric unit. Moreover, the two molecules in the asymmetric unit have been independently fitted and refined resulting in slight conformational differences (Not shown).

AMXI-5001 is a week tankyrase inhibitor

The PARP protein superfamily, particularly PARP1 and PARP2, has wide-ranging roles in cellular processes such as DNA repair, opening of the chromatin and transcription of various genes. Recent reports highlighting the role of another family member, tankyrase 1 (TNKS1; also known as PARP5A and ARTD5), in the control of oncogenic WNT signaling have fueled interest in the development of additional inhibitors to target this enzyme class [20, 21]. Tankyrase function is also implicated in other processes such as the regulation of telomere length, lung fibrogenesis and myelination, suggesting that tankyrase inhibitors could have broad clinical utility.

The effect of AMXI-5001 towards TNKS1 was determined using a commercially available Tankyrase 1 colorimetric activity assay (BPS BIOSCIENCE INC). XAV939 a small molecule inhibitor of TNKS1, and Olaparib were used as controls for TNK1 inhibition. AMXI-5001 exhibited only a weak inhibition of TNKS1 activity when compared to XAV939 (Figure S9 and Table S5). Olaparib also demonstrated a weak TNKS1 inhibitory activity compared to XAV939, albeit stronger than AMXI-5001. AMXI-5001 inhibited TNKS1 activity with an IC50 value >800-fold lower than its corresponding IC50 towards either PARP1 or PARP2 enzymes.

AMXI-5001 is a potent tubulin polymerization inhibitor

Microtubules have pivotal roles in fundamental cellular processes, such as mitosis, cell division, intracellular transport and cell migration [22, 23]. They are highly dynamic filaments assembled from αβ-tubulin heterodimers [24-27]. MTAs interact with tubulin and alter one or more of the three characteristic phases of polymerization, namely nucleation, growth and steady state equilibrium.

To evaluate the direct effect of AMXI-5001 on tubulin polymerization, we used a standard cell free fluorescence-based tubulin polymerization assay, which generates a polymerization curve representing the three phases of microtubule formation. Vinblastine was used as a positive

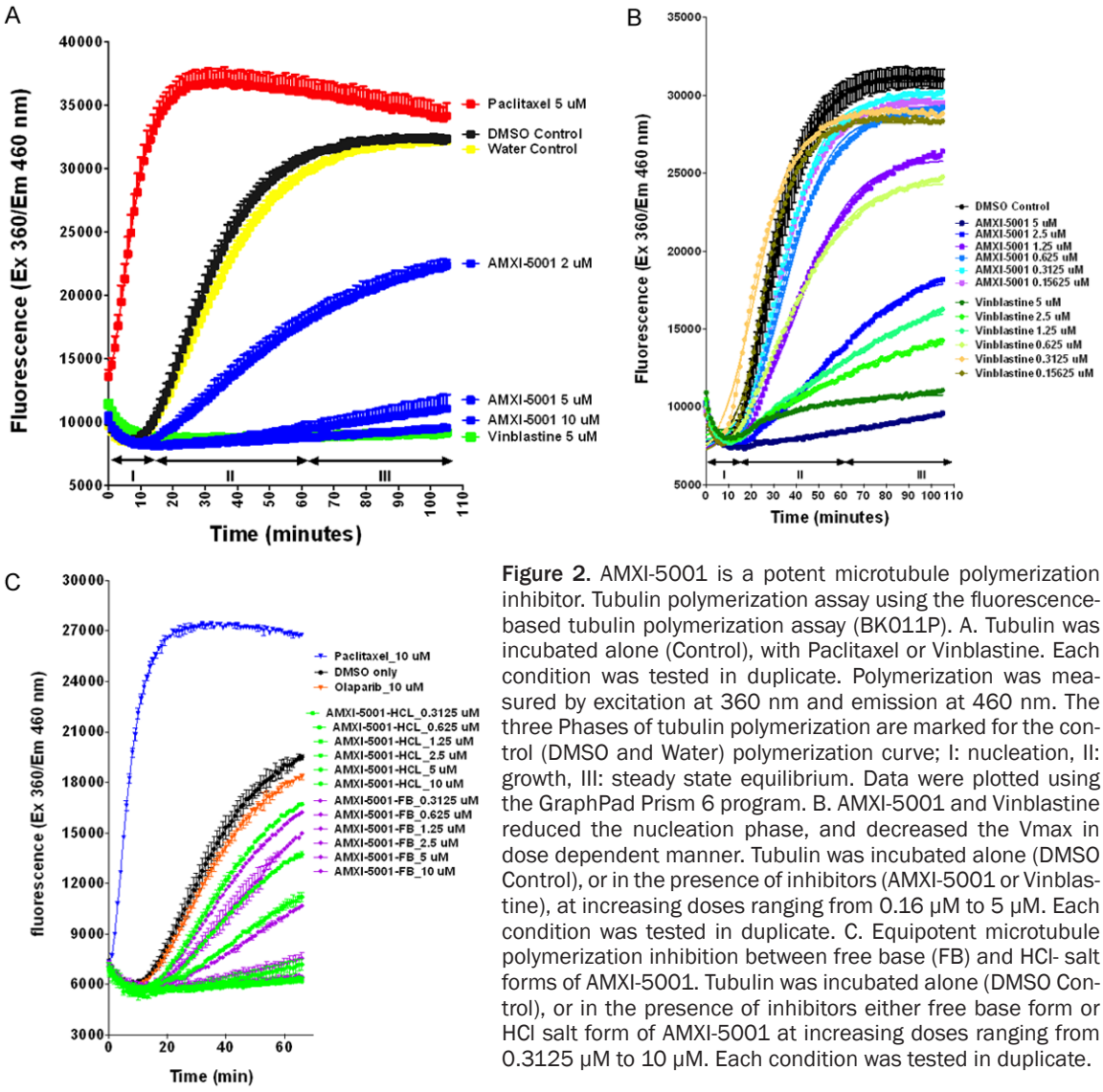

Figure 2. AMXI-5001 is a potent microtubule polymerization inhibitor. Tubulin polymerization assay using the fluorescence-based tubulin polymerization assay (BK011P). A. Tubulin was incubated alone (Control), with Paclitaxel or Vinblastine. Each condition was tested in duplicate. Polymerization was measured by excitation at 360 nm and emission at 460 nm. The three Phases of tubulin polymerization are marked for the control (DMSO and Water) polymerization curve; I: nucleation, II: growth, III: steady state equilibrium. Data were plotted using the GraphPad Prism 6 program. B. AMXI-5001 and Vinblastine reduced the nucleation phase, and decreased the Vmax in dose dependent manner. Tubulin was incubated alone (DMSO Control), or in the presence of inhibitors (AMXI-5001 or Vinblastine), at increasing doses ranging from 0.16 μM to 5 μM. Each condition was tested in duplicate. C. Equipotent microtubule polymerization inhibition between free base (FB) and HCl- salt forms of AMXI-5001. Tubulin was incubated alone (DMSO Control), or in the presence of inhibitors either free base form or HCl salt form of AMXI-5001 at increasing doses ranging from 0.3125 μM to 10 μM. Each condition was tested in duplicate.

control for tubulin polymerization inhibition, and Paclitaxel was used as a positive control for tubulin polymerization enhancement.

As shown in **Figure 2A**, AMXI-5001 inhibited tubulin polymerization in a dose-dependent manner, thereby indicating that AMXI-5001 inhibited the polymerization of tubulin in a direct manner. Both AMXI-5001 and Vinblastine reduced the nucleation phase, and decreased the Vmax and polymer in comparable fashion (**Figure 2**). The Vmax value was decreased by 4.9, 4.2, and 2.1 fold in the presence of AMXI-5001 at 10 μM, 5 μM and 0.5 μM, respectively, as compared to DMSO control (CTL) (Table S6). The Vmax value was decreased by 5.3 fold in the presence of Vinblastine. Conversely, the addition of paclitaxel at 5 μM final concentration eliminated the nucleation phase, enhanced the Vmax by 4 fold and increased the maximum fluorescence of the reaction.

To measure the compound's IC50, we conducted the standard BK011P Tubulin polymerization assay in presence of increasing doses of either AMXI-5001 or Vinblastine (**Figure 2B**). The Vmax were determined as described in the experimental section. The Vmax of the DMSO control was set to 100% polymerization. The percentages of compounds Vmax over DMSO control Vmax were plotted against the compound concentrations, and IC50s were determined (Figure S10).

The Vmax value was decreased in dose dependent manner in presence of either AMXI-5001

or Vinblastine (**Figure 2B**). AMXI-5001 inhibited tubulin polymerization with an IC50 comparable to Vinblastine (Table S7).

As shown in **Figures 2C**, S11 and Table S8, both the salt and free base forms of AMXI-5001 strongly inhibited tubulin polymerization with an equipotent inhibitory activity and an IC50 of 0.92 μM and 0.86 μM, respectively. Paclitaxel induced a marked (~2 fold) increase in the polymerized (P) tubulin fraction as compared to DMSO control (**Figure 2C**). In contrast, Olaparib had no effect on tubulin polymerization (**Figure 2C**).

Since AMXI-5001 has an inhibitory effect on microtubule dynamics in vitro, in cell free assay, we sought to determine its influence on the dynamics of cellular microtubules in dividing A549 cells as described in the experimental section. Paclitaxel was used as a positive control for tubulin polymerization enhancement; and Vinblastine was used as a positive control for tubulin polymerization inhibition. Medium alone (untreated) or medium with 0.1% DMSO were used as negative controls. AMXI-5001 depolymerized microtubules in a dose-dependent manner and in comparable manner as Vinblastine (**Figures 3** and S12). When treated with 0.05 μM AMXI-5001, the polymerization of microtubules was moderately inhibited (**Figures 3** and S12). However, when cells were treated with 0.5 μM AMXI-5001, the microtubules polymerization was significantly inhibited; Moreover, when cells were treated with 5 μM AMXI-5001 (**Figures 3** and S12), almost all microtubules were depolymerized compared with the control group. Analysis of Paclitaxel-treated cells showed the formation of thickened microtubule bundles that encircled the nucleus (**Figures 3** and S12), consistent with a tubulin polymerization enhancement and increased microtubule polymers mass. Given that, AMXI-5001 is a dual PARP and microtubule inhibitor, we investigated cellular microtubule dynamics in cells treated with clinical PARP inhibitors Olaparib and Talazoparib (**Figures 3** and S12), and showed that PARP inhibition does not affect the status of cellular microtubule polymerization compared to controls.

In vitro, the equilibrium between the dimeric and polymeric forms of tubulin can be altered by different effecters and microtubule targeting agents (MTA) which alter the stability of tubulin dimers or the polymerization process. Three unique binding sites for MTAs are known and are responsible for the interactions and pharmacologic effect of paclitaxel, vinblastine and colchicine [28-30]. Paclitaxel, which preferably binds to polymeric tubulin as opposed to its dimeric form. Paclitaxel, a classic type of microtubule-stabilizing agent, binds at the inner surface of the β -subunit known as the Taxane -binding domain. Vinblastine and colchicine are microtubule destabilizing agents, which prefer to bind to dimeric tubulin. Vinblastine binds to the β-tubulin subunit at a distinct region known as the Vinca alkaloid -binding domain, while colchicine binds to the β-subunit at the interface with α-monomer of the same tubulin molecule.

The Competitive MS binding assay was conducted to characterize the binding site of AMXI-5001 on tubulin. Tubulin was incubated with colchicine, vinblastine and paclitaxel. Both colchicine- and vinblastine-tubulin binding studies were examined in the absence of GTP without preincubation. Paclitaxel-tubulin binding studies were performed after pre-incubation of tubulin with GTP for 1 h. Nocodazole, vincristine and docetaxel are well-known competitors for colchicine, vinblastine and paclitaxel, respectively, binding to tubulin. As shown in Figure S13A-C, the MS competitive binding assay demonstrated that Nocodazole, vincristine and docetaxel effectively competed for the colchicine-, vinblastine- and paclitaxel-tubulin binding sites, respectively, indicating that competitive displacement of the known ligand can be quantified and identified using this assay. The MS competitive binding method was further employed to determine the binding site of AMXI-5001 (Figure S13A-C) on tubulin. AMXI-5001 is a novel dual PARP and anti-tubulin agent that potently inhibits tubulin polymerization as demonstrated above. AMXI-5001 microtubule targeting moiety is a benzimidazole known to interact with Colchicine binding site on tubulin. Varying concentrations of AMXI-5001were used to compete with colchicine-, vinblastine- and paclitaxel-tubulin binding. Figure S13A-C show that AMXI-5001 competed specifically with colchicine-tubulin binding, but not to the Vinca alkaloid or paclitaxel sites, suggesting that AMXI-5001 binds to the colchicine-binding site on tubulin. AMXI-5001 competitive binding was less potent than that of Nocodazole

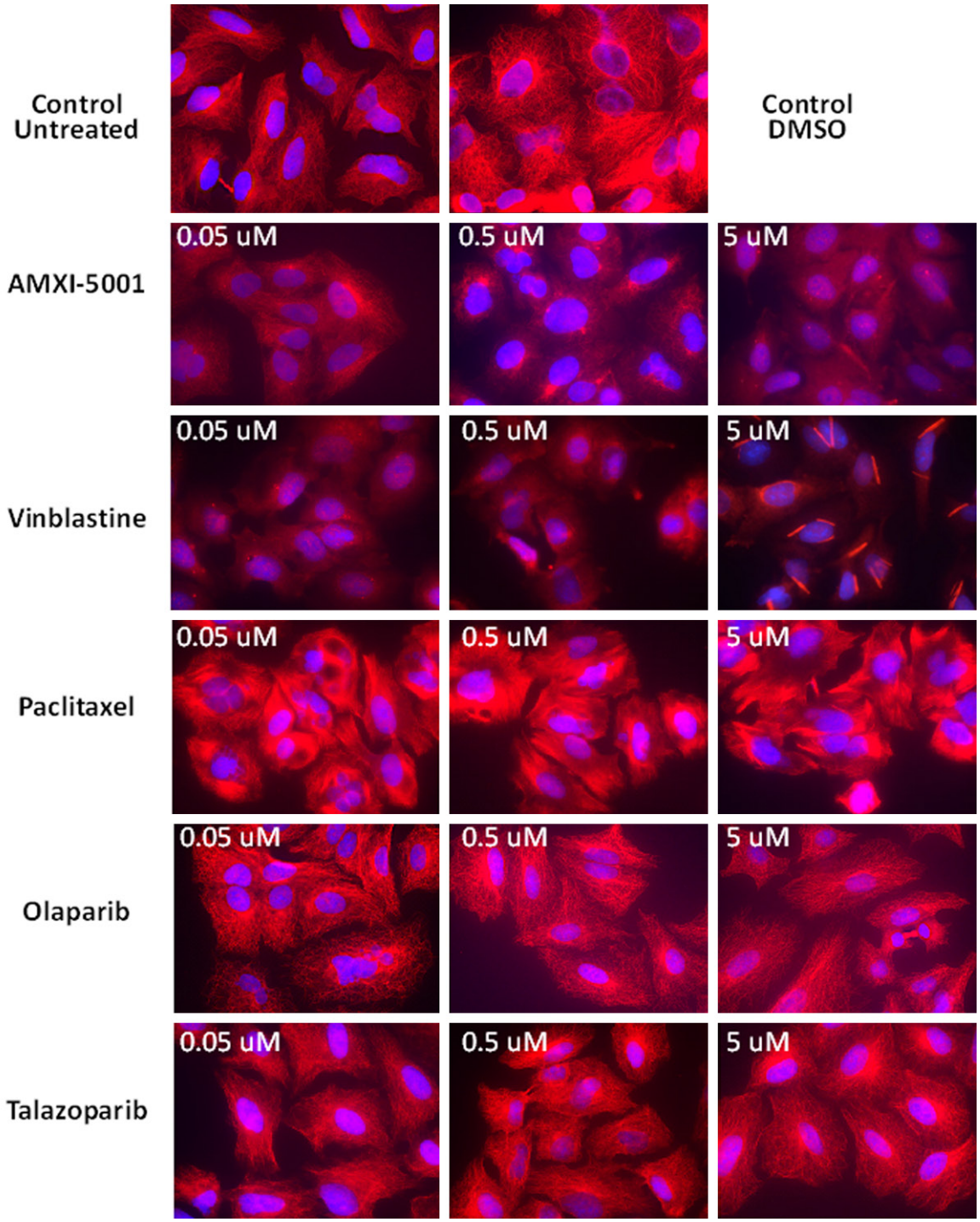

Figure 3. Comparaison of the anti-microtubule effect for AMXI-5001 versus standard microtubule targeting agents and PARP inhibitors. A549 cells were treated with either AMXI-5001, Vinblastine, Paclitaxel, Olaparib or Talazoparib at 0.05 μM, 0.5 μM, or 5 μM for 24 h. 0.1% DMSO or PARP inhibitors (Olaparib and Talazoparib) were used as a negative control. Vinblastine was used as a positive control for tubulin polymerization inhibition. Paclitaxel was used as a positive control for tubulin polymerization enhancement. Samples were then prepared as in the "Experimental" section, and the status of microtubules was observed using a Zeiss AxioImager 2 microscope; 63x objective, DAPI and RFP channels. Microtubule filaments are stained in red, and cell nuclei are stained in blue. AMXI-5001 inhibited the polymerization of microtubules in comparable manner as Vinblastine. PARP inhibitors does not affect the status of cellular microtubule polymerization when compared to controls.

(Figure S13A). Vinca alkaloid. These results indicate that AMXI-5001 specifically binds only to the colchicine-binding site, but not to Vinca alkaloid - or Taxane sites.

The effect of the AMXI-5001 treatment on the tubulin polymerization in situ were evaluated using the cell-based intracellular tubulin polymerization assay. Both AMXI-5001 and Vinblastine treatments resulted in a significant decrease in polymerized (P) tubulin, and thus microtubule assembly, compared with the negative control DMSO-treated cells (Figure S14). Conversely, Paclitaxel induced a marked (~2 fold) increase in the polymerized (P) tubulin fraction as compared to DMSO control. The density of the (P) tubulin protein band was decreased in dose dependent manner in presence of either AMXI-5001 or Vinblastine (Figures S14, S15). Both AMXI-5001 and Vinblastine strongly inhibited in situ tubulin polymerization with an IC50 of 0.67 mM and 0.17 mM, respectively (Figure S14 and Table S9).

Furthermore, treatment with AMXI-5001, or with Paclitaxel resulted in a significant decrease in the cellular levels of total tubulin protein expression, as compared to DMSO treatment (Figure S16). The density of the total tubulin protein band was decreased in dose dependent manner in presence of AMXI-5001 or Paclitaxel (Figure S16). In contrast vinblastine and the benzimidazoles (Nocodazole, Flubendazole, or Mebendazole) induced only a very modest inhibition of the cellular total tubulin protein expression. AMXI-5001 and Paclitaxel strongly inhibited in situ tubulin polymerization with an IC50 of 0.26 mM and 0.02 mM, respectively (Figure S17 and Table S10). IC50s for Vinblastine or Colchicine site- bonding benzimidazoles (Nocodazole, Flubendazole, and Mebendazole) could not be determined. These data confirm that AMXI-5001 engages the microtubule target inside the cells leading to microtubule destabilization. These findings also suggest that the levels of total alpha/beta-tubulin could be a potential simple and reliable pharmacodynamic marker of AMXI-5001-induced microtubule polymerization inhibition. in keeping, a previous study has reported a decrease in total a alpha/beta-tubulin levels in PBMCs from patients treated with ixabepilone (a microtubule polymerization stabilizer) [31].

AMXI-5001 has no significant off target effect

The potential for AMXI-5001 to inhibit off target kinases was assessed in a panel of 156 recombinant human kinase activity and binding assays including cytoplasmic and receptor tyrosine kinases, serine/threonine kinases and lipid kinases. The kinase profiling assays were performed using Life Technologies' SelectScreen® Profiling Service, (Thermo Fisher Scientific, Madison, WI), with a broad coverage of the human kinome. AMXI-5001 was tested at 8 μM in triplicate against each kinase and the mean % inhibition values was determined. At the concentration of 8 mM, AMXI-5001 did not have any significant inhibitory effects on most of the kinases tested (Data not shown).

Furthermore, AMXI-5001 was also profiled in radioligand binding assays as part of in vitro compound selection to detect potential off-target activity. AMXI-5001 was evaluated at a concentration of 10 μM against 38 targets in a binding screening assay that included primary molecular targets, transmembrane and soluble receptors, ion channels, and monoamine transporters. No receptors or enzymes were inhibited ≥50% (Data not shown).

AMXI-5001 targets tumor cells with or without defects in homologous recombination

The objective of this study was to evaluate the cell growth inhibitory activity of AMXI-5001 as well as clinical PARPis (Olaparib, Tlazoparib, Niraparib and Rucaparib), and MTAs (Paclitaxel and Vinblastine) in a panel of 110 cancer cell lines using the Cell Titer Glo assay. The panel included a wide variety of cancer cell lines of various origins, with proficient DNA damage response genes (BRCA-1 or BRCA-2) or defective for BRCA-1 or BRCA-2 expression or expressing mutant forms of the two genes.

Following a 3 days treatment, AMXI-5001 resulted in a robust cytotoxicity in a wide variety of human cancer cell lines (110 lines) of various origins, with very low IC50s and a potency that is far superior than all clinical PARPis. AMXI-5001 potency was 20, to >10000-fold *more than* that of the clinical PARPis. Importantly, AMXI-5001 was highly active in both BRCA1/2-deficient cancer cells (Homologous recombination (HR) deficient) and BRCA1/2 wild type can-

cer cells (HR proficient) (Table S11). Cell lines with BRCA1/2 mutations or low expression of homologous recombination repair (HRR) genes/proteins were more sensitive (IC50 ranging from 18 nM to 26 nM) (Table S11) to cell growth inhibitory activity by AMXI-5001, as compared to HR proficient cancer lines (IC50 ranging from 4 nM to >5000 nM) (Table S11). In contrast, clinic PARP inhibitors were mostly inactive in HR proficient cancers and only modestly active in HR deficient cancers (Table S11).

On account of the different doubling time between the various tested cancer cell lines, we have also assessed AMXI-5001 anti-growth potency in a 6 days treatment cell viability assay. 6 days drug exposure, resulted in a dramatic increase in the apparent drug potency as reflected by a decreased IC50 in the majority of the tested lines, as compared 3 days drug exposure (Table S12).

Moreover, AMXI-5001 inhibited colony formation in a various cell lines, including ovarian, non-small cell lung, and prostate. AMXI-5001 inhibited colony formation with stronger potency (5 to 200-fold greater) than all the clinical PARPis or standard chemotherapy carboplatin, as determined by a decreased IC50, in all the tested lines (Figures S18, S19 and S20 and Tables S13, S14 and S15).

One of the hallmarks of aggressive tumor cells is an ability to migrate and to invade surrounding tissue. The ability of AMXI-5001 to inhibit cell migration which may be an important process in tumor metastasis, was tested using in vitro scratch assay that assess cell migration by recovery of the scratch wound in A549 lung cancer cells. AMXI-5001 effectively inhibited scratch wound recovery in A549 cells as compared to control-treated cells (Figures S21, S22). Importantly, AMXI-5001 demonstrated greater cell migration inhibition than both the clinical PARPis, Olaparaib and Talazoparib. AMXI-5001 showed a comparable inhibitory effect to MTAs, against scratch wound recovery (Figures S21, S22). However, Clinical MTAs inhibitory effect was largely due to a significant cell death induction by these agents (Figures S21, S22).

The effect of AMXI-5001 on cell-cycle progression in dividing MDA-MB-436, OVCAR8 and A549 cells, was evaluated following 24 Hrs treatment with medium alone (untreated CTL) or medium containing either 0.1% DMSO (DMSO CTL), or increasing concentrations of AMXI-5001. Clinical MTAs (Paclitaxel and Vinblastine) were used as positive controls for cell cycle arrest. Cell cycle analyses revealed that similar to Vinblastine, AMXI-5001 induced a concentration dependent cell cycle arrest in G2/M phase in all three tested cancer cells (Figures S23, S24 and S25). 5 mM Paclitaxel also induced G2/M cell cycle arrest in all three tested cancer cells (Figures S24 and S25). Furthermore, dose-response analysis of AMXI-5001 effect on the cell cycle, showed that low (equal or lower than 2 mM) concentrations induced cell cycle arrest chiefly at G2/M phase, while increasingly higher (greater than 2 mM) concentrations caused arrest at late, mid or early S phase in addition to G2M phase arrest (Figures S24 and S25). In contrast, drug-induced S-phase arrest was not observed with either the low and high Vinblastine concentrations, or with a high concentration (5 mM) of Paclitaxel (Figures S24 and S25). Cell cycle arrest in S-phase with high doses of AMXI-5001, implies that the treated cells are unable to duplicate their DNA due to a significant DNA damage induced by AMXI-5001 potent and simultaneous PARP and microtubule polymerization inhibition in situ.

AMXI-5001 effect on cellular checkpoint, regulatory, and signaling proteins

To better understand the mechanisms by which S and G2/M arrest are regulated in response to AMXI-5001, western blot analyses were performed on cell lysates to assess the status of various checkpoint-related proteins. Cells were incubated with AMXI-5001 at various concentrations that causes cell cycle arrest after a 24 h incubation. In MDA-MB-436 cells and A549 cells, AMXI-5001 treatment resulted in modulation of its direct targets as shown by decreased levels of PAR and total tubulin (Figure S26A). In addition, AMXI-5001 treatment increased phosphorylation of cell cycle checkpoint kinases CHK1 and CHK2 at ser296Chk1 and thr68Chk2 sites, respectively, indicating activation of these kinases (Figure S26A, S26B). Clinical PARPi (Olaparib and Talazoparib) also activated both CHK1 and CHK2, whereas clinical MTAs (Vinblastine and Paclitaxel) had no effect on either of these kinases (Figure S26B). CHK1 is

implicated in several checkpoints of the cell cycle acting as a key player in the signal transduction pathway activated in response to either or both DNA damage and mitotic spindle damage. CHK2 is primarily involved in cell cycle checkpoints in response to DNA double-strand breaks (DSBs). Furthermore, AMXI-5001 induced modulation of the phosphorylation levels of serine 10 in histone H3 (pH3) in a dose dependent manner (Figure S26A, S26C, S26D). There was no significant overall change in total H3 protein expression (Figure S26A). At low doses (less than 1 mM), AMXI-5001 resulted in an increase in the pH3 level, suggesting a cell cycle arrest in prometaphase (G2/M phase) (Figure S26A, S26D). However, treatment with higher AMXI-5001 concentrations (>1 mM) triggers loss of pH3 signal (Figure S26A, S26D). Clinical PARPis (Olaparib and Talazoparib) induced inhibition of cellular PAR but had no significant effect on pH3 level (Figure S26D). Cell treatment with clinical MTAs (Vinblastine and Paclitaxel) resulted in decreased tubulin levels and increased pH3 levels (Figure S26C), suggesting that AMXI-5001-induced pH3 modulation is principally due to its anti-microtubule activity. AMXI-5001-induced pH3 loss at higher concentration, could be attributed to either or both enhanced rates of apoptosis and significant increase in DNA damage and cell cycle arrest at S phase, as demonstrated by increased expression of p21, a growth arrest and a proapoptotic protein (Figure S26E). In keeping, AMXI-5001 also induced an enhanced expression of rH2AX, a marker for double strand DNA damage (Figure S26F).

Previous studies demonstrated a role for PARP activity in cancer cell resistance to clinical MTAs [12]. These studies showed that microtubule inhibition by MTAs results in stimulation of cellular PARP1 activity. Subsequently, the activated PARP stabilizes important mitotic checkpoint proteins such as E3 ubiquitin ligase (CHFR), and thus lead to inhibition of cell cycle progression to M phase in the replicating cancer cells [12]. Consequently, cancer cells avoid mitotic catastrophe induced by MTAs. Our results showed that treatment with AMX-5001, a dual PARP and microtubule polymerization inhibitor, results in decreased expression of CHFR protein in cancer cells (Figure S26F). These results are exciting as they indicate that AMXI-5001dual mechanism of action may override the potential for cancer cells resistance to microtubule damage through its synchronous inhibition of both PARP and microtubule polymerization in the same cells. In agreement with these findings, AMXI-5001 also resulted in activation of Cyclin A-associated kinases, CDK1 and CDK2, as indicated by decreased phosphorylation of CDK1 at Tyr15 site (an inhibitory site), and increased phosphorylation of CDK2 at Tyr160 site (an activating site) (Figure S26A, S26B). CDK1 and CDK2, participate in regulating cellular progression into mitosis. CDK2 drives the progression of cells into the S- and M-phases of the cell cycle. Cdk1 is a central regulator that drives cells through G2 phase and mitosis. Activation of CDK1/2 with AMXI-5001, suggests that the AMXI-5001-treated cancer cells may progress to the irreversible M phase before the AMXI-5001-induced damage of mitotic spindle and/or DNA is resolved, and thus resulting in an enhanced cancer cell death. In agreement with this, previous investigations reported that cancer cells sensitivity to MTAs requires CDK1/2 kinase activity [32, 33].

Treatment with chemotherapies including MTAs, DNA-damaging agents, and PARPis are known to result in neoantigen expression in various human cancers. The chemotherapy-induced neoantigen expression may increase cancer cells immunogenicity and thus prime cancers to respond to immunotherapy. We sought to assess the effect of AMXI-5001 treatment on some predicted immunomodulatory neoantigen expression in various cancer cell lines including. Our results showed that AMXI-5001 treatment induced a concentration-dependent increase protein expression of either or both the natural killer (NK) cells activating antigens DR4 and CD155, and the T regulatory cells immunomodulatory antigen PDL-L1 (Figure S27A-C). In contrast, neither clinical PARPis (Olaparib ad Talazoparib) or Paclitaxel had any significant effect on the protein expression of these antigens as assessed in MDA-MB-436 breast cancer cells (Figure S27C). However, Vinblastine, a microtubule polymerization inhibitor, resulted in increased expression of both DR4 and PDL1 in a similar manner as AMXI-5001 (Figure S27C). These results suggest that the increased expression of death receptors and PD-L1 is chiefly associated with its inhibitory effect on the microtubule polymerization.

Our aforementioned findings are interesting as they suggest potential synergy of AMXI-5001 in combination with the immunotherapy to include the immune checkpoint PD1/PDL-1 inhibitors. In addition, AMXI-5001-induced expression of NK activating antigens (DR4/5 and CD155) is exciting as it indicates a potential for AMXI-5001 to illicit a NK driven anti-tumor response. Furthermore, death receptors including DR4/5 can selective trigger apoptosis in cancer cells through interaction with TNF-related apoptosis-inducing ligand (TRAIL) on NK cells. In keeping, AMXI-5001 demonstrated synergistic cytotoxicity, in vitro, when combined with TRAIL in various cancer cells (Figure S28; Table S16). In contrast, there was no significant synergy in combination of TRAIL with other clinical PARP inhibitors (Olaparib and Talazoparib).

Moreover, increased expression of CD155 (necl-5) on cancer cells, may induced NK and T cell-mediated anti-tumor immunity through its interaction with CD226 on these immune cells. Previous studies have shown that tumor cells with higher CD155 expression are more susceptible to CD226-induced killing [34, 35]. In addition, CD155-CD226 interaction can mediate the inhibition of CD155-positive tumor metastasis by NK [36]. Cell surface expression for both DR4/5 and PD-L1 antigens is *required for binding* to their respective ligands/receptors on the target cells and thus exerting their full effect. Flow cytometry analysis demonstrated a marked increase in cell surface expression of both Death receptors DR4 and DR5, as well as PD-L1, in A549 cells following either 24 Hr or 48 Hr treatment with AMXI-5001 (Figures S29 and S30). The abovementioned increase in cell surface expression for these antigens was demonstrated by the conspicuous shift to the right (increase) in fluorescence intensity for cells treated with AMXI-5001 (1 mM or 5 mM) compared to vehicle treated controls (Figures S29 and S30).

Synergistic anticancer activity of AMXI-5001 with approved anticancer therapies in vitro

To evaluate the potential synergistic effect of AMXI-5001 when combined with some selected clinically approved anticancer therapies to include DNA damaging chemotherapies (Gemcitabine, Cisplatin or Etoposide) or Topoisomerase inhibitor (Topotecan) or PI3K inhibitor (Idelalisib). Our results showed that a 1/10 ratio combination of AMXI-5001 with the aforementioned anticancer therapies resulted in more potent anti-proliferative effect in MDA-MB-436 cell line than either single agents alone (Figure S31 and Table S17). Moreover, AMXI-5001 demonstrated stronger synergy when combined with Gemcitabine or Topotecan (Figure S31 and Table S17).

Metabolism and PK properties of AMXI-5001

Currently, there are no approved orally bioavailable microtubule targeting agent. One of the objectives of our dual PARP and microtubule inhibitor discovery program was to develop an orally bioavailable dual PARP and microtubule inhibitor and to improve metabolic stability, PK properties and oral bioavailability over existing PARP1/2 inhibitors. In vitro metabolism studies of AMXI-5001 in hepatocytes from rats, dogs, cynomolgus monkeys, and humans demonstrated that AMXI-5001 had excellent liver stability; The half-life of AMXI-5001 (2 μM) during incubation with hepatocytes (500,000 cells/mL) from Sprague-Dawley rats, beagle dogs, cynomolgus monkeys, or humans was estimated to be 217 min, 812 min, 185 min, and 417 min, respectively. After incubation 1 μM concentration for 120 min at 37°C, the percentage of AMXI-5001 remaining was 63.6%, 85.4%, 64.1%, and 78.5% for rat, dog, monkey, and human hepatocytes, respectively (Not shown). These data suggest AMXI-5001 will have human clearance approximately similar to that of the animal species.

AMXI-5001 has been given orally to rats and dogs at various dose levels (*manuscript in preparation*). AMXI-5001 was absorbed and bioavailable in all species tested. In rats and dogs, exposure increased with the increase in dose level, supporting the use of these species in the toxicity studies of AMXI-5001. A variety of formulations were tested, eventually leading to selection of 10% TPGS (D-α-tocopherol polyethylene glycol-1000-succinate; Vitamin E) in 0.01 N HCl, pH 2.1-2.3, because of its suitable toxicity profile and ability to deliver adequate AMXI-5001 systemic exposure. AMXI-5001 demonstrated an absolute bioavailability in rats and dogs of 31% and 64%, respectively with this formulation, and PK properties that would predict a human half-life that is sufficient to

support a regimen of twice daily administration (*manuscript in preparation*).

In vitro studies assessing the potential for inhibition of human cytochrome P450 enzymes (CYP450s) showed that AMXI-5001 did not inhibit any of the major human hepatic CYP450 enzymes CYP1A2, CYP2B6, CYP2D6, and CYP-3A4/5. There was weak (and not time-dependent) inhibition of CYP2C9, and CYP2C19 (Data not shown).

Overall, AMXI-5001 demonstrated excellent metabolic stability, oral bioavailability and PK properties.

Anti-tumor effect of AMXI-5001 oral administration in xenograft tumor models

AMXI-5001 pharmacokinetic assessment: To support the in vivo primary pharmacodynamic studies in xenograft models, pharmacokinetic parameters of AMXI-5001 were determined in female BALB/C mice. AMXI-5001 free base or hydrochloride salt forms were formulated either as N-methyl-pyrrolidine/carboxymethylcellulose (NMP/CMC) suspension or in 10% D-α-tocopherol polyethylene glycol-1000-succinate; Vitamin E (TPGS) suspension, respectively and administered orally. AMXI-5001 was absorbed and bioavailable in this strain of mice, enabling its testing in murine xenograft models with oral dosing (Table S18).

Initial 5-day study in MDA-MB-436 xenografts

AMXI-5001 (HCl salt form) was formulated in 10% TPGS and administered orally to female athymic nude mice bearing established MDA-MB-436 xenograft tumors, an aggressive basal breast carcinoma cell line cell line that harbors BRCA1 deletion and is BRCA1 deficient. When tumors reached average volume of 350 mm^3, AMXI-5001 suspension was administered orally at doses of 12.5, 25, or 50 mg/kg/dose BID for 5 days. Five days of twice per day (BID) oral administration of AMXI-5001 caused a rapid and marked tumor growth inhibition at doses of 25 and 50 mg/kg/dose BID, and clear tumor regression at 50 mg/kg/dose BID compared to the vehicle group (Figure S32A).

Moreover, plasma and tumor tissue bioanalyses revealed a dose dependent increase in AMXI-5001 plasma concentration and a corresponding dose dependent increase in AMXI-5001 tumor concentration (Figure S32B). However, there was no significant changes in AMXI-5001 concentration in either plasma or tumor tissues between tissues harvested after 4th and 10th repeat oral dose (Figure S32B). These results suggest that there is no significant increase in the accumulation of AMXI-5001 in either blood or tumor tissue with repeat treatment.

Western Blot analyses of tumor lysates showed that AMXI-5001 modulates its targets in vivo in a dose dependent manner (Figure S33). Particularly, AMXI-5001 inhibition of its targets was more evident at 25 and 50 mg/kg BID doses as indicated by a noticeable decrease in polymeric adenosine diphosphate (ADP) ribose (PAR) expression, a surrogate marker for PARP activity, and in total tubulin expression, a surrogate marked for microtubule polymerization inhibition (Figure S33). This provides support for the hypothesis that the anti-tumor efficacy of AMXI-5001 potentially results from inhibition of both PARP and microtubule polymerization. In general, there was a good correlation between increases in plasma and tumor drug concentrations and increased inhibition of either or both of these AMXI-5001 targets at the doses tested.

Confirmatory 31-day study in MDA-MB-436 xenografts

The efficacy of AMXI-5001 seen in the 5-day study was confirmed in this subsequent study of a longer dosing duration. MDA-MB-436 xenografts tumors were established by inoculation of female athymic nude mice with 3.5×10^6 MDA-MB-436 cells subcutaneously in the third mammary fat. When the tumors reached approximately 100 mm^3, mice were randomized to five treatment groups (8 animals per group): 1) Vehicle control, oral; 2) 10 mg/kg PO BID AMXI-5001 on 5-day ON/2-day OFF cycles, oral; 3) 50 mg/kg PO BID AMXI-5001 on 5-day ON/2-day OFF cycles, oral; 4) 50 mg/kg BID Olaparib on 5-day ON/2-day OFF cycles, oral; 5) 1 mg/kg vinblastine once weekly (Q1W), intraperitoneally. All animals were treated over a 31-day dosing period. Tumor size for each animal was measured twice a week (**Figure 4A**).

AMXI-5001 exhibited significant, dose-dependent tumor growth inhibition. In addition to

tumor growth inhibition, AMXI-5001 also exhibited clear tumor regression in this model. For the 50-mg/kg AMXI-5001 group, all tumors experienced a complete regression. By Day 31 of the dosing schedule, tumors were either too small to be accurately measured or non-palpable. Comparison to Olaparib revealed that the anti-tumor growth effect observed with AMXI-5001 at a dose of either 10 or 50 mg/kg/dose BID was superior to Olaparib at a dose of 50 mg/kg/dose BID. In contrast to AMXI-5001, Olaparib did not exhibit any tumor regression activity in this model and vinblastine given at a dose of 1 mg/kg Q1W showed no significant effect on tumor growth in this model (**Figure 4A**).

Animals treated with AMXI-5001 doses of 10 and 50 mg/kg/dose BID on 5-day ON/2-day OFF cycles for 31 days, did not display any physical symptoms of compound-related toxicity, nor did Olaparib and vinblastine treated animals. There was no significant effect on the body weight during the entire course of treatment in any group (**Figure 4B**).

In order to assess treatment related histological changes, paraffin sections of harvested tumors taken at the end of treatment were stained with hematoxylin-eosin (*H&E)*. H&E staining revealed dramatic hemorrhagic tumor necrosis in tumors treated with AMXI-5001 at 50 mg/kg dose (**Figure 4C**). The harvested tumors from the mice treated with AMXI-5001 at 50 mg/kg were nonpalpable by the end of the treatment. Tumor sections from this group showed a few remaining xenograft cancer cells dispersed through extensive fibrosis, which were surrounded by skin, skeletal muscle and fat from the host animal. At higher magnification a photograph of these tumors showed a significant treatment effect with evidence of necrosis and hemorrhage, with hemosiderin filled macrophage accumulation, cholesterol granuloma, chronic inflammation and fibrosis (**Figure 4C**). The tumors from mice treated with AMXI-5001 at 10 mg/kg also showed reduced density of xenograft cells with areas of necrosis, inflammation, and fibrosis. Tumor sections from vehicle-treated, Olaparib-treated or vinblastine-treated mice, contained mostly vital tumor cells without any fibrosis (**Figure 4C**).

At the end of the study, tumors were resected and processed for analysis of microtubule filament formation. Sections from paraffin embedded tumors were stained with an antibody specific to alpha/beta-tubulin, and visualized by fluorescent microscopy. Cell nuclei were stained with 4',6-diamidino-2-phenylindole (DAPI). Repeat oral dose of AMXI-5001 at either 10 mg/kg or 50 mg/kg BID resulted in a striking dose dependent inhibition of microtubule filament formation in MDA-MB-436 cells derived tumors (Figure S34). Vinblastine treatment also induced a marked inhibition of microtubule filament in MDA-MB-436 tumors. Conversely, repeat oral treatment with Olaparib at 50 mg/kg BID dose showed no effect on tumor cells microtubule filaments formation.

Pharmacodynamic parameters for AMXI-5001 treatment, were also determined using lysate prepared with xenograft tumor specimens from each group in this study. For PARP inhibition, PAR levels were evaluated, and for microtubule destabilization, total alpha/beta tubulin expression levels were assessed by western blot analyses with their specific corresponding antibodies. AMXI-5001 treatment at either 10 or 50 mg/kg inhibited dramatically, and in a dose dependent manner, PAR expression in MDA-MB-436 derived tumors (Figure S35). AMXI-5001 treatment also resulted in a significant and dose dependent decrease in the expression levels of total alpha/beta-tubulin in MDA-MB-436 derived tumors (Figure S35). Olaparib treatment resulted in a significant inhibition of PAR expression but had no effect on tubulin expression in MDA-MB-436 derived tumors. In contrast, vinblastine treatment showed no effect on levels of PAR or total tubulin expression in MDA-MB-436 derived tumors (Figure S35). Consistent with PARP inhibition effect, both AMXI-5001 treatment and Olaparib treatment resulted in a conspicuous inhibition of the tumor protein expression of the cell cycle checkpoint protein (CHFR), as compared to vehicle control treatment (Figure S35).

Collectively, the aforementioned results, indicate that AMXI-5001 modulates in a dose dependent manner, both its intended targets in vivo in tumors. These results also suggest that antitumor activity of AMXI-5001 might be attributed to its dual mechanism of action through its synchronous inhibition of both PARP and microtubule polymerization in the tumor cells.

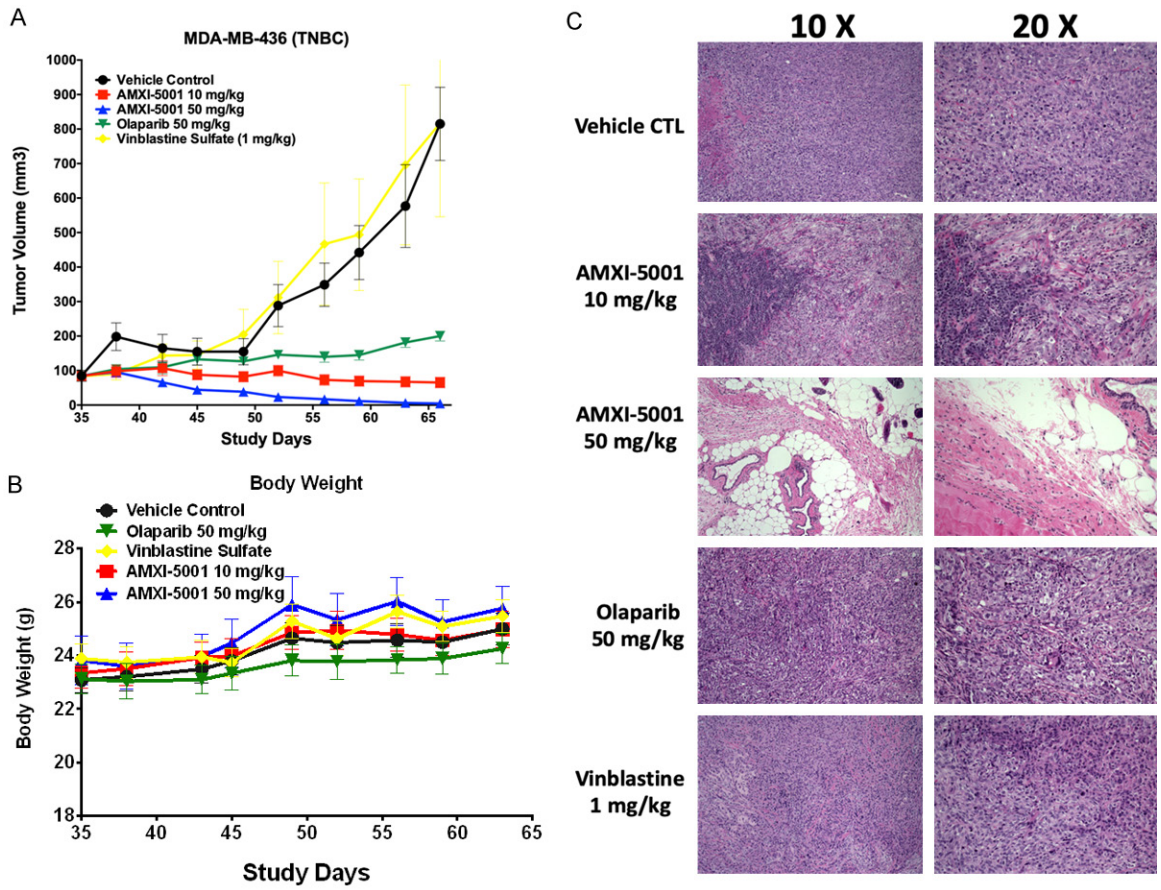

Figure 4. A. Effect of AMXI-5001 on MDA-MB-436 Xenograft Growth and Body Weight in Female Athymic Nude Mice (31-Day Dosing). A. MDA-MB-436 xenografts tumors were established by inoculation of female athymic nude mice with 3.5 × 10^6 MDA-MB-436 cells subcutaneously in the third mammary fat. When the tumors reached approximately ~100 mm^3, mice were randomized to five treatment groups (8 animals per group): 1) Vehicle control administered BID orally on 5 day ON and 2 day OFF cycles, or AMXI-5001 administered at 2) 10 and 3) 50 mg/kg orally BID on 5 day ON and 2 day OFF cycles, or 4) Olaparib at 50 mg/k BID on 5 day ON and 2 day OFF cycles, or 5) vinblastine at IP 1 mg/kg once a week. All animals were treated over a 31 day dosing period. Tumor size for each animal was measured twice a week. B. Body weights were recorded twice a week for animals in each group. C. Histologic therapy response. Histological analysis using H&E staining at low *(10 ×)* and high *(20 ×)* magnifications of representative paraffin embedded MDA-MB-436 xenograft tumor sections form mice treated with: vehicle control, AMXI-5001 at 10 mg/kg or 50 mg/kg BID, Olaparib at 50 mg/kg BID 5 day on 2 day off cycles, vinblastine at 1 mg/kg once a week. All treatments were administered over 31 days dosing period.

Complete regression of established large tumors (600-1300 mm^3) in MDA-MB-436 xenografts with single agent AMXI-5001 treatment

Based on the anti-tumor efficacy in the above study in MDA-MB-436 xenografts when tumors were staged at 100-150 mm^3 before initiation of dosing, the anti-tumor effect of AMXI-5001 was tested in larger, more well-established tumors (**Figure 5A**).

At the end of the 31-day dosing period of the above described study, 5 out of 8 mice from the control group with tumor sizes of 554-1318 mm^3 received AMXI-5001 at a dose of 50 mg/kg/dose BID on 5-day ON/2-day OFF cycles, 2 mice from the vinblastine group, and 1 mouse from the control group (tumor size 458-953 mm^3) received vehicle control on the same schedule. Remarkably, all large tumors treated with AMXI-5001 exhibited gradual and approximatively complete tumor regression starting in the first week of treatment initiation (**Figure 5A**). Notably, following AMXI-5001 treatment, there was no sign of tumor recurrence 2 weeks after mice stopped treatment (**Figure 5A**).

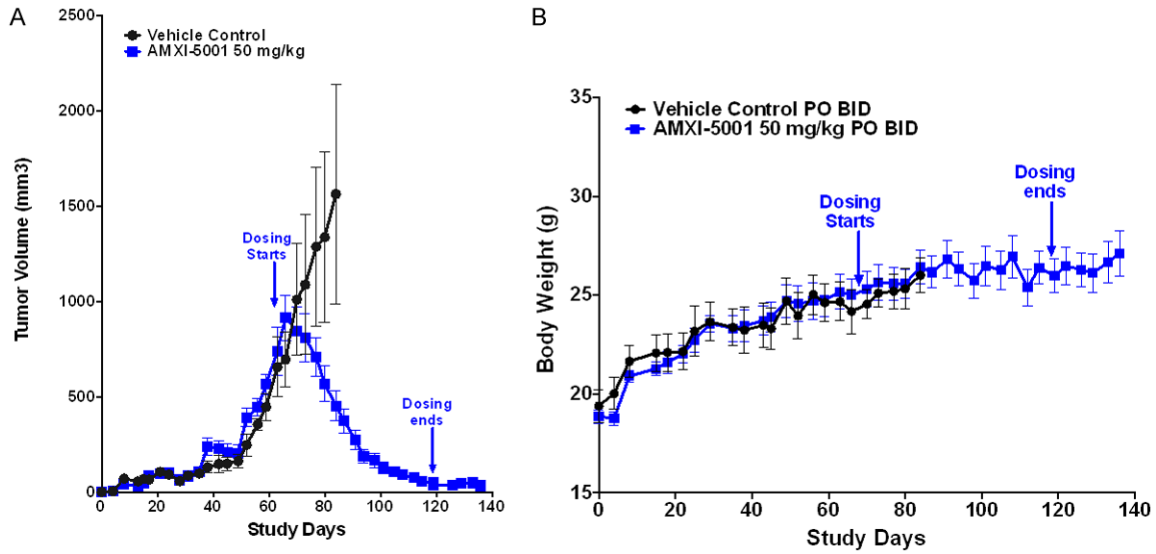

Figure 5. Effect of AMXI-5001 on Large MDA-MB-436 Xenograft Growth and Body Weight in Female Athymic Nude Mice. A. AMXI-5001 causes uniformly growth inhibition and complete regression without recurrence of large MDA-MB-436 mammary fat xenograft tumors in all treated mice. Five mice bearing large tumors (Tumor size ranging from ~554 to ~1318 mm^3) in each group. B. Body weights were recorded twice a week for animals in each group. No significant effect on the body weight during the entire course of treatment with AMXI-5001 at 50 mg/kg as compared to vehicle control treated group was observed.

Conversely, in the new vehicle treated group, tumors continued to grow rapidly and the mice were terminated, less than three weeks after vehicle treatment was initiated, because of excessive tumor growth and the consequent poor animal health. There was no significant effect on the body weight during the entire course of treatment with AMXI-5001 at 50 mg/kg/dose BID as compared to vehicle control treated group (**Figure 5B**).

Superior antitumor effect of AMXI-5001 compared to combination therapy of single-agent PARP and microtubule inhibitors in MDA-MB-436 xenograft model

The objective of this study was to compare the in vivo anti-tumor efficacy of AMXI-5001 treatment to either single agent Olaparib (a clinical PARP inhibitor), or single agent paclitaxel (a potent clinical microtubule polymerization inhibitor), and to combination therapy of Olaparib and paclitaxel in MDA-MB-436 Xenograft model. Olaparib and paclitaxel were administered at clinically relevant doses and schedules.

MDA-MB-436 xenografts tumors were established by inoculation of female athymic nude mice with 3.5 × 10^6 MDA-MB-436 cells subcutaneously. Mice were randomized when the tumors reached approximately an average of 220 mm^3 prior to dosing (**Figure 6**).

AMXI-5001 induced complete or near-complete tumor regression in all treated animals, and this effect was superior to either single agent Olaparib or paclitaxel, or combination treatment with both agents (**Figure 6A**). In this tumor model, single agent paclitaxel treatment displayed weak anti-tumor activity, whereas treatment with single agent Olaparib induced a clear but modest inhibition of the tumor growth. Combination therapy of Olaparib and paclitaxel resulted in a greater tumor growth inhibition than either of these single agents alone. However, the combination therapy of Olaparib and paclitaxel failed to induce tumor regression and the tumors continued to grow, albeit, at slower rate than the vehicle treated or single agent (Olaparib or paclitaxel) treated tumors. AMXI-5001 was much more effective in this model than the combination of single agent Olaparib with single agent paclitaxel.

Animals treated with AMXI-5001, single agent Olaparib, or combination treatment of Olaparib with paclitaxel did not show any notable treatment-related toxicity (**Figure 6B**). However, 3

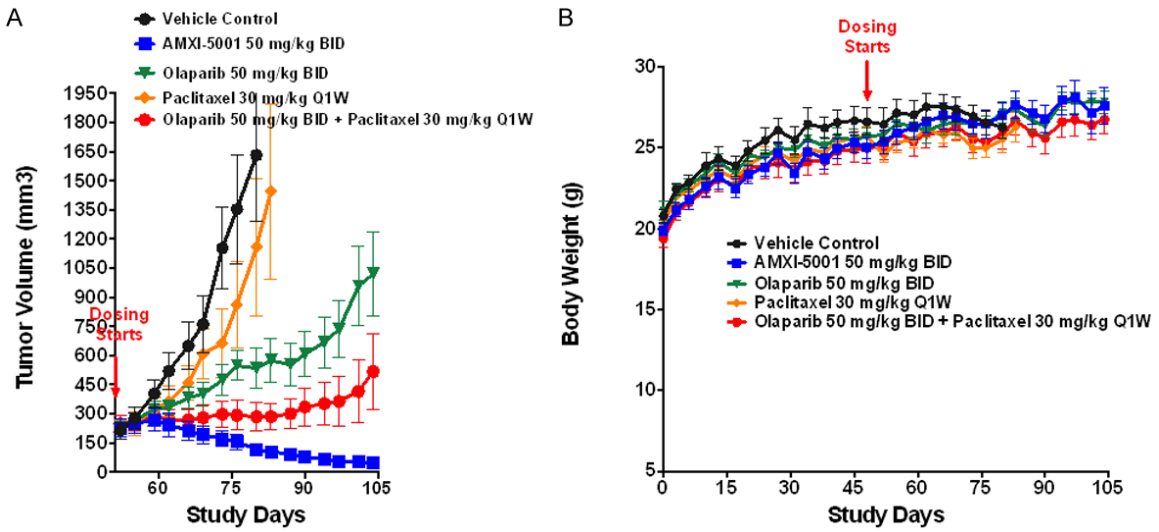

Figure 6. Effect of AMXI-5001, Olaparib, Paclitaxel, and Olaparib/Paclitaxel on MDA-MB-436 Xenograft Growth and Body Weight in Female Athymic Nude Mice (56-Day Dosing). MDA-MB-436 xenografts tumors were established by inoculation of female athymic nude mice with 3.5 × 10^6 MDA-MB-436 cells subcutaneously in the third mammary fat. When the tumor size average reached approximately ~200 mm^3, mice were randomized to five treatment groups (8 animals/group): vehicle control, administered BID orally on 5 day ON and 2 day OFF cycles, AMXI-5001 (50 mg/kg) orally BID on 5 day ON and 2 day OFF cycles, Olaparib (50 mg/kg) BID on 5 day ON and 2 day OFF cycles, paclitaxel IV (30 mg/kg) once a week, or a combination therapy of Olaparib (50 mg/kg PO BID 5 day ON 2 day OFF) with paclitaxel (30 mg/kg) IV once per week. A. Tumor size for each animal was measured twice a week. B. Body weights were recorded twice a week for animals in each group.

out of 8 mice in the single-agent paclitaxel group showed lethargy, lack of response to external stimuli, loss of consciousness, and labored respiration within a few minutes after first intravenous (IV) administration of paclitaxel (30 mg/kg). The 3 affected animals in this group were euthanized. Nevertheless, all remaining 5 animals in the single agent paclitaxel treated group did not show any notable treatment-related toxicity for the duration of treatment. There were no significant treatment-related effects on body weight during the entire course of treatment with any of the treatment modalities as compared to the vehicle control treatment.

Discussion

Standard treatment available to most patients with advanced cancers is inadequate with most approved therapies for advanced cancers having response rates ≤ 20-30% and modest survival benefits. The ineffectiveness of standard therapies for advanced cancers has a number of causes, including that cancers are quite heterogeneous, especially at the molecular level. There are ongoing advances in our understanding of the genetic and molecular drivers of cancer as well as our ability to molecularly characterize cancers [37-39].

Over the past 50 years, chemotherapy, to include microtubule targeting agents (MTAs), and DNA damaging agents (DDAs), has been and remains the standard of care in cancer treatment. Despite all the recent advances in targeted cancer therapy, these chemotherapeutic agents are still the most potent agents to kill cancer cells owing to their ability to target critical mechanisms for cancer cells proliferation, DNA repair, mitosis, migration, and cytoskeleton. Unfortunately, the dose limiting toxicity along with drug resistance, remain the most significant barriers to delivering curative doses for cancer with these agents.

Preclinical studies have demonstrated that PARP inhibitors act synergistically with other chemotherapy agents, including platinum compounds and microtubule targeting agents. However, due to limited dosing schedule options for chemotherapy agents, combination of single agent PARP inhibitors with chemotherapy do not allow for a synchronous and continuous effect of these mutually reinforcing treatments. Accordingly, synchronous delivery of both PARP

inhibition and chemotherapy may result in a synthetically lethal anti-cancer therapeutic strategy, and is therefore a desirable profile for a small molecule dual-inhibitor. In addition, synchronous delivery of both PARP inhibition and chemotherapy with one drug, could theoretically accentuate the efficacy of these mutually reinforcing therapies at lower doses, thereby decreasing off-target side effects and, consequently, increasing the therapeutic indices of either therapy.

Here we describe a novel and first in class small-molecule dual PARP and microtubule polymerization inhibitor AMXI-5001. AMXI-5001 was designed to inhibit PARP and the microtubule polymerization synchronously and thus sensitize cancer cells to spindle damage resulting in suppression of mitotic checkpoints and cell death. Microtubule inhibition may also sensitize cancer cells to PARP inhibition by impairing the trafficking of critical DNA repair proteins, and resulting in prolonged DNA damage and enhanced cell death.

In vitro, AMXI-5001 inhibits with high potency both PARP and tubulin polymerization. AMXI-5001 shows comparable IC50 inhibition profiles against PARP1/2 and microtubule polymerization as clinical PARP inhibitors (Olaparib, Rucaparib, Niraparib, and Talazoparib) and the potent polymerization inhibitor (vinblastine), respectively. AMXI-5001 resulted in a robust cytotoxicity across a wide variety of human cancer cell lines (110 lines) of various origins, with very low IC50s (low nanomolar concentrations) and a potency that is far superior than all currently approved PARP inhibitors (Olaparib, Rucaparib, Niraparib, and Talazoparib). Importantly, AMXI-5001 was highly active in both BRCA mutated and thus homologous recombination deficient and BRCA wild type and HR proficient cancer cells. In contrast, the clinic PARPis which were mostly inactive in HR proficient cancers and modestly active in HR deficient cancers when used at micromolar concentrations. AMXI-5001 potency was 20, to >10000-fold more than that of the clinical PARPis. Cell lines with BRCA1/2 mutations or low expression of homologous recombination repair (HRR) genes/proteins were more sensitive (IC50 ranging from 18 nM to 26 nM) (Figure S7) to cell growth inhibitory activity by AMXI-5001, as compared to HR proficient cancer lines (IC50 ranging from 4 nM to >5000 nM).

Furthermore, AMXI-5001 treatment results in PARP1 and PARP2 trapping to chromatin in human cancer cells lines. AMXI-5001 is a very potent PARP-DNA complexes trapper, far superior (~10 fold greater) than most of the clinically approved PARP inhibitors (Olaparib, Rucaparib, Niraparib, and veliparib) and comparable in potency to Talazoparib (the most potent clinical PARP inhibitor). The PARP-DNA complexes trapping process may interfere with DNA replication, causing cell death preferentially in cancer cells, which grow faster than non-cancerous cells. Preclinical studies have demonstrated that PARPi trapping ability contributes significantly to their monotherapy activity in vitro and potentiate their synergistic activity with chemotherapy including DNA damaging agents in vivo [40].

Also, AMXI-5001 demonstrated strong anti-tubulin polymerization activity, with a comparable potency and IC50 to Vinblastine, an FDA approved and a clinically-used potent microtubule destabilizer compound. Noteworthy, through its simultaneous PARP and microtubule polymerization inhibition, AMXI 5001 may mitigate the peripheral neuropathy commonly associated with MTAs. MTAs-induced peripheral neuropathy is a major dose limiting toxicity for which no therapy is approved. Recent reports demonstrated that PARP inhibition protects against microtubule targeting agent-induced painful neuropathy in rats [9], and thus support that PARP inhibition may represent a novel therapeutic approach for the dose limiting toxicity associated with MTAs. Additionally, unlike the standard MTAs used in cancer treatment, AMXI-5001 is a non-taxane and non-vinca alkaloid microtubule inhibitor. AMXI-5001 targets the colchicine-binding motif on tubulin, and thus inhibits its polymerization into microtubules. Microtubule inhibitors that target the colchicine binding site are emerging as promising anticancer with reduced risk for dose limiting neuropathy. Therefore, AMXI-5001 has a potential to lowering the risk of neuropathy commonly associated with the microtubule inhibition.

AMXI-5001 demonstrated a remarkable In vivo preclinical anti-tumor activity in BRCA mutated triple negative breast cancer (TNBC) model, a cancer with currently no effective therapy. Oral administration of single agent AMXI-5001 in-

duced complete regression of established tumors, including exceedingly large tumors (**Figures 4**-**6**). Most importantly, none of the AMXI-5001 treated mice had tumor re-growth until the end of the study, two weeks after AMXI-5001 dosing stopped. Furthermore, AMXI-5001 resulted in superior anti-tumor effects when compared to either single agent (PARP inhibitor (Olaparib) or microtubule targeting agent (Paclitaxel or Vinblastine)) or combination treatment with both agents which were given at clinically relevant doses (**Figures 4A**, **6A**). Importantly, the AMXI-5001 anti-tumor effect was achieved with tolerable toxicity, evidence of PARP and microtubule inhibition in vivo in tumors and favorable PK properties that allow twice-a-day oral dosing in human patients.

AMXI-5001 is the first in class small-molecule inhibitor reported to date that offers a continuous and synchronous PARP and microtubule polymerization inhibitions, and thus results in synthetic lethality, particularly in cancer cells vulnerable to DNA damage. The discovery and characterization of AMXI-5001 as an orally bioavailable dual PARP and microtubule polymerization inhibitor, provides a welcome addition to the oncology field and we believe the pharmacological properties of AMXI-5001 warrant further investigation, and its advancement into clinical studies in cancer patients.

Materials and methods

Drugs and cell lines

Synthesis of AMXI-5001 is described elsewhere (patent). Olaparib, rucaparib, and veliparib, Paclitaxel, Vincristine, Colchicine, Nocodazole, Mebendazole, docetaxel and Carboplatin were obtained from Selleck Chemicals, LLC. Olaparib was obtained from LC laboratories, LLC Talazoparib (BMN-673) and Rucaparib were obtained from MedChemExpress, Inc. Cell Titer Glo reagent was purchased from Promega. Human TRAIL antibodies were obtained from R&D systems. The colorimetric Universal PARP Assay, HT PARP *In Vivo* Pharmacodynamic Assay II, and Anti-PAR antibody from BPS Trevigen Inc. Tubulin polymerization assay (BK011P) and Anti-alpha/beta tubulin antibody were obtained from Cytoskeleton, Inc. PD-L1, DR4 antibodies and all other antibodies used in this study were purchased from Cell signaling Technology, Inc.

All cell lines were obtained from American Type Culture Collection and maintained as exponentially growing monolayers according to the supplier's instructions.

PARP enzyme assays

The inhibitory action of the test compounds towards PARP1 was determined using a commercially available microplate assay kit (Universal Colorimetric PARP Assay from Trevigen, Inc., Gaithersburg, MD) and in accordance with the instructions provided by the manufacturer. Briefly, stock solutions of the various test compounds were made in dimethyl sulfoxide (DMSO). For the assay, each strip well was filled with 10 µL of the inhibitor solution, 20 µL of diluted PARP1 enzyme (providing 0.5 Unit/well), and 25 µL of PARP Cocktail (consisting of biotinylated NAD, activated DNA in Tris-Cl pH 8.0, and EDTA). The strip wells were incubated at room temperature for 60 min, and then washed 4 times with phosphate buffered saline (PBS: Na_2HPO_4, NaH_2PO_4, and NaCl) and 0.1% Triton X-100, and 2 times with PBS. Then, 50 µL of diluted Strep-HRP (blocking solution) was added to each well, and the strips were further incubated at room temperature for 60 min. After washing the wells 2 times each with PBS and with 0.1% Triton X-100, and 2 times with PBS they were mixed with 50 µL of TACS-Sapphire™ colorimetric substrate, and allowed to stand in the dark for 15 min. After stopping the reaction by adding 50 µL of 0.2 N hydrochloric acid (HCl) to each well, the absorbance was measured at 450 nm. Parallel experiments were conducted by substituting the test solution with an equivalent volume of DMSO to verify the effect of the vehicle on the enzyme activity. All the assays were conducted in at least two separate occasions, each time in duplicates Subsequently, the IC50s for the PARP1 inhibition were determined after non-linear fit using GraphPad Prism. The results of these studies are reported in µM. DMSO was used as a negative control. Clinically approved PAPR inhibitors (olaparib, talazoparib, niraparib, or rucaparib) were used as a positive control for PARP inhibition. In some instances, paclitaxel was also used as a negative control.

PARP2 inhibition assay

The inhibitory action of the test compounds towards PARP2 was determined using a commercially available microplate assay kit (BPS BIOSCIENCE INC., San Diego, CA) and in accordance with the instructions provided by the

manufacturer. Subsequently, the IC50s for the PARP2 inhibition were determined after non-linear fit using GraphPad Prism.

HT PARP in vivo pharmacodynamic assay

The HT PARP In Vivo Pharmacodynamic Assay (Trevigen, Inc. #4520-096-K) is a high-throughput, chemiluminescent ELISA designed to quantify poly (ADP-ribose) (PAR) in cellular extracts. The assay employs a two-site sandwich technique in which two different anti-PAR antibodies are used to capture and detect the target analyte. This assay is useful for measuring PAR in extracts from peripheral blood mononuclear cells (PBMC), cultured cells, and tissues. Additionally, this assay can be used to monitor the efficacy of PARPi or anti-cancer drugs on cellular PAR formation and cancer cell cytotoxicity. The inhibitory effect of AMXI-5001 on cellular PAR formation was quantified with this HT PARP In Vivo Pharmacodynamic Assay in accordance with the instructions provided by the manufacturer. Each ELISA plate contains serial dilutions of purified PAR standard used to plot the PAR standard curve. The net mean RLU (Relative Light Units) values of the PAR standards were calculated by subtracting the background (without PAR) from the RLU values, then plotted as a function of the corresponding PAR values (pg/ml). The PAR standard curve was plotted using the GraphPad Prism 6 program (GraphPad Software Inc., San Diego, CA). Typically, the linear dynamic range for the PAR standard curve is from 10 to 1000 pg/ml. The net RLU values for each cell lysate sample was calculated by subtracting the background from the RLU values. Subsequently, the PAR levels in each sample was determined using the PAR standard curve. The PAR level of DMSO-treated control was set to 100% PAR level. The percentages of test compounds-treated samples over DMSO-treated control PAR levels were plotted against the compound concentrations. Subsequently, the IC50s for the cellular PAR formation inhibitors were determined after non-linear fit using GraphPad Prism.

Cellular PAR western blot assay

The effect of AMXI-5001 on the cellular PAR levels was also assessed by standard western blotting procedures. Briefly, cancer cells were cultured overnight in 6 wells plates, followed by incubation with vehicle control or test compound for 24 h. The cells were then washed and cell lysates were prepared for western blotting as described below. Protein concentration in each cell lysate was quantified using BCA method. Immunoblotting was subsequently performed using standard procedures. A total of 10 μg of protein was resolved by SDS-PAGE, transferred to polyvinylidene difluoride (PVDF) membranes, and probed with Anti-PAR (Trevigen, MD) and secondary antibodies (Jaskson ImmunoResearch Inc). Clinically approved PARPi (olaparib, talazoparib, or rucaparib) were used as a positive control for PAR inhibition and γ H2AX induction. β-actin (Cell Signaling Technology, MA) was used as the loading control.

Cellular PARP-DNA trapping assays

To assess the PARP trapping ability of AMXI-5001, standard cellular trapping assays were performed as previously described [18]. Briefly, cancer cells were cultured overnight in 6 wells plates, followed by cotreatment with alkylating agent methyl methanesulfonate (MMS) and vehicle control, or cotreatment with alkylating agents and varying concentrations of the test PARPi for 1 or 3 hr. Cells were then washed and collected by trypsinization. Subsequently chromatin fractions were prepared using Thermo Scientific subcellular protein fractionation kits (#PI78840) per manufacturer protocol. Samples were normalized for protein concentration and analyzed by immunoblotting by anti-PARP1, anti-TOP1, and anti-H3. Clinically approved PARPi (olaparib, talazoparib, or rucaparib) were used as a positive control for PARP-DNA trapping. To quantify the PARPi-induced PARP1-DNA trapping in human cancer cells, densitometry was performed on immunoblots. DNA-bound PARP1 levels were normalized to total cellular PARP1 levels (chromatin-bound PARP1+ Unbound PARP1). Each experiment was conducted at least three independent times. Representative results are depicted in the result section below.

Crystal structure of AMXI-5001 in complex with human PARP1

The crystal structure of AMXI-5001 compound in complex with Human PARP1 protein was determined using Charles River's structural biology platform support Charles River's structu-

ral biology platform (Report ATLAS-AMXI-5001-PRE-CLIN PHARM-PARP1 structure AMXI-5001). Briefly, PARP1 (residues 611-1011) was cloned into pET24 and expressed in *E.coli* (BL21DE3), then PARP1 protein was purified. Subsequently, crystallization studies were conducted. The formed co-crystal of the PARP protein complexed with AMXI-5001 was collected and analyzed examined by Synchrotron X-ray diffraction analysis. X-ray data was collected and processed using AUTOPROC to a resolution of 2.43 Å and the structure solved by molecular replacement using PHASER using the PDB structure 5WRZ as a search model. The model was then rebuilt in COOT and refined using REFMAC and anisotropic B factors. The ligand dictionary was prepared using ACEDRG and modelled into the protein active site and further rounds of TLS and isotropic B factor refinement and placement of solvent molecules carried out.

Tankyrase 1 activity assay

The effect of AMXI-5001 towards TNKS1 was determined using a commercially available Tankyrase 1 colorimetric activity assay (#80573, BPS BIOSCIENCE INC) in accordance with the instructions provided by the manufacturer.

In vitro tubulin polymerization assay

An in vitro fluorescence-based tubulin polymerization assay kit (#BK011, Cytoskeleton, Inc) was used according to the manufacturer's protocol for monitoring the time-dependent polymerization of tubulin to microtubules. The reaction mixture, containing porcine brain tubulin, fluorescent reporter and GTP in presence or absence of test compounds, was prepared. Tubulin polymerization was followed by monitoring fluorescence enhancement due to the incorporation of a fluorescent reporter into microtubules as polymerization proceeded. Fluorescence emission (excitation at 360 nm and elimination at 460 nm wavelength) was measured for one hour and 45 minutes at one min intervals in a Biotek Synergy Plate Reader. Under the conditions described above, approximately 45% of the tubulin is polymerized, leaving flexibility for detecting enhancers and inhibitors of polymerization. DMSO was used as a negative control. Paclitaxel was used as a positive control for tubulin polymerization enhancement. Vinblastine was used as a positive control for tubulin polymerization inhibition. The incorporation of the fluorescent reporter into microtubules as polymerization proceeded was measured. The fluorescence absorbance, at 360 nm excitation and 460 nm elimination wavelengths, was plotted against the reaction time using the GraphPad Prism 6 program (GraphPad Software Inc., San Diego, CA). The Vmax were determined after non-linear fit using GraphPad Prism. The Vmax of DMSO control was set to 100% polymerization The Vmax of the DMSO control was set to 100% polymerization. The percentages of compounds Vmax over DMSO control Vmax were plotted against the compound concentrations. Subsequently, The IC50s for the tubulin polymerization inhibitors were determined after non-linear fit using GraphPad Prism.

Cellular microtubule polymerization Immunocytochemistry assay

The effects of drugs on cellular microtubules were observed using an immunocytochemistry assay with the anti-alpha/beta tubulin: (ATN02: sheep polyclonal, Cytoskeleton) as previously described [41].

Competitive MS binding assay

To determine the binding site of AMXI-5001 on tubulin, competitive MS binding assay was conducted as previously described [42] but with slightly different conditions for Colchicine, vinblastine and paclitaxel binding. This assay was used to assess the tubulin binding of Colchicine, Vinblastine and Paclitaxel and to identify which of these three binding sites that AMXI-5001 binds. The method involves a very simple step of separating the unbound ligand from macromolecules using ultrafiltration. The unbound ligand in the flow through fraction can be accurately determined using highly sensitive and specific HPLC-MS/MS method. Briefly, Nocodazole Colchicine, and Vinblastine were incubated with tubulin in the incubation buffer at 37°C for 1 h. Paclitaxel was incubated with performed tubulin in the incubation buffer at 37°C for 1 hr. Performed tubulin was prepared by incubating tubulin with GTP in the incubation buffer at 37°C for 1 hr. Varying concentrations of Nocodazole, vincristine and Docetaxel were used to compete with Colchicine-, Vinblastine- and Paclitaxel-tubulin binding, respectively. After incubation, reaction samples were centri-

fuged in an Ultracel-30 microconcentrators. The flow through (unbound ligands) was collected and analyzed by HPLC MS/MS, as described below. Varying concentrations of AMXI-5001 were examined to individually compete with colchicine-, vinblastine- and paclitaxel-tubulin binding. The ability of the competitor or AMXI-5001 to inhibit the binding of ligands was expressed as a percentage of unbound ligand control in the absence of any competitor.

Tubulin protein expression assay

The effect of AMXI-5001 on the levels of total tubulin was evaluated by western blot analysis as described above. Briefly, MDA-MB-436 breast cancer cells were seeded into 6-well plates and cultured until attached (~5 hours), then changed to serum-free medium and cultured overnight. Cells were treated in 1% FBS medium for 24 hrs with either control DMSO (0.1%) or varying concentrations of test drugs. Treated cells were then lyzed in M-PER buffer in wells, scrapped cells off wells. and rocked at 4°C for 10 minutes. The cell lysates were centrifuged at 14 kg, 4°C, 10 minutes and supernatants were harvested. The total protein concentration was assessed by BCA quantification method. 6 ug of each of these lysates was added to 4x sample buffer, in 3:1 mixture ratio, and boiled at 95-100° for 10 minutes, cooled down and centrifuged for 10 seconds. Subsequently, the sample were loaded on SDS-PAGE gels, and western blots were probed with antibodies specific for total alpha/beta-tubulin or GAPDH as described above. The densities of the detected tubulin and actin protein bands were quantified with ImageJ software (NIH). For each sample, the tubulin band density was normalized to the GAPDH band density. Normalized band density of DMSO control was set to 100% density. The percentages of compounds band density over DMSO control band density were plotted against the compound concentrations. Subsequently, The IC50s for the tubulin polymerization inhibition were determined after non-linear fit using GraphPad Prism. DMSO was used as a negative control. Paclitaxel was used as a positive control for tubulin polymerization enhancement. Vinblastine was used as a positive control for tubulin polymerization inhibition. Benzimidazoles (Nocodazole, Flubendazole, and Mebendazole) were used as controls for Colchicine-site binding tubulin polymerization inhibitors.

In vitro kinase inhibition assays

The potential for AMXI-5001 to inhibit off target kinases was assessed in a panel of 156 recombinant human kinase activity and binding assays including cytoplasmic and receptor tyrosine kinases, serine/threonine kinases and lipid kinases. The kinase profiling assays were performed using Life Technologies' SelectScreen® Profiling Service, (Thermo Fisher Scientific, Madison, WI), with a broad coverage of the human kinome. The kinase activity assays measure peptide phosphorylation (Z'-LYTE®) or ADP production (Adapta®) while the kinase binding assays monitor displacement of ATP site-binding probes (LanthaScreen®). The ATP concentrations used in the activity assays were within 2-fold of the experimentally determined apparent Michaelis constant (K_m^{app}) value for each kinase while the competitive binding tracer concentrations used in the binding assays were within 3-fold of the experimentally determined dissociation constant (K_d) values. AMXI-5001 was tested at 8 μM in triplicate against each kinase and the mean % inhibition values are reported. For selected kinases, 10-point inhibitor titrations were carried out using the same kinase assays as used in the single point tests in order to determine the inhibitor concentration providing 50% inhibition (IC50). Details regarding the kinase proteins used and the assay protocols are on file and also available online (thermofisher.com).

Cell titer Glo assay

Antiproliferative activity of AMXI-5001 was evaluated in a panel of 110 cancer cell lines of various origins, either proficient or defective for BRCA-1 or BRCA-2 expression or expressing mutant forms of the two genes. Proliferation was assessed after cells were exposed for 3 days or 6 days with AMXI-5001 doses ranging from 8 nM to 5 μM. Briefly, 5000 or 1000 cells (In 3 days or 6 days exposure, respectively) were cultured in a 96-well plate and incubated at 37°C and 5% CO_2 prior to adding serial dilutions of AMXI-5001. Cells were then incubated for 3-6 days at 37°C and 5% CO_2. Cell viability was assessed by Cell Titer Glo assay. The number of living cells was determined by reading the plate on a GloMax Luminametor. Cell growth

was expressed as percentage growth with respect to vehicle (DMSO control) treated cells. The concentration required to inhibit cell growth by 50% (IC50) was determined after non-linear fit using GraphPad Prism. DMSO treated cells were used as a vehicle control. MTAs (Paclitaxel and Vinblastine) as well as clinical PARPis (Olaparib, Talazoparib, Niraparib, and Rucaparib) were used as comparative controls.

Clonogenic assay

The effect of AMXI-5001 on cell viability was also evaluated using colony formation assay in cells lines of ovarian, non-small cell lung cancer, and prostate origin. In brief, cell lines were incubated in 0.1% (v/v) DMSO (vehicle control) or 0.008, 0.04, 0.2, 1, 5 mM AMXI-5001 at 37°C until > 50 colonies have formed (6-28 days). Seeding cell density was determined from preliminary experiments and is defined as seeding density producing linear cell growth after cell incubation in 0.1% (v/v) DMSO (vehicle control). Cell viability was determined using the colony formation assay by counting Crystal Violet-stained colonies using ImageJ software. IC50 values were defined as the AMXI-5001 concentrations producing 50% cell viability when compared to vehicle control cells (100% cell viability). Clinical PARPis (Olaparib, Talazoparib, Niraparib, and Rucaparib) were used as comparative controls.

Wound healing assay/scratch assay

The ability of AMXI-5001 to inhibit cell migration was tested using in vitro scratch assay that assess cell migration by recovery of the scratch wound in A549 lung cancer cells grew into monolayer. Briefly, A549 lung cancer cells were seeded onto 12-well plates. When the cell confluence reached about 80% and above, scratch wounds were made by scraping the cell layer across each culture plate using the tip of 200 µl pipette. After wounding, the debris was removed by washing the cells with PBS. Wounded cultures were incubated in culture medium alone (Untreated control), or medium containing 0.1% (v/v) DMSO (DMSO control) or 0.04, 0.2, 1 mM AMXI-5001 at 37°C for 24 hr. Subsequently, 3 fields (40 Å~) were randomly picked from each scratch wound and visualized by microscopy to assess cell migration ability. Clinical PARPis (Olaparib and Talazoparib) and clinical MTAs (Paclitaxel and Vinblastine) were used as positive controls for cell migration inhibition.

Cell cycle analysis

The effect of AMXI-5001 on cell-cycle progression in dividing MDA-MB-436, OVCAR8 and A549 cells, was evaluated. Briefly, the cells were grown in T75 flasks and treated with 0.1% DMSO (vehicle control), Vinblastine, or AMXI-5001 at varying concentrations for 24 Hr. After incubation, the cells were trypsinized, washed with PBS and fixed. After fixation, the cells were centrifuged, washed with once with PBS and stained with propidium iodide. Finally, the distributions of treated cells at different phases of cell cycle (G1, S, G2/M) were analyzed using flow cytometry. The percentage of cells in each mitotic phase pre- and post-treatment with AMXI-5001 for 24 Hr was determined. MTAs (Paclitaxel and Vinblastine) were used as positive controls for cell cycle arrest.

Western blot analysis of cellular checkpoint and signaling proteins

To better understand the mechanisms by which AMXI-5001 regulates the cell cycle arrest in cancer cells, standard western analysis was performed on cell lysates to assess the status of various checkpoint-related proteins and cell signaling proteins (**Figure 3**). Briefly, cancer cells were cultured overnight in 6 wells plates in serum free medium, followed by incubation with vehicle control or test compound for 24 h. The cells were then washed and cell lysates were prepared for western blotting as described below. Protein concentration in each cell lysate was quantified using BCA method. Immunoblotting was subsequently performed using standard procedures. a total of 10 µg of protein was resolved by SDS-PAGE, transferred to polyvinylidene difluoride (PVDF) membranes, and probed with checkpoint proteins corresponding antibodies, and secondary antibodies. Clinically approved PARPi (Olaparib, Talazoparib) or MTAs (Paclitaxel, Vinblastine) were used as controls. β-actin and GAPDH (Cell Signaling Technology) were used as the loading control.

Flow cytometry analysis-cell surface marker staining

A549 cells were cultured overnight in 100 mm culture dishes, followed by incubation with vehi-

cle control or AMXI-5001 at 1 mM or 5 mM for either 24 hr or 48 hr then harvested by trypsinization, as described below in method section. For PDL1 and death receptors (DR4 and DR5) cell surface staining, harvested cells were washed with PBS, and stained with respective antibodies in cell staining buffer and processed for flow cytometry analysis. (BD FACS Calibur). BD CellQuest Pro software (Franklin Lakes, NJ) was used for flow cytometric data analysis.

Pharmacokinetic evaluations of AMXI-5001 in mice

The objective of these studies was to determine pharmacokinetic and bioavailability profile following a single dose oral administration of either free base form or HCl salt forms of AMXI-500 in BALB/c mice. The In-Life procedures for these studies were conducted using Explora Bioloabs contract research services (San Diego, CA). The in vitro bioanalyses of the plasma samples were performed using Integrated Analytical Solutions contract research services (Berkeley, CA). Briefly, AMXI-5001 free base and HCl salt form were formulated either as NMP/CMC suspension or in 10% TPGS suspension, respectively and administered orally to female BALB/c mice. The formulations protocols used for the PK studies are described below. The bioavailability for AMXI-5001 free base form was assessed following a single oral dose administration at either 50 or 100 mg/kg per mouse. The bioavailability for AMXI-5001 HCL form was assessed following a single oral dose administration at 50 mg/kg per mouse. Blood samples were collected at pre-dose, 0.5, 1, 2, 4, 8 and 24 hours after AMXI-5001 single dose oral administration. For each mouse, one-two time points were assigned. Each group had 3 blood samples per time point. The first blood collection was survival bleed and the second blood collection was terminal. Blood samples were collected into tubes containing K2EDTA anticoagulant and stored on wet ice until centrifuged and processed for plasma. Plasmas were stored at -80°C until analysis. The peak concentration (Cmax), the time to maximum concentration (Tmax), the half-life, and the AUC were determined from composite mean plasma concentration-time data. All doses and plasma concentrations of AMXI-5001 were presented as free base.

Plasma samples were analyzed by high performance liquid chromatography (HPLC) in conjunction with a triple quadrupole mass spectrometer that used electrospray ionization in tandem with positive ionization (MS/MS). The lower limit of quantitation (LLOQ) was 5 ng/ml. The quantitative range of the assay was 5 to 10000 ng/ml.

The pharmacokinetic modeling was performed using PK Solver software (Version 2.0) and the following PK parameters were reported: Cmax: Maximum (peak) plasma concentration DN-Cmax: Dose-normalized Cmax; Tmax: Time at Cmax; AUC: Area under the concentration-time curve; DN-AUC: Dose-normalized AUC; T1/2: Terminal half-life; and VF: Apparent volume of distribution. The PK parameters were determined based on a Non-Compartmental PK model Analysis of Plasma Data after Extravascular Input.

Pharmacodynamic evaluations of AMXI-5001 in mice bearing MDA-MB-436 tumors

The primary objective of this study was to determine the relationship between AMXI-5001 dose, plasma concentration, tumor concentration and inhibition of PARP and microtubule polymerization In vivo in MDA-MB-436 Xenograft Tumors. The In-Life procedures for this study were conducted using Explora Bioloabs contract research services (San Diego, CA). The in vitro bioanalyses of the plasma samples were performed using Integrated Analytical Solutions contract research services (Berkeley, CA). Briefly, AMXI-5001 HCL salt form was formulated in 10% TPGS suspension, as described below and administered orally to female athymic nude mice bearing established MDA-MB-436 Xenograft Tumors (When tumors reach average volume of 500 mm^3). AMXI-5001 suspension was administered orally BID at 6.25, or 12.5, or 25 mg/kg per mouse for 5 days. At 3 hr post the 4th and 10th dose, n=3 mice per group, or each AMXI-5001-dose and the vehicle control group, were euthanized and blood collected in EDTA tubes for plasma processing. At necropsy the tumor tissues from all groups, as well as stomach, small intestine, large intestine, caecum, kidneys, and liver from the vehicle control group and the group treated with AMXI-5001 at 50 mg/kg BID, were individually collected, placed into cryotubes and flash fro-

zen in liquid nitrogen. The frozen plasma and tissue samples were kept at -80°C until bioanalysis for AMXI-5001 concentration. Plasma samples were analyzed by high performance liquid chromatography (HPLLC) in conjunction with a triple quadrupole mass spectrometer that used electrospray ionization in tandem with positive ionization (MS/MS). The lower limit of quantitation (LLOQ) was 5 ng/ml. The quantitative range of the assay was 5 to 10000 ng/ml.

In vivo xenograft models

In the present studies, the MDA-MB-436 (triple negative human breast carcinoma with BRCA1 mutation) was utilized to explore the efficacy and potency of AMXI-5001 with regard to tumor growth inhibition and regression in vivo. The In-Life procedures for these studies were conducted using the Explora Biolabs contract research services (San Diego, CA). The standard experimental design for these studies involved twice daily (BID) daily oral administration (PO) of AMXI-5001, following a 5-day ON and 2-day OFF cycles, beginning when the established solid tumors were staged (~100 -150 mm^3 for most xenografts, ~700 mm^3 and up to 1500 mm^3 for xenograft regression studies). Throughout the dosing period of 10-60 days, tumor size and body weight were measured twice weekly.

At the end of the study, tumors were resected and processed for analysis of microtubule filament formation. Sections from paraffin embedded tumors were stained with an antibody specific to for alpha/beta-tubulin, and visualized by fluorescent microscopy.

In order to assess treatment related histological changes, paraffin sections of harvested tumors taken at the end of treatment were also stained with hematoxylin-eosin (H&E) and analyzed by a certified pathologist.

Pharmacodynamic parameters for AMXI-5001 treatment, were also determined using lysate prepared with xenograft tumor specimens from each group in this study. For poly {adenosine diphosphate (ADP)}-ribose polymerase (PARP) inhibition (PARPi), Poly (ADP-ribose) (PAR) levels were evaluated, and for microtubule destabilization, total alpha/beta tubulin expression levels were assessed by Western blot analyses with their specific corresponding antibodies.

Disclosure of conflict of interest

AMXI-5001 is currently developed by AtlasMedx, Inc. Lemjabbar-Alaoui Hassan, Csaba Peto, and David Jablons may benefit financially from the development of AMXI-5001 through patents held jointly with University of California, San Francisco and AtlasMedx, Inc.

Address correspondence to: Dr. Hassan Lemjabbar-Alaoui, Department of Surgery, Thoracic Oncology Program, University of California, 2340 Sutter Street N-224, Box 1724, San Francisco, CA 94143, USA. Tel: 415-476-9303; Fax: 415-476-4845; E-mail: hassan.lemjabbar-alaoui@ucsf.edu

References

[1] Society AAC: American Cancer Society. Cancer Facts & Figures 2020. In. Atlanta, GA: American Cancer Society; 2020: volumes.

[2] Lord CJ and Ashworth A. PARP inhibitors: synthetic lethality in the clinic. Science (New York, NY 2017; 355: 1152-1158.

[3] O'Neil NJ, Bailey ML and Hieter P. Synthetic lethality and cancer. Nat Rev Genet 2017; 18: 613-623.

[4] Canaani D. Application of the concept synthetic lethality toward anticancer therapy: a promise fulfilled? Cancer Lett 2014; 352: 59-65.

[5] Fouquin A, Guirouilh-Barbat J, Lopez B, Hall J, Amor-Gueret M and Pennaneach V. PARP2 controls double-strand break repair pathway choice by limiting 53BP1 accumulation at DNA damage sites and promoting end-resection. Nucleic Acids Res 2017; 45: 12325-12339.

[6] Ray Chaudhuri A and Nussenzweig A. The multifaceted roles of PARP1 in DNA repair and chromatin remodelling. Nat Rev Mol Cell Biol 2017; 18: 610-621.

[7] Ronson GE, Piberger AL, Higgs MR, Olsen AL, Stewart GS, McHugh PJ, Petermann E and Lakin ND. PARP1 and PARP2 stabilise replication forks at base excision repair intermediates through Fbh1-dependent Rad51 regulation. Nat Commun 2018; 9: 746.

[8] Balko RA, Hendrickson AW, Grudem ME, Klampe CM and Jatoi A. Can Poly (ADP-ribose) polymerase inhibitors palliate paclitaxel-induced peripheral neuropathy in patients with cancer? Am J Hosp Palliat Care 2019; 36: 72-75.

[9] Brederson JD, Joshi SK, Browman KE, Mikusa J, Zhong C, Gauvin D, Liu X, Shi Y, Penning TD, Shoemaker AR and Giranda VL. PARP inhibi-

tors attenuate chemotherapy-induced painful neuropathy. J Peripher Nerv Syst 2012; 17: 324-330.
[10] Brodie SA, Li G, Harvey D, Khuri FR, Vertino PM and Brandes JC. Small molecule inhibition of the CHFR-PARP1 interaction as novel approach to overcome intrinsic taxane resistance in cancer. Oncotarget 2015; 6: 30773-30786.
[11] Dent RA, Lindeman GJ, Clemons M, Wildiers H, Chan A, McCarthy NJ, Singer CF, Lowe ES, Watkins CL and Carmichael J. Phase I trial of the oral PARP inhibitor olaparib in combination with paclitaxel for first- or second-line treatment of patients with metastatic triple-negative breast cancer. Breast Cancer Res 2013; 15: R88.
[12] Kashima L, Idogawa M, Mita H, Shitashige M, Yamada T, Ogi K, Suzuki H, Toyota M, Ariga H, Sasaki Y and Tokino T. CHFR protein regulates mitotic checkpoint by targeting PARP-1 protein for ubiquitination and degradation. J Biol Chem 2012; 287: 12975-84.
[13] Poruchynsky MS, Komlodi-Pasztor E, Trostel S, Wilkerson J, Regairaz M, Pommier Y, Zhang X, Kumar Maity T, Robey R, Burotto M, Sackett D, Guha U and Fojo AT. Microtubule-targeting agents augment the toxicity of DNA-damaging agents by disrupting intracellular trafficking of DNA repair proteins. Proc Natl Acad Sci U S A 2015; 112: 1571-1576.
[14] Lord CJ and Ashworth A. The DNA damage response and cancer therapy. Nature 2012; 481: 287-294.
[15] Kinner A, Wu W, Staudt C and Iliakis G. Gamma-H2AX in recognition and signaling of DNA double-strand breaks in the context of chromatin. Nucleic Acids Res 2008; 36: 5678-5694.
[16] Solier S and Pommier Y. The nuclear gamma-H2AX apoptotic ring: implications for cancers and autoimmune diseases. Cell Mol Life Sci 2014; 71: 2289-2297.
[17] Oliver AW, Ame JC, Roe SM, Good V, de Murcia G and Pearl LH. Crystal structure of the catalytic fragment of murine poly(ADP-ribose) polymerase-2. Nucleic Acids Res 2004; 32 456-464.
[18] Murai J, Huang SY, Das BB, Renaud A, Zhang Y, Doroshow JH, Ji J, Takeda S and Pommier Y. Trapping of PARP1 and PARP2 by clinical PARP inhibitors. Cancer Res 2012; 72: 5588-5599.
[19] Cepeda V, Fuertes MA, Castilla J, Alonso C, Quevedo C, Soto M and Perez JM. Poly(ADP-ribose) polymerase-1 (PARP-1) inhibitors in cancer chemotherapy. Recent Pat Anticancer Drug Discov 2006; 1: 39-53.
[20] Kim MK. Novel insight into the function of tankyrase. Oncol Lett 2018; 16: 6895-6902.
[21] Riffell JL, Lord CJ and Ashworth A. Tankyrase-targeted therapeutics: expanding opportunities in the PARP family. Nat Rev Drug Discov 2012; 11: 923-936.
[22] Etienne-Manneville S. Microtubules in cell migration. Annu Rev Cell Dev Biol 2013; 29: 471-499.
[23] Ganguly A, Yang H, Sharma R, Patel KD and Cabral F. The role of microtubules and their dynamics in cell migration. J Biol Chem 2012; 287: 43359-43369.
[24] Akhmanova A and Steinmetz MO. Control of microtubule organization and dynamics: two ends in the limelight. Nat Rev Mol Cell Biol 2015; 16: 711-726.
[25] Bowne-Anderson H, Zanic M, Kauer M and Howard J. Microtubule dynamic instability: a new model with coupled GTP hydrolysis and multistep catastrophe. Bioessays 2013; 35: 452-461.
[26] Desai A and Mitchison TJ. Microtubule polymerization dynamics. Annu Rev Cell Dev Biol 1997; 13: 83-117.
[27] Mitchison T and Kirschner M. Dynamic instability of microtubule growth. Nature 1984; 312: 237-242.
[28] Gigant B, Wang C, Ravelli RB, Roussi F, Steinmetz MO, Curmi PA, Sobel A and Knossow M. Structural basis for the regulation of tubulin by vinblastine. Nature 2005; 435: 519-522.
[29] Lu Y, Chen J, Xiao M, Li W and Miller DD. An overview of tubulin inhibitors that interact with the colchicine binding site. Pharm Res 2012; 29: 2943-2971.
[30] Nogales E, Wolf SG and Downing KH. Structure of the alpha beta tubulin dimer by electron crystallography. Nature 1998; 391: 199-203.
[31] Zhuang SH, Hung YE, Hung L, Robey RW, Sackett DL, Linehan WM, Bates SE, Fojo T and Poruchynsky MS. Evidence for microtubule target engagement in tumors of patients receiving ixabepilone. Clin Cancer Res 2007; 13: 7480-7486.
[32] Bae T, Weon KY, Lee JW, Eum KH, Kim S and Choi JW. Restoration of paclitaxel resistance by CDK1 intervention in drug-resistant ovarian cancer. Carcinogenesis 2015; 36: 1561-1571.
[33] Nakayama S, Torikoshi Y, Takahashi T, Yoshida T, Sudo T, Matsushima T, Kawasaki Y, Katayama A, Gohda K, Hortobagyi GN, Noguchi S, Sakai T, Ishihara H and Ueno NT. Prediction of paclitaxel sensitivity by CDK1 and CDK2 activity in human breast cancer cells. Breast Cancer Res 2009; 11: R12.
[34] Castriconi R, Dondero A, Corrias MV, Lanino E, Pende D, Moretta L, Bottino C and Moretta A. Natural killer cell-mediated killing of freshly isolated neuroblastoma cells: critical role of DNAX accessory molecule-1-poliovirus receptor interaction. Cancer Res 2004; 64: 9180-9184.

[35] Pende D, Spaggiari GM, Marcenaro S, Martini S, Rivera P, Capobianco A, Falco M, Lanino E, Pierri I, Zambello R, Bacigalupo A, Mingari MC, Moretta A and Moretta L. Analysis of the receptor-ligand interactions in the natural killer-mediated lysis of freshly isolated myeloid or lymphoblastic leukemias: evidence for the involvement of the Poliovirus receptor (CD155) and Nectin-2 (CD112). Blood 2005; 105: 2066-2073.

[36] Chan CJ, Andrews DM, McLaughlin NM, Yagita H, Gilfillan S, Colonna M and Smyth MJ. DNAM-1/CD155 interactions promote cytokine and NK cell-mediated suppression of poorly immunogenic melanoma metastases. J Immunol 2010; 184: 902-911.

[37] Markman M. The promise and perils of 'targeted therapy' of advanced ovarian cancer. Oncology 2008; 74: 1-6.

[38] Berger MF and Mardis ER. The emerging clinical relevance of genomics in cancer medicine. Nat Rev Clin Oncol 2018; 15: 353-365.

[39] Hyman DM, Taylor BS and Baselga J. Implementing genome-driven oncology. Cell 2017; 168: 584-599.

[40] Hopkins TA, Ainsworth WB, Ellis PA, Donawho CK, DiGiammarino EL, Panchal SC, Abraham VC, Algire MA, Shi Y, Olson AM, Johnson EF, Wilsbacher JL and Maag D. PARP1 trapping by PARP inhibitors drives cytotoxicity in both cancer cells and healthy bone marrow. Mol Cancer Res 2019; 17: 409-419.

[41] Jenks AD, Vyse S, Wong JP, Kostaras E, Keller D, Burgoyne T, Shoemark A, Tsalikis A, de la Roche M, Michaelis M, Cinatl J Jr, Huang PH and Tanos BE. Primary cilia mediate diverse kinase inhibitor resistance mechanisms in cancer. Cell Rep 2018; 23: 3042-3055.

[42] Li CM, Lu Y, Ahn S, Narayanan R, Miller DD and Dalton JT. Competitive mass spectrometry binding assay for characterization of three binding sites of tubulin. J Mass Spectrom 2010; 45: 1160-1166.

Table S1. PARP1 Activity Inhibition

	AMXI-5001 HCL	AMXI-5001 FB	Olaparib	Talazoparib	Niraparib	Rucaparib	Paclitaxel
IC50 μM	0.0053	0.0050	0.0022	0.0010	0.0047	0.0016	NA

The inhibitory action of the test compounds towards PARP1 was determined using a commercially available microplate assay (Universal Colorimetric PARP Assay from Trevigen, Inc., Gaithersburg, MD). To determine the IC50 value for the inhibitors, the compounds were tested using increasing concentrations of the test compounds and the average absorbance of each inhibitor concentration was plotted against the log of the concentration of inhibitor using the GraphPad Prism 6 program (GraphPad Software Inc., San Diego, CA). Subsequently, the IC50s for the PARP1 inhibition were determined after non-linear fit using GraphPad Prism. The inhibitory effects of both the free base form (AMXI-5001 Free-base [FB]) and the HCl salt form (AMXI-5001 HCl) of AMXI-5001 were evaluated. DMSO was used as a negative control. Clinically approved PAPR inhibitors Olaparib (**Figure 1A**), Talazoparib (**Figure 1A**), Niraparib (**Figure 1B**), or Rucaparib (**Figure 1B**) were used as a positive control for PARP1 inhibition. Paclitaxel (**Figure 1B**) was also used as a negative control. (NA = Not Active).

Table S2. PARP2 Activity Inhibition

	AMXI-5001	Olaparib	Talazoparib
IC50 μM	0.00005	0.00003	0.00009

The inhibitory action of the test compounds towards PARP2 was determined using a commercially available microplate assay kit (BPS BIOSCIENCE INC., San Diego, CA). To determine the IC50 value for the inhibitors, the compounds were tested using increasing concentrations of the test compounds and the normalized average absorbance of each inhibitor concentration was plotted against the log of the concentration of inhibitor using the GraphPad Prism 6 program (GraphPad Software Inc., San Diego, CA). Subsequently, the IC50s for the PARP2 inhibition were determined after non-linear fit using GraphPad Prism. DMSO was used as a negative control. Clinically approved PAPR inhibitors, Olaparib and Talazoparib, were used as a positive control for PARP1 inhibition.

Table S3. Cellular PARP Activity Inhibition

	AMXI-5001	Olaparib	Talazoparib
IC50 μM	0.007	0.008	0.003

HT PARP In Vivo Pharmacodynamic Assay: The normalized ratio of pg PAR/ug total protein for cells treated with increasing doses of test compounds (AMXI-5001, Olaparib or Talazoparib) over normalized ratio for DMSO Control-treated cells, were plotted against the compound concentrations, and IC50s were determined using non-linear fit using GraphPad Prism.

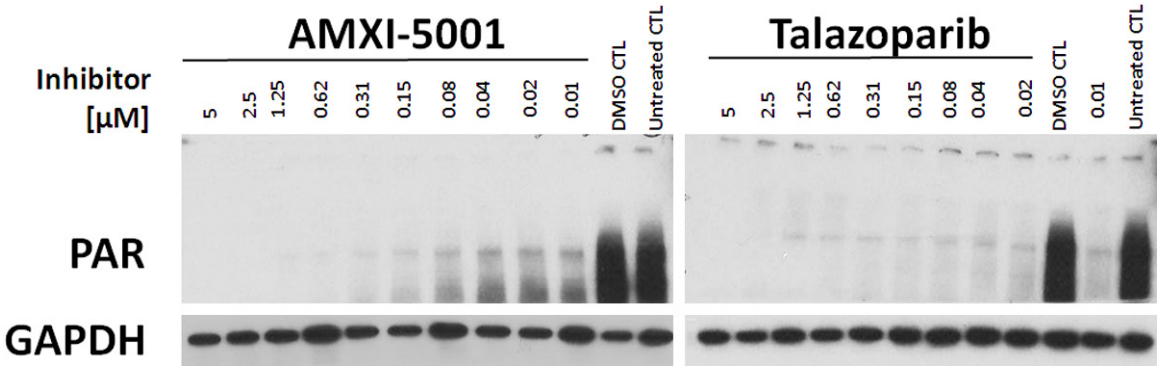

Figure S1. Cellular PAR Inhibition. Western Blot Assay: AMXI-5001 strongly inhibited PAR levels in situ in MDA-MB-436 human breast cancer cells. Cells were grown for 26 hr in media with or without varying concentrations of AMXI-5001 or Talazoparib. Cell lysates were analyzed by western blot with an anti-PAR or anti-GAPDH antibodies. Both AMXI-5001 and Talazoparib treatment resulted in a dramatic and dose dependent decrease in PAR expression in situ, when compared to the negative control DMSO-treatment (DMSO CTL) or untreated control (Untreated CTL).

Table S4. Cellular PAR Inhibition

	AMXI-5001	Talazoparib
IC50 μM	0.007	0.003

Western blot analysis: Cells were grown for 26 hr in media with or without varying concentrations of AMXI-5001 or Talazoparib. Cell lysates were analyzed by western blot with an anti-PAR or anti-GAPDH antibodies. The percentages of the normalized cellular PAR bands densities of test compounds over DMSO control, were plotted against the compound concentrations using non-linear fit using GraphPad Prism, and IC50s were determined. Talazoparib was used as positive control for cellular PAR inhibition. AMXI-5001 and Talazoparib inhibited the cellular PAR expression in dose dependent manner.

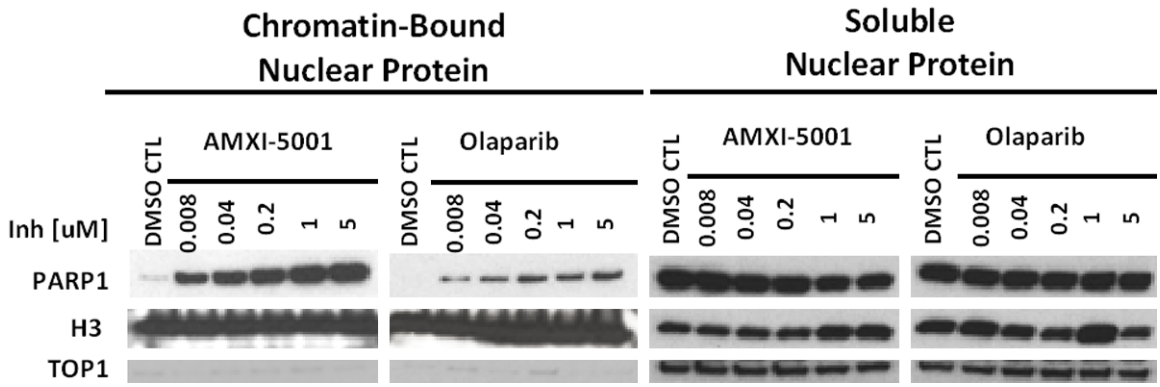

Figure S2. PARP1-DNA Complex Trapping by AMXI-5001 in Ovcar-8 Ovarian Cancer Cells. Ovcar8 cell lines were co-treated for 1 hr with 0.01% MMS and vehicle controls or increasing doses of AMXI-5001 or Olaparib. Subsequently, cell lysates were prepared and fractionated into nuclear-soluble and chromatin-bound fractions then analyzed by western blot with an anti-PARP1. Anti-H3 and anti TOP1 antibodies were used as markers for chromatin- bound or soluble nuclear fractions, respectively. AMXI-5001 treatment induced a strong and dose dependent chromatin binding of both PARP1. AMXI-5001 is a superior PARP1-DNA complex trapper than Olaparib.

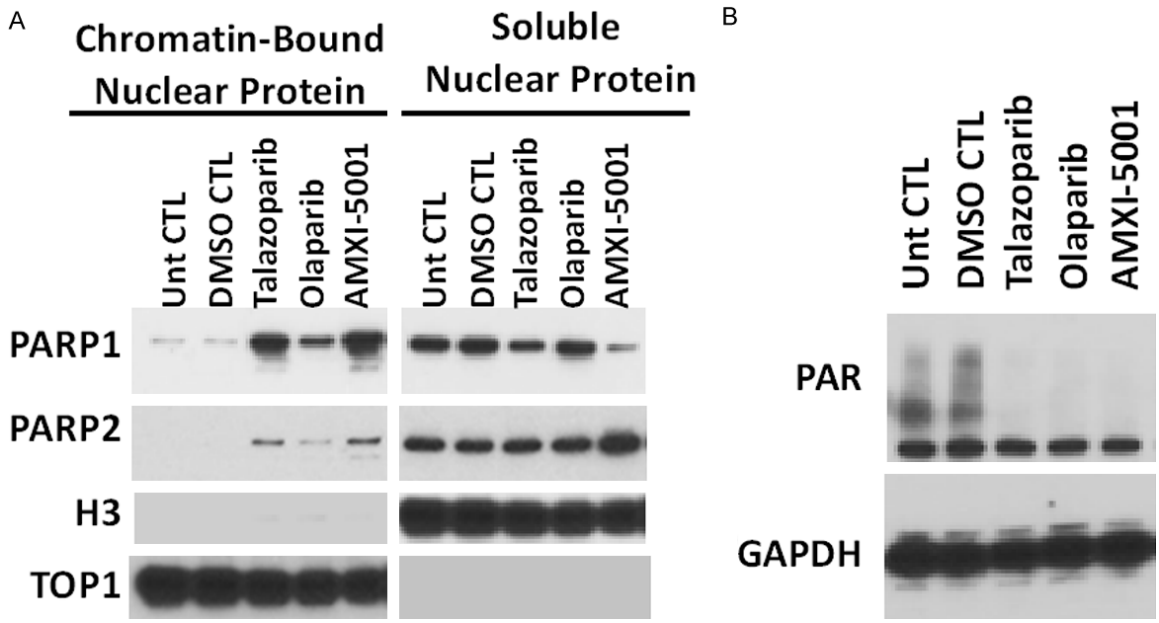

Figure S3. Concurrent Cellular PARP Activity Inhibition and PARP1-DNA Complex Trapping. Western Blot Assay: MDA-MB-436 cells were co-treated for 3 hr with 0.01% MMS and vehicle controls or 5 uM of AMXI-5001, or 5 uM Olaparib, or 5 uM Talazoparib. Subsequently, cell lysates were prepared and (A) fractionated into nuclear-soluble and chromatin-bound fractions then analyzed by western blot with an anti-PARP1 or anti-PARP2. Anti-H3 and anti TOP1 antibodies were used as markers for chromatin- bound or soluble nuclear fractions, respectively; (B) Total cell lysates were analyzed by western blot with an anti-PAR or anti-GAPDH antibodies. AMXI-5001 induced equipotent inhibition of the PAR formation in situ when compared to Olaparib and Talazoparib. Simultaneously, AMXI-5001 induced a potent PARP1-chromatin binding in a fashion comparable to Talazoparib but more potent than Olaparib.

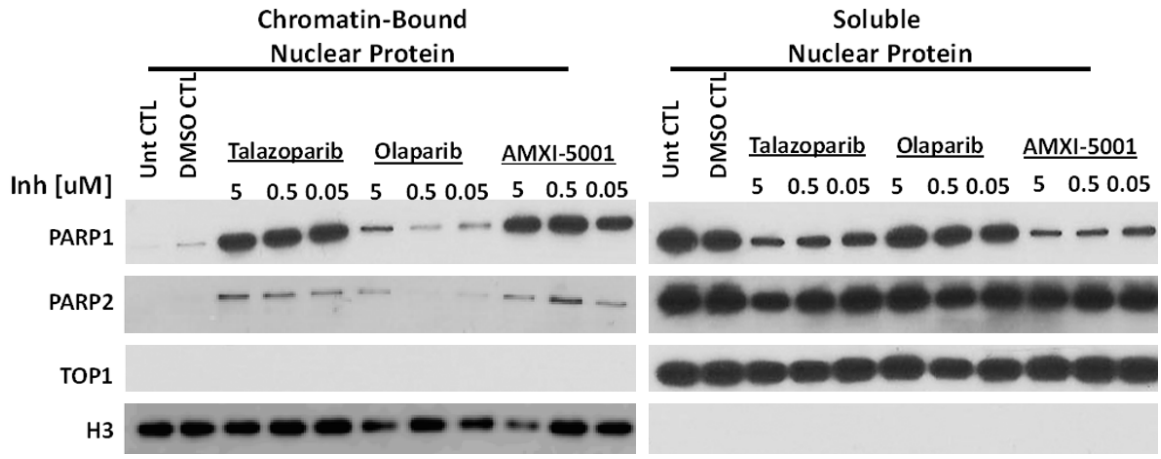

Figure S4. PARP1- and PARP2- DNA Complex Trapping by AMXI-5001 in MDA-MB-436 Breast Cancer Cells. MDA-MB-436 cell lines were co-treated for 3 hr with 0.01% MMS and vehicle controls or increasing doses of AMXI-5001. Subsequently, cell lysates were prepared and fractionated into nuclear-soluble and chromatin-bound fractions then analyzed by western blot with an anti-PARP1 or anti-PARP2. Anti-H3 and anti TOP1 antibodies were used as markers for chromatin- bound or soluble nuclear fractions, respectively. AMXI-5001 treatment induced a strong and dose dependent chromatin binding of both PARP1, and to a lesser extent PARP2, in the presence of 0.01% MMS. AMXI-5001 induced a PARP1/2-DNA complex trapping in an equipotent manner as Talazoparib, but more potent than Olaparib. Accordingly, AMXI-5001 treatment resulted in a dose dependent decrease of soluble level of PARP1 in the soluble nuclear protein fraction.

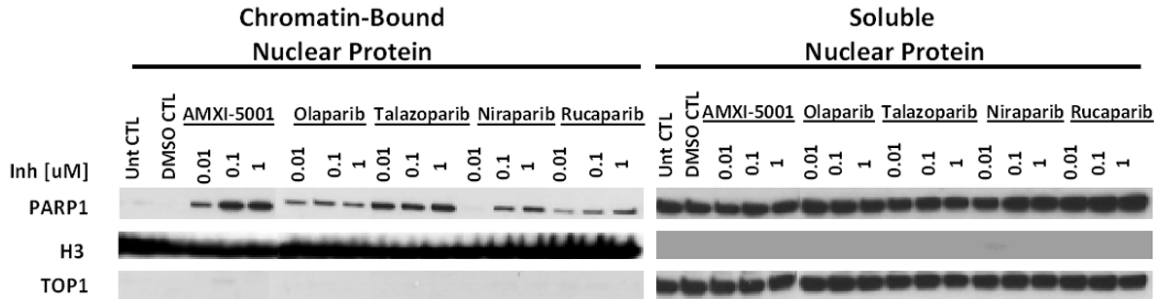

Figure S5. PARP1-DNA Complex Trapping by AMXI-5001 in MDA-MB-436 Breast Cancer Cells. MDA-MB-436 cell lines were co-treated for 1 hr with 0.01% MMS and vehicle controls or increasing doses of AMXI-5001 or clinical PARPis (Olaparib, Talazoparib, Niraparib, or Rucaparib). Subsequently, cell lysates were prepared and fractionated into nuclear-soluble and chromatin-bound fractions then analyzed by western blot with an anti-PARP1. Anti-H3 and anti TOP1 antibodies were used as markers for chromatin- bound or soluble nuclear fractions, respectively. AMXI-5001 treatment induced a strong and dose dependent chromatin binding of PARP1, in the presence of 0.01% MMS. AMXI-5001 induced a PARP1/2-DNA complex trapping to a similar extent as Talazoparib, but more potent than all the other clinical PARPis (Olaparib, Niraparib, and Rucaparib).

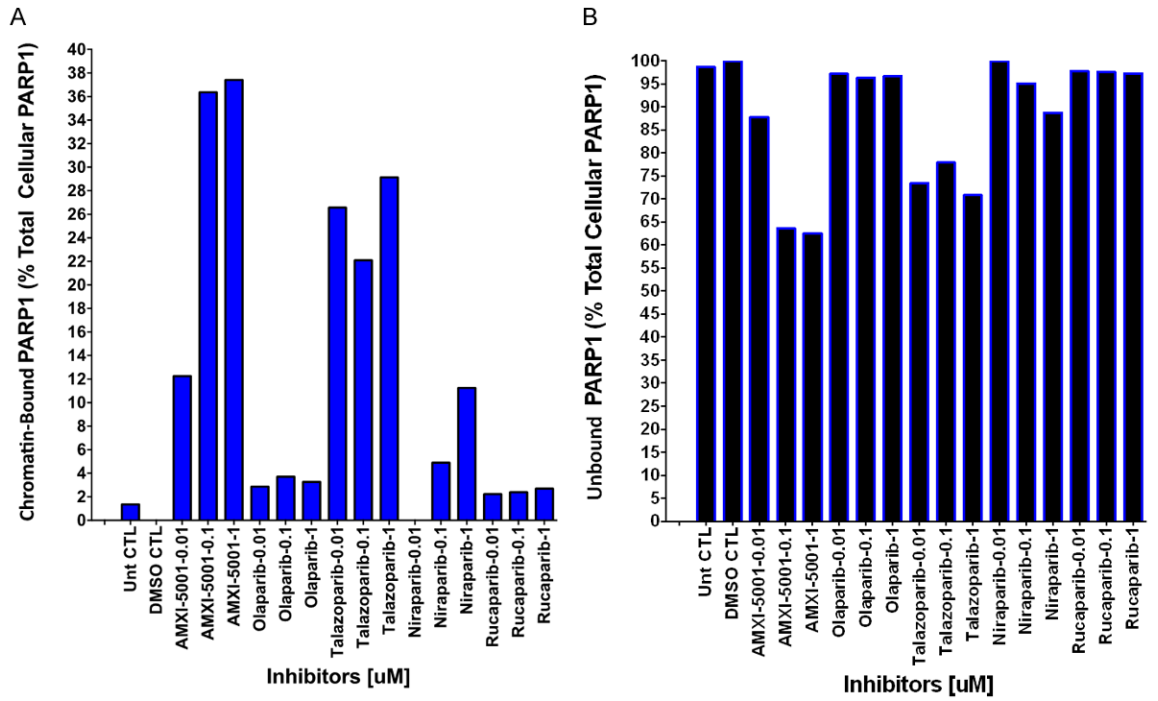

Figure S6. PARP1-DNA Complex Trapping by AMXI-5001 in MDA-MB-436 Breast Cancer Cells. MDA-MB-436 cell lines were co-treated for 1 hr with 0.01% MMS and vehicle controls or increasing doses of AMXI-5001 or clinical PARPis (Olaparib, Talazoparib, Niraparib, or Rucaparib). Subsequently, cell lysates were prepared and fractionated into nuclear-soluble and chromatin-bound fractions then analyzed by western blot with an anti-PARP1 (Figure S5). The PARP1 protein bands were quantified with ImageJ software (NIH). For each compound and for each concentration, the band density of total PARP1 (chromatin-bound PARP1 + Unbound-PARP1 in soluble nuclear fraction) was set to 100% intensity. The percentages of chromatin-bound PARP1 band density over total PARP1 band density were calculated and plotted using GraphPad Prism. AMXI-5001 treatment induced a strong and dose dependent chromatin binding of PARP1, in the presence of 0.01% MMS. AMXI-5001 induced a PARP1-DNA complex trapping to a similar extent as Talazoparib, but more potent than all the other clinical PARPis (Olaparib, Niraparib, and Rucaparib). Accordingly, AMXI-5001 treatment resulted in a dose dependent decrease of soluble level of PARP1 in the soluble nuclear protein fraction.

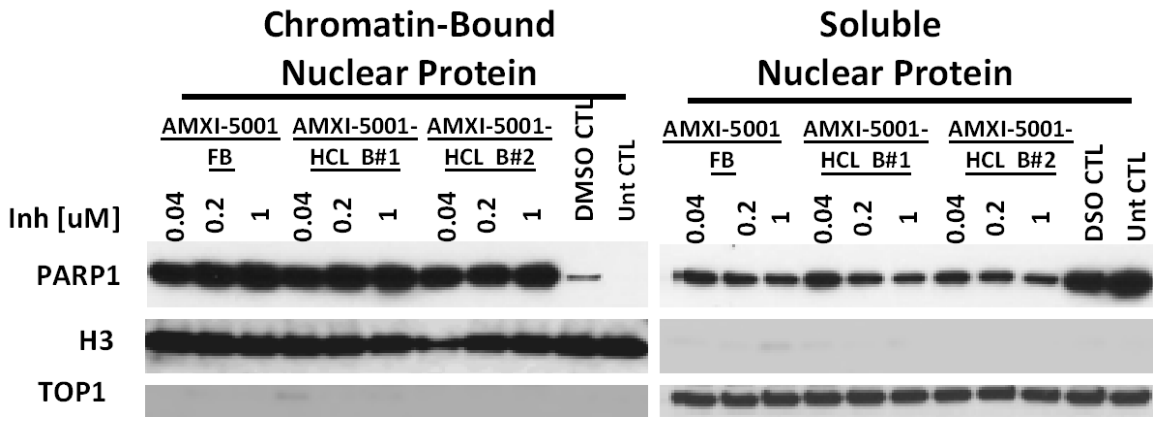

Figure S7. Equipotent PARP1-DNA Complex Trapping Potency Between Free Base (FB) and HCl- salt Forms of AMXI-5001 in MDA-MB-436 Breast Cancer Cells. MDA-MB-436 cell lines were co-treated for 3 hr with 0.01% MMS and vehicle controls or increasing doses of free base form of AMXI-5001 (AMXI-5001 FB) or its hydrochloride salt form (AMXI-5001 HCl). Here two different batches of AMXI-5001 HCl were tested B#1 and B#2. Subsequently, cell lysates were prepared and fractionated into nuclear-soluble and chromatin-bound fractions then analyzed by western blot with an anti-PARP1. Anti-H3 and anti TOP1 antibodies were used as markers for chromatin- bound or soluble nuclear fractions, respectively. Both the free base and HCl salt forms of AMXI-5001 induced an equipotent and strong dose dependent chromatin binding of PARP1, in the presence of 0.01% MMS. Also, both the free base and HCl salt forms of AMXI-5001 resulted in a dose dependent decrease of unbound PARP1 levels in the soluble nuclear protein fraction.

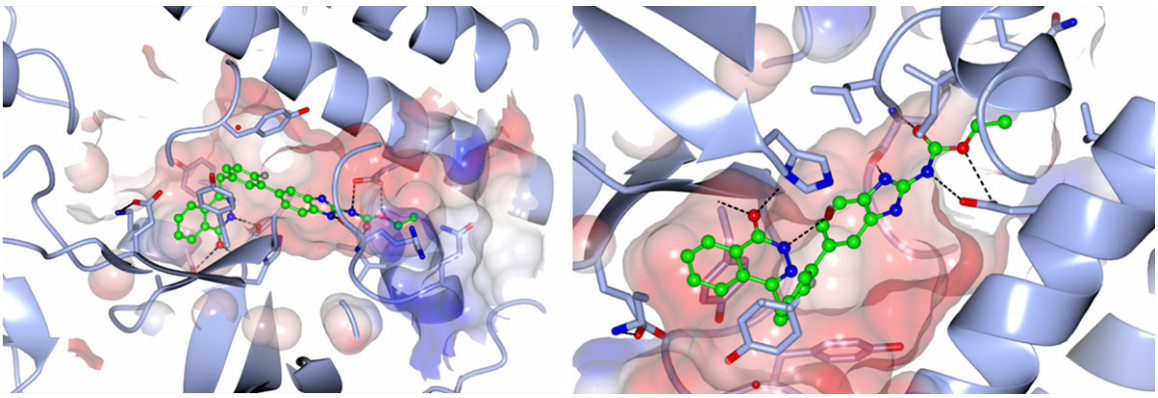

Figure S8. AMXI-5001 Binds to the Active Site of Human PARP1. AMXI-5001 (C in green ball and stick representation) in complex with PARP1 (chain B ice blue) showing some binding site interactions and with electrostatic surface representation of compound binding site.

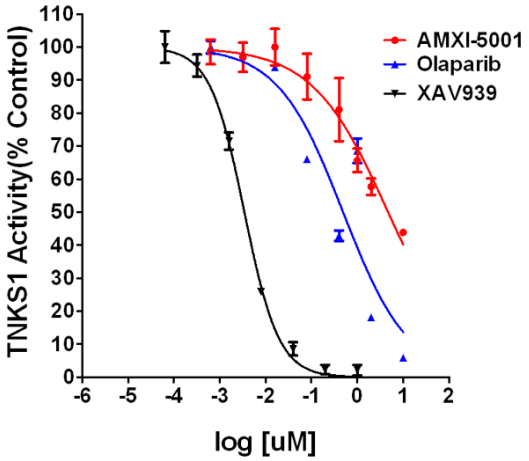

Figure S9. TNKS1 Activity Inhibition. The effect of AMXI-5001 towards TNKS1 was determined using a commercially available Tankyrase 1 colorimetric activity assay (#80573, BPS BIOSCIENCE INC). To determine the IC50 value for the inhibitors, the compounds were tested using increasing concentrations of the test compounds and the normalized average absorbance of each inhibitor concentration was plotted against the log of the concentration of inhibitor using the GraphPad Prism 6 program (GraphPad Software Inc., San Diego, CA). Subsequently, The IC50s for the TNKS1 inhibition were determined after non-linear fit using GraphPad Prism. Untreated DMSO control was set as 100% TNKS1 activity. XAV939, a small molecule inhibitor of TNKS1, and Olaparib were used as controls for TNK1 inhibition.

Table S5. TNKS1 Activity Inhibition

	AMXI-5001	Olaparib	XAV939
IC50 μM	4.721	0.492	0.004

The effect of AMXI-5001 towards TNKS1 was determined using a commercially available Tankyrase 1 colorimetric activity assay (#80573, BPS BIOSCIENCE INC). To determine the IC50 value for the inhibitors, the compounds were tested using increasing concentrations of the test compounds and the normalized average absorbance of each inhibitor concentration was plotted against the log of the concentration of inhibitor using the GraphPad Prism 6 program (GraphPad Software Inc., San Diego, CA). Subsequently, the IC50s for the TNKS1 inhibition were determined after non-linear fit using GraphPad Prism. Untreated DMSO control was set as 100% TNKS1 activity. XAV939, a small molecule inhibitor of TNKS1, and Olaparib were used as controls for TNK1 inhibition.

Table S6. Dose-dependent Tubulin Polymerization inhibition by AMXI-5001 and Vinblastine

	Water CTL	DMSO CTL	AMXI-5001 (0.5 μM)	AMXI-5001 (5 μM)	AMXI-5001 (10 μM)	Vinblastine (5 μM)	Paxlitaxel (5 μM)
FLmax	31983	32158	22474	11236	9532	8907	35724
Tmax (minutes)	84	72	105	105	105	105	20
Vmax (Fl max/Tmax)	380.8	446.6	214.0	107.0	90.8	84.8	1786.2
Vmax Fold change vs. DMSO CTL	1.2	1.0	2.1 (Fold Decrease)	4.2 (Fold Decrease)	4.9 (Fold Decrease)	5.3 (Fold Decrease)	4.0 (Fold Increase)

Standard Tubulin polymerization reactions alone (DMSO CTL) and in the presence of inhibitors (AMXI-5001 or Vinblastine), at increasing doses ranging from 0.16 μM to 5 μM. The Vmax value was decreased in dose dependent manner in presence of AMXI-5001 and Vinblastine. FLmax= Maximum reached fluorescence of the reaction. Tmax = Time to achieve FLmax.

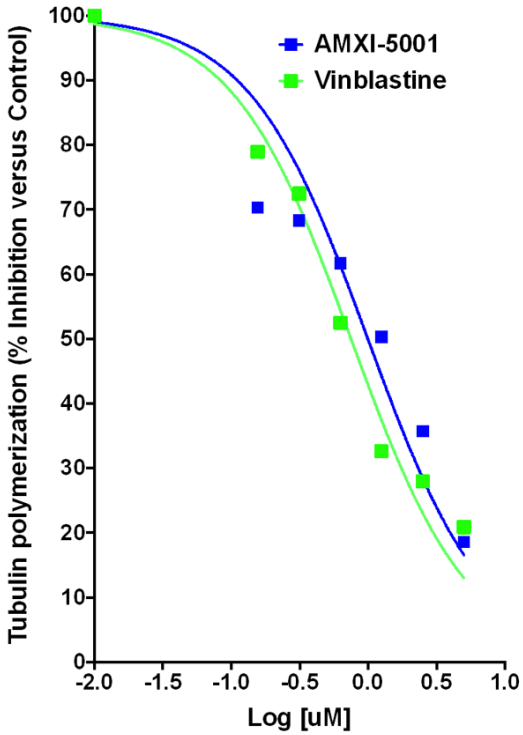

Figure S10. AMXI-5001 and Vinblastine inhibited tubulin polymerization in dose dependent manner. The Vmax were determined as described above (experimental). The Vmax of DMSO control was set to 100% polymerization. The percentages of compounds Vmax over DMSO control Vmax were plotted against the compound concentrations, and IC50s were determined. Data were plotted using the GraphPad Prism 6 program. Both AMXI-5001 and Vinblastine decreased the Vmax in dose dependent manner.

Table S7. Tubulin polymerization inhibition

	AMXI-5001	Vinblastine
IC50 μM	0.99	0.75

The Vmax percentages for compounds (AMXI-5001 or Vinblastine) over DMSO control Vmax, were plotted against the compounds (Figure S9) The Polymerized tubulin densities concentrations, and IC50s were determined using non-linear fit using GraphPad Prism.

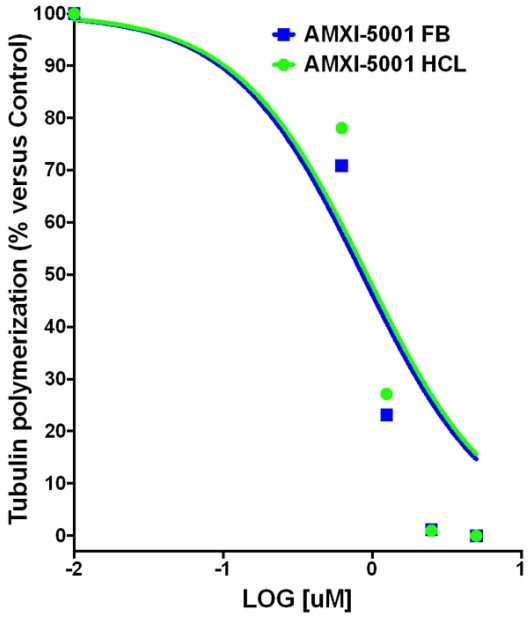

Figure S11. Equipotent microtubule polymerization inhibition between free base (FB) and HCl- salt forms of AMXI-5001. The Vmax were determined as described above (experimental). The Vmax of DMSO control was set to 100% polymerization. The percentages of compounds Vmax over DMSO control Vmax were plotted against the compound concentrations, and IC50s were determined. Data were plotted using the GraphPad Prism 6 program. The inhibitory effects of both the free base form (AMXI-5001-FB) and the HCL salt form (AMXI-5001-HCL) of AMXI-5001 were evaluated.

Table S8. Equipotent microtubule polymerization inhibition between free base (FB) and HCL- salt forms of AMXI-5001

	AMXI-5001-HCl	AMXI-5001-FB
IC50 μM	0.92	0.86

The effects of the HCl salt form and the Free base form of AMXI-5001 was compared using the fluorescence-based tubulin polymerization assay (BK011P) was conducted. Tubulin was incubated alone (DMSO Control), or in the presence of inhibitors either free base form or HCl salt form of (AMXI-5001 at increasing doses ranging from 0.3125 μM to 10 μmol/The Vmax percentages for compounds (AMXI-5001 or Vinblastine) over DMSO control Vmax, were plotted against the compound concentrations (Figure S10), and IC50s were determined using non-linear fit using GraphPad Prism.

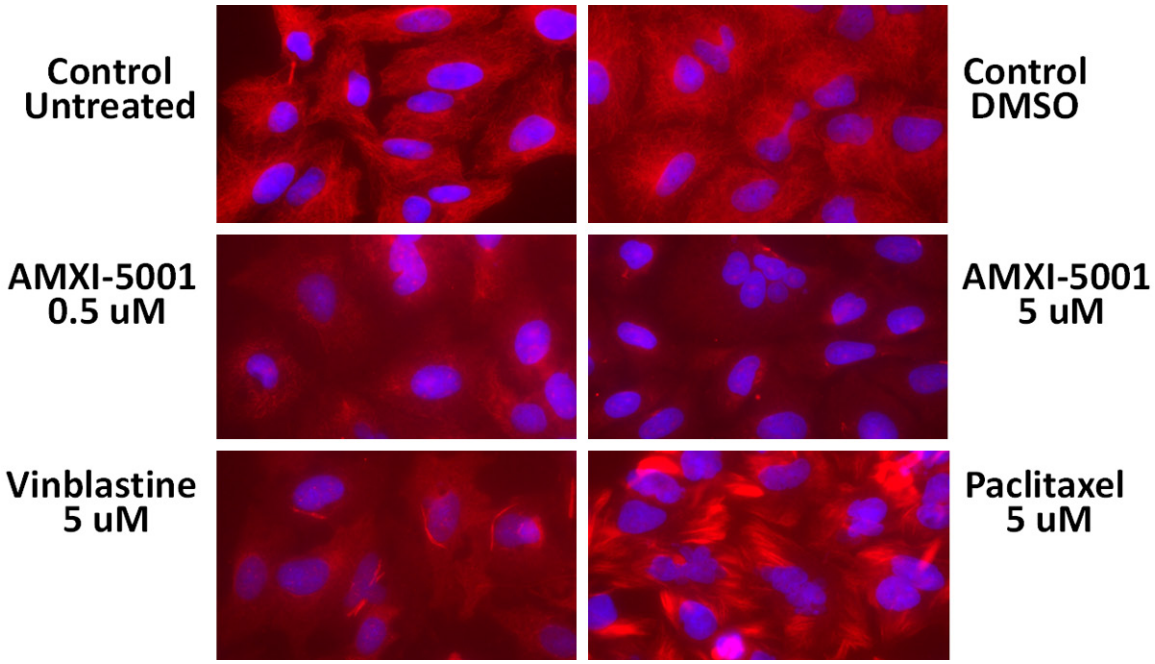

Figure S12. AMXI-5001 effect on microtubule network organization inside the cells. AMXI-5001 inhibited the polymerization of microtubules. A549 cells were treated with either AMXI-5001 at 0.5 μM or 5 μM for 24 h. 0.1% DMSO was used as a negative control. Vinblastine at 5 μM was used as a positive control for tubulin polymerization inhibition. Paclitaxel 5 μM was used as a positive control for tubulin polymerization enhancement. Samples were then prepared as in the "Experimental" section, and the status of microtubules was observed using a Zeiss AxioImager 2 microscope; 63x objective, DAPI and RFP channels. Microtubule filaments are stained in red, and cell nuclei are stained in blue.

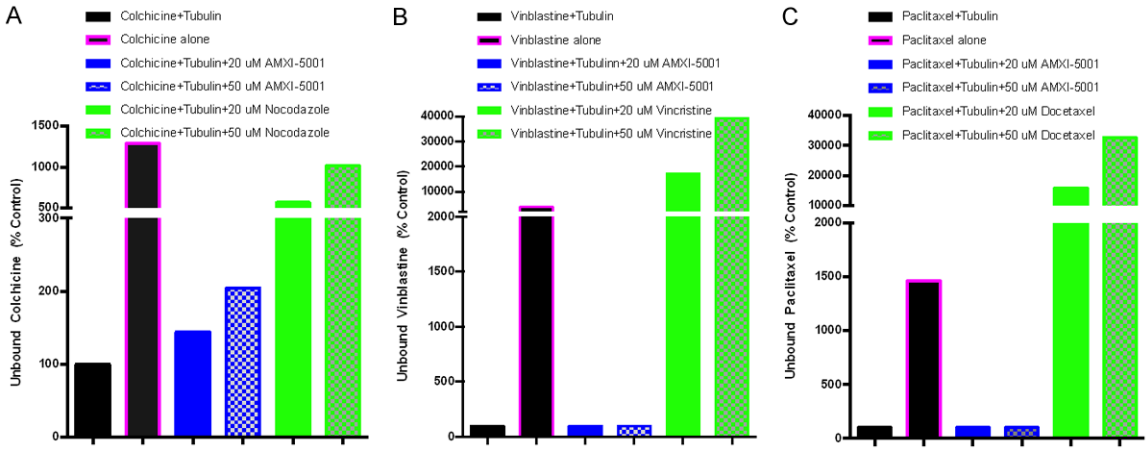

Figure S13. MS competitive binding studies. AMXI-5001 competes with colchicine (A), but not with vinblastine (B) or paclitaxel (C) to bind to tubulin. In panel (A and B), tubulin was incubated with colchicine or vinblastine in the absence of GTP with varying concentrations of either the test compound (AMXI-5001) or a known competitor (nocodazole or vincristine, respectively). In panel (C), preformed microtubules were incubated with paclitaxel and 1 mM GTP, and varying concentrations of either the test compound (AMXI-5001) or a known competitor (docetaxel). As a no tubulin binding control, colchicine, or vinblastine, or paclitaxel were incubated in reaction buffer alone without tubulin. Data were plotted using the GraphPad Prism 6 program.

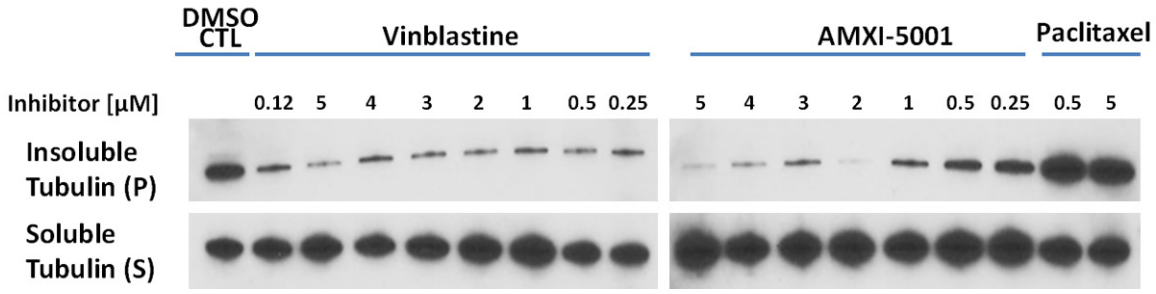

Figure S14. AMXI-5001 inhibited tubulin polymerization in situ in MDA-MB-436 human breast cancer cells. Cells were grown for 24 hr in media with or without varying concentrations of AMXI-5001, Vinblastine, or Paclitaxel. Cell lysates were fractionated into soluble and insoluble (polymerized) tubulin fractions. The two tubulin fractions were then analyzed by western blot with an anti-α/b tubulin. AMXI-5001 and Vinblastine treatments resulted in a significant decrease in polymerized (P) tubulin when compared to the negative control DMSO-treatment. Paclitaxel induced a conspicuous increase in the polymerized (P) tubulin fraction as compared to DMSO control.

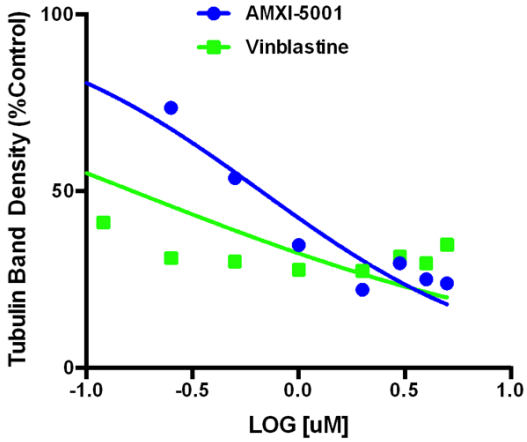

Figure S15. Intracellular tubulin polymerization assay. The Polymerized tubulin densities were determined as described above (experimental). The Polymerized tubulin densities of DMSO control was set to 100% density. The percentages of Polymerized tubulin densities with compounds treatment over DMSO control treatment were plotted against the compound concentrations, and IC50s were determined (Table S4). Data were plotted using the GraphPad Prism 6 program. AMXI-5001 decreased the polymerized tubulin density in dose dependent manner.

Table S9. In situ Cellular Tubulin polymerization inhibition

	AMXI-5001	Vinblastine
IC50 µM	0.67	0.17

The Polymerized tubulin densities percentages for compounds (AMXI-5001 or Vinblastine) over DMSO control, were plotted against the compounds' concentrations, and IC50s were determined using non-linear fit using GraphPad Prism.

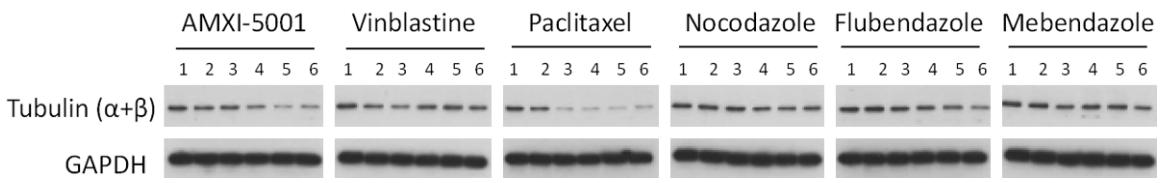

Figure S16. Total tubulin protein expression assay. AMXI-5001 reduced total tubulin protein expression in situ in MDA-MB-436 human breast cancer cells. Cells were grown for 24 hr in media with or without varying concentrations of AMXI-5001, Vinblastine, Paclitaxel, Nocodazole, Flubendazole, or Mebendazole. Cell lysates were analyzed by western blot with an anti-α/b tubulin. AMXI-5001 treatment resulted in a significant and dose dependent decrease in total tubulin protein expression in situ, when compared to the negative control DMSO-treatment.

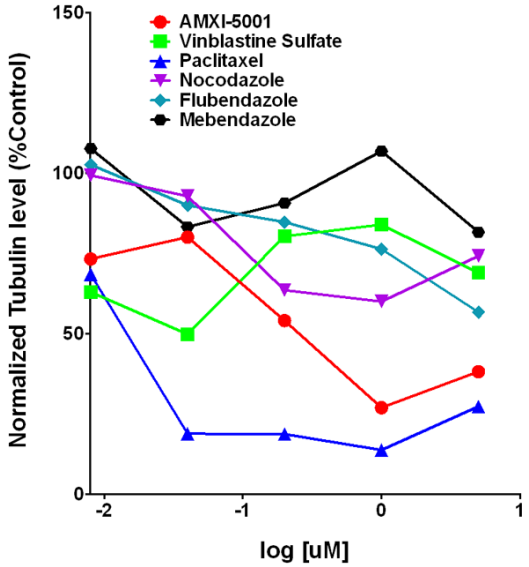

Figure S17. Total cellular tubulin protein expression inhibition. The percentages of the normalized total cellular tubulin protein band densities of test compounds over DMSO control, were plotted against the compound concentrations using non-linear fit using GraphPad Prism, and IC50s were determined (Table S5). AMXI-5001 and Paclitaxel inhibited the cellular tubulin expression in dose dependent manner and their respective IC50 were determined. percentages However, Vinblastine or Colchicine site- bonding benzimidazoles (Nocodazole, Flubendazole, and Mebendazole) induced only a modest inhibition of total cellular tubulin expression.

Table S10. Total cellular tubulin protein expression inhibition

	AMXI-5001	Paclitaxel
IC50 μM	0.26	0.02

The percentages of the normalized total cellular tubulin protein band densities test compounds over DMSO control, were plotted against the compounds' concentrations, and IC50s were determined using non-linear fit using GraphPad Prism. AMXI-5001 and Paclitaxel inhibited the cellular tubulin expression in dose dependent manner and their respective IC50 were determined. percentages However, IC50s for Vinblastine or Colchicine site- bonding benzimidazoles (Nocodazole, Flubendazole, and Mebendazole) could not be determined.

Table S11. Effect of AMXI-5001 on Cell Viability in a Panel of Human Cancer Cell Lines

Cell line	Tumor type	AMXI-5001 IC50 (μM)	TALA IC50 (μM)	OLA IC50 (μM)	NIRA IC50 (μM)	RUCA IC50 (μM)	BRCA1/ BRCA2 mutation
HuCCT1	Cholangiocarcinoma	0.004		NR			
Jurkat	*Acute T Cell Leukemia.*	0.013	0.01	0.083			
H322	Non-small lung cancer	0.023	NR	NR	NR	NR	
Calu-6	Non-small lung cancer	0.026	3.364				
DU145	Prostate	0.026	NR				BRCA1, BRCA2
CCRF-CEM (CCL-119)	*Acute lymphoblastic leukemia*	0.028	0.431	5.869	2.53	8.395	BRCA1, BRCA2
MS-1	Mesothelioma	0.028	1.885	NR	10.15	NR	
HCT15	Colorectal	0.032	NR	NR	NR	NR	
OE21	Oesophageal	0.037	15.45	9.791	NR	NR	
U2OS	Osteosarcoma	0.037	NR				
MES-SA	Uterine sarcoma	0.044					
MM1.R	Myeloma	0.047					
H290	Mesothelioma	0.048	0.171	7.729	5.555	NR	
H1299	Non-small lung cancer	0.052	6.75	NR	NR	NR	
SK-OV-3	Ovarian	0.053	1.053				
MOLM-13	Acute lymphoblastic leukemia	0.055	0.766	NR	2.837	1.666	
MV4-1	Acute lymphoblastic leukemia	0.057	0.19	2.768	1.567	0.83	
MG63	Osteosarcoma	0.059	0.448				
H1975	Non-small lung cancer	0.061	6.85	NR	NR	NR	
647-V	Urothelial	0.062	0.005				
H1703	Non-small lung cancer	0.063	NR	NR	NR	NR	
A-673	Ewing's sarcoma	0.066	2.47	NR	NR	NR	
Saos-2	Osteosarcoma	0.068					
K562	Acute lymphoblastic leukemia	0.074	1.517	5.453			
HCC2998	Colorectal	0.078	0.218				
RPMI 8226/CCL-155	Myeloma	0.082	NR	5.248	NR	NR	
SK-UT-1	Uterine leiomysarcoma	0.082					
KG-1	Chronic myeloid Leukemia	0.084	0.14	3.788			
MOLM-14	Acute lymphoblastic leukemia	0.088	0.972	4.773	2.069	1.669	
LNCAP C4-2	Prostate	0.09	1.145	NR			BRCA1, BRCA2
REN	Mesothelioma	0.091	3.412				
Caco2	Colorectal	0.092	2.37				
HT-1080	Fibrosarcoma	0.092	0.758	6.159			
MiaPaca2	Pancreatic	0.1	0.59				
Hela	Cevical cancer	0.104	10.96				
Colo201	Colorectal	0.105	NR	NR	NR	NR	
A427	Non-small lung cancer	0.105	4.135	9.294	15.17	NR	
LN-18	Glioblastoma	0.106		1.283			BRCA2
BxPC3	Pancreatic	0.107					
H838	Non-small lung cancer	0.114	NR	NR	NR	NR	
HOS	Osteosarcoma	0.117					
H69	Small Cell lung cancer	0.12	4.232	NR	NR	NR	
OVCAR8	Ovarian	0.129	NR	NR	6.06	6.965	BRCA1 (MET)
H82	Small Cell lung cancer	0.13	6.254	NR	NR	NR	
H2052	Mesothelioma	0.13	1.895	NR	9.224	NR	BRCA1
HCC2998	Colorectal	0.132	NR	NR	NR	NR	
LOX	Melanoma	0.147					
A204	Rhabdomyosarcoma	0.149					
HL-60	Acute lymphoblastic leukemia	0.154	3.151	NR			
CFPAC-1	Pancreatic	0.156	0.155		0.155		
RD-ES	Ewing's sarcoma	0.16					
A549	Non-small lung cancer	0.168	14.03	NR	6.237	5.906	
MSTO-211H	Mesothelioma	0.173	2.675	NR	NR	NR	

MES-SA-DX5	Uterine Sarcoma	0.176					
22RV1	Prostate	0.189					BRCA2
MDA-MB-436	Breast	0.192	NR	15.13	13.84	NR	BRCA1
H292	Non-small lung cancer	0.195	0.51				
VcaP	Prostate	0.202	NR	NR	NR	NR	
Calu3	Non-small lung	0.214	0.241				BRCA1
PANC1	Pancreatic	0.234	NR	15.3	18.48	9.993	
OE33	Oesophageal	0.242					
U521	Glioblastoma	0.247	8.115	46.25	18.11	33.85	
HCC2935	Non-small lung cancer	0.258	3.888	NR	NR	NR	
A2058	Melanoma	0.263	0.161				BRCA2
HCC1954	Breast	0.273	6.343	NR	NR	1.578	
H28	Mesothelioma	0.273					BRCA2
Colo320	Colorectal	0.274					BRCA2
H2452	Mesothelioma	0.304	16.92	16.92	NR	NR	
MDA-MB-231	Breast	0.307	1.705				
H441	Non-small lung	0.308					BRCA2
OE19	Oesophageal	0.308					
PEO1	Ovarian	0.336	NR	NR	NR	NR	BRCA2
H460	Non-small lung cancer	0.344	NR	NR	NR	NR	
HT-144	Melanoma	0.406	0.963				
MCF7	Breast	0.461	2.5	10.12			
PEO4	Ovarian	0.465	NR	NR	NR	NR	BRCA2
HCT116	Colorectal	0.49	NR	NR	11.1	17.77	BRCA2
Capan-1	Pancreatic	0.496	0.336		0.336		BRCA2
HCC827	Non-small lung cancer	0.523					
H2170	Non-small lung cancer	0.537	2.787	NR	NR	NR	
H226	Mesothelioma	0.537	4.433	NR			
H2030	Non-small lung cancer	0.556	7.327				
EKVX	Non-small lung cancer	0.667	4.794				
HCC1937	Breast	0.675	NR	3.495			BRCA1
PEO23	Ovarian	0.731	NR	NR	NR	NR	
SNB-75	Glioblastoma	0.896	7.554	82.83	14.9	30.57	
HCC1569	Breast	5.428	NR	NR	NR	NR	BRCA2
U87	Glioblastoma	6.169	177.8	110.8	37.39	25.4	
HCC1428	Breast	17.27	NR	NR	NR	NR	BRCA2
PEO14	Ovarian	NR	NR	NR	NR	NR	

The effect on cell viability of increasing concentrations of AMXI-5001 or clinical PARPis (Olaparib (OLA), Talazoparib (TALA), Niraparib (NIRA), or Rucaparib (RUCA)) was assessed in a wide panel of cancer cell of various origins. Proliferation was assessed using Cell Titer Glo assay after cells were incubated for 3 days with AMXI-5001. The concentration required to inhibit cell growth by 50% (IC50) was determined after non-linear fit using GraphPad Prism. DMSO treated cells were used as a vehicle control. Known BRAC1/2 mutation status is indicated. NR = Non-Responsive. (MET) = Methylated gene.

Table S12. Effect of AMXI-5001 on Cell Viability in a Panel of Human Cancer Cell Lines

Cell Line Name	Tumor Type	AMXI-5001 IC50 (μM)	*BRCA1/BRCA2* mutation
MDA-MB-436	Breast (TNBC)	0.013	*BRCA1*
DU4475	Breast (TNBC)	0.013	
Jurkat	Hematologic	0.019	
Calu-6	Lung (NSCLC)	0.02	
RPMI-2650	Nasal	0.022	
MDA-MB-157	Breast (TNBC)	0.027	
MDA-MB-468	Breast (TNBC)	0.028	
SKLU-1	Lung (NSCLC)	0.029	
H82	Lung (SCLC)	0.033	
HCC1428	Breast	0.034	*BRCA2*
PEO1	Ovarian	0.047	*BRCA2*
OE21	Oesophageal	0.049	
CCRF-HSB-2	Hematologic	0.052	
Capan-1	Pancreatic	0.054	*BRCA2*
SK-UT-1	Sarcoma	0.056	
MV4-11	Hematologic	0.056	
HCC2998	Colorectal	0.057	
K562	Hematologic	0.059	
CCL119	Hematologic	0.059	*BRCA1, BRCA2*
H2170	Lung (NSCLC)	0.061	
H1703	Lung (NSCLC)	0.062	
H209	Lung (SCLC)	0.064	
HCT-15	Colorectal	0.064	
HT-144	Skin	0.064	
RD-ES	Sarcoma	0.065	
A427	Lung (NSCLC)	0.067	
H69	Lung (SCLC)	0.068	
LNCAP C4-2	Prostate	0.069	
KG-1	Hematologic	0.070	
Hela	Cervical	0.071	
A673	Sarcoma	0.072	
MG63	Sarcoma	0.074	
MOLM-14	Hematologic	0.076	
Raji	Hematologic	0.076	
MES-SA	Sarcoma	0.077	
22RV1	Prostate	0.078	*BRCA2*
HL-60	Hematologic	0.079	
MOLM-13	Hematologic	0.083	
DU145	Prostate	0.086	*BRCA1*, *BRCA2*
8226	Hematologic	0.086	
H322	Lung (NSCLC)	0.087	
H520	Lung (NSCLC)	0.087	
MSTO-211H	Mesothelioma	0.091	
VCaP	Prostate	0.091	
H838	Lung (NSCLC)	0.092	

LOX	Skin	0.092	
HT-1080	Sarcoma	0.092	
U251	Brain	0.093	
Mel-201	Hematologic	0.093	
H2058	Lung (NSCLC)	0.097	
Mel-juso	Skin	0.097	
H1975	Lung (NSCLC)	0.097	
MCF7	Breast	0.098	
SK-OV-3	Ovarian	0.100	
Calu-3	Lung (NSCLC)	0.101	*BRCA1*
Colo201	Colorectal	0.102	
LNCAP	Prostate	0.102	*BRCA1, BRCA2*
HCC1954	Breast	0.103	
H2052	Mesothelioma	0.103	*BRCA1*
EKVX	Lung (NSCLC)	0.103	
SOAS-2	Sarcoma	0.103	
PC3TriGFP	Prostate	0.104	
H1299	Lung (NSCLC)	0.104	
LN-18	Brain	0.106	*BRCA2*
DLD1	Colorectal	0.107	
OE19	Oesophageal	0.108	
MS-1	Mesothelioma	0.109	
HOS	Sarcoma	0.113	
Colo357	Colorectal	0.113	
H226	Mesothelioma	0.116	
CFPAC-1	Pancreatic	0.117	
OE33	Oesophageal	0.118	
PEO4	Ovarian	0.119	*BRCA2*
A204	Sarcoma	0.120	
MES-SA-DX5	Sarcoma	0.123	
HuCCT1	Cholangiocarcinoma	0.125	
OVCAR8	Ovarian	0.126	*BRCA1* (MET)
H28	Mesothelioma	0.127	*BRCA2*
Colo320	Colorectal	0.127	*BRCA2*
BT-20	Breast (TNBC)	0.131	
HCC1569	Breast	0.135	*BRCA2*
A549	Lung (NSCLC)	0.140	
H2452	Mesothelioma	0.141	
MDA-MB-231	Breast (TNBC)	0.145	
H460	Lung (NSCLC)	0.146	
HCT116	Colorectal	0.147	*BRCA2*
SNB-75	Brain	0.147	
U2OS	Sarcoma	0.151	
U87	Brain	0.158	
H2030	Lung (NSCLC)	0.162	
BT-549	Breast (TNBC)	0.169	
SK-MES-1	Lung (NSCLC)	0.174	
PEO23	Ovarian	0.174	
H292	Lung (NSCLC)	0.195	

Panc-1	Pancreatic	0.208	
Hcc2935	Lung (NSCLC)	0.225	
HCC827	Lung (NSCLC)	0.236	
PEO14	Ovarian	0.268	
H596	Lung (NSCLC)	0.301	
HCC1937	Breast	0.481	*BRCA1*
GS2	Brain	0.489	

The effect on cell viability of increasing concentrations of AMXI-5001 was assessed in a wide panel of cancer cell of various origins. Proliferation was assessed after cells were incubated for 6 days with AMXI-5001 using Cell Titer Glo assay. The concentration required to inhibit cell growth by 50% (IC50) was determined after non-linear fit using GraphPad Prism. DMSO treated cells were used as a vehicle control. Known BRAC1/2 mutation status is indicated. (MET) = Methylated gene.

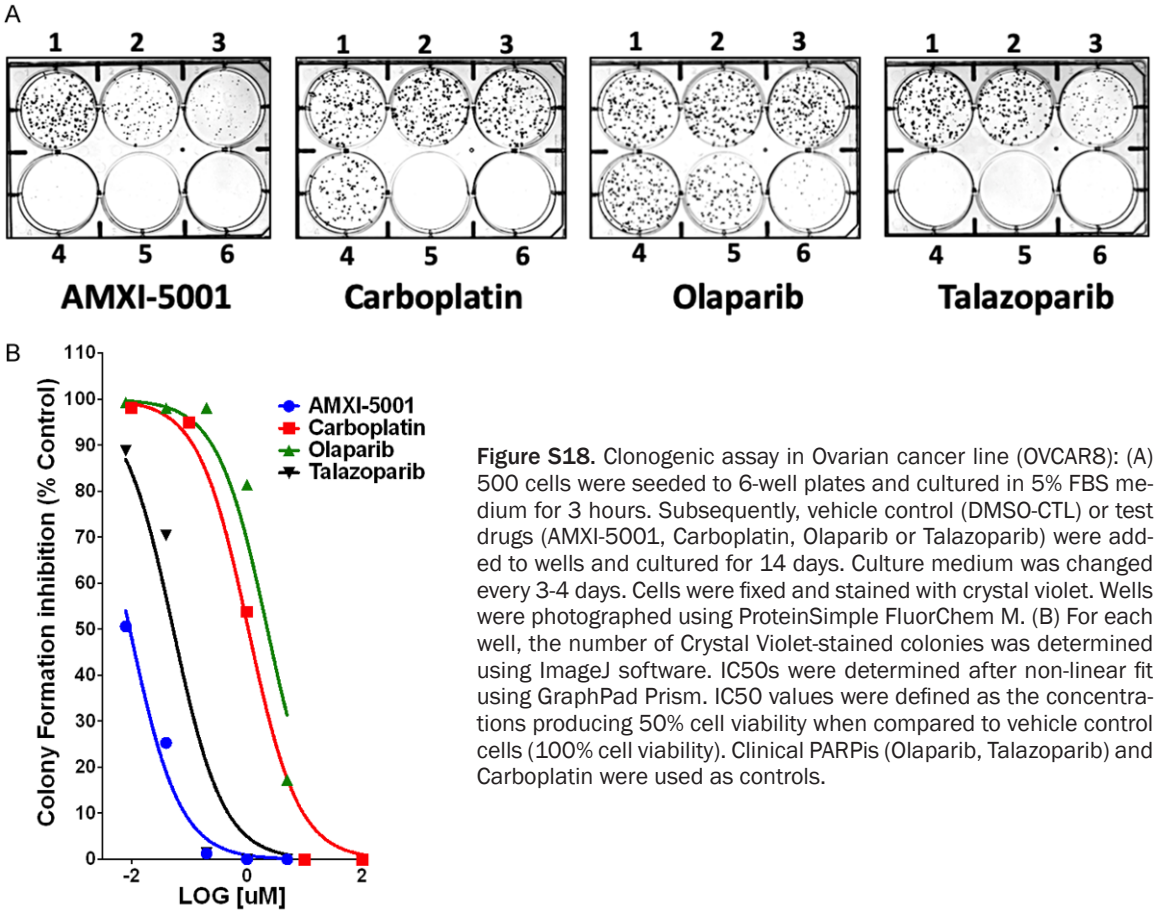

Figure S18. Clonogenic assay in Ovarian cancer line (OVCAR8): (A) 500 cells were seeded to 6-well plates and cultured in 5% FBS medium for 3 hours. Subsequently, vehicle control (DMSO-CTL) or test drugs (AMXI-5001, Carboplatin, Olaparib or Talazoparib) were added to wells and cultured for 14 days. Culture medium was changed every 3-4 days. Cells were fixed and stained with crystal violet. Wells were photographed using ProteinSimple FluorChem M. (B) For each well, the number of Crystal Violet-stained colonies was determined using ImageJ software. IC50s were determined after non-linear fit using GraphPad Prism. IC50 values were defined as the concentrations producing 50% cell viability when compared to vehicle control cells (100% cell viability). Clinical PARPis (Olaparib, Talazoparib) and Carboplatin were used as controls.

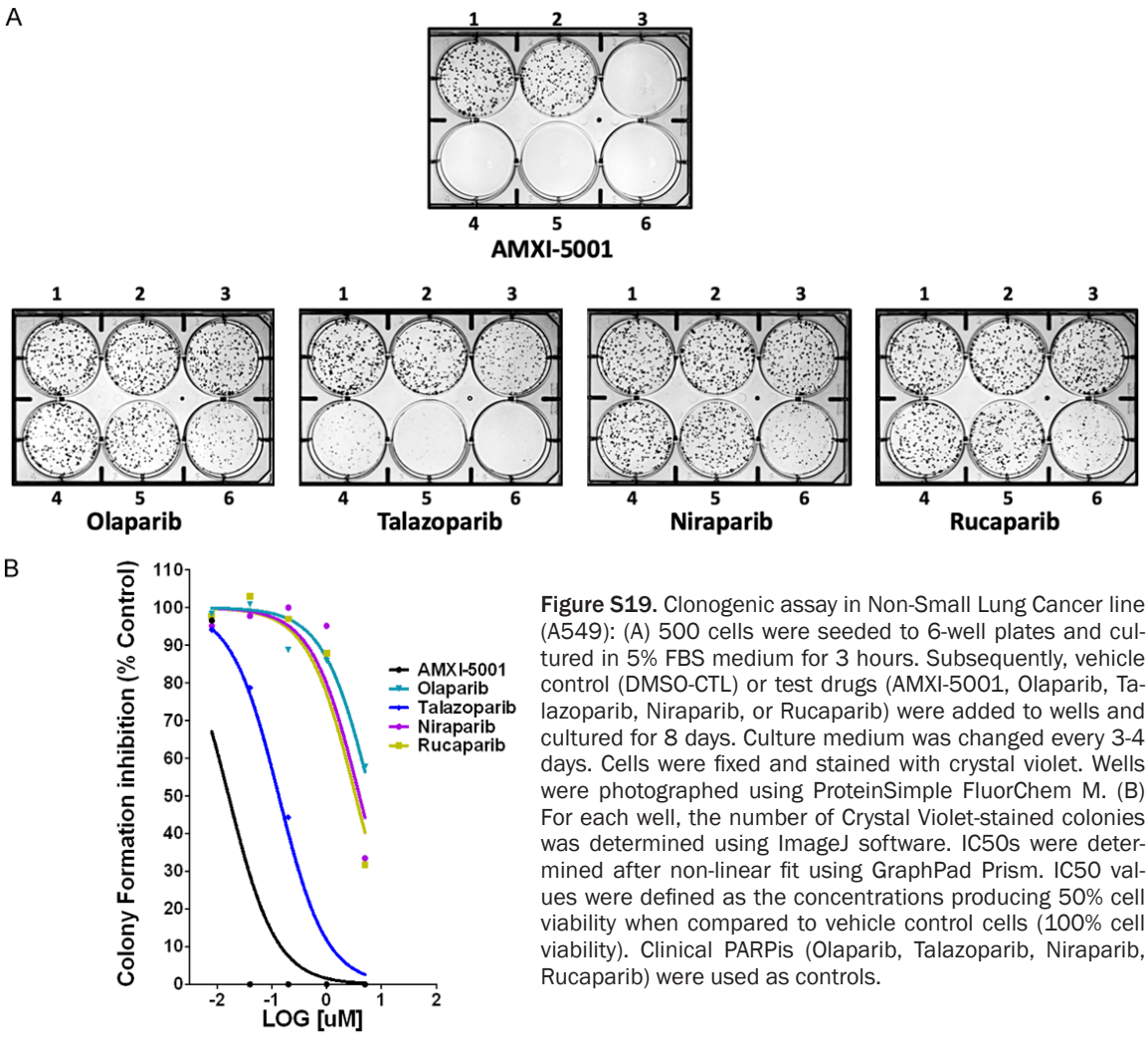

Figure S19. Clonogenic assay in Non-Small Lung Cancer line (A549): (A) 500 cells were seeded to 6-well plates and cultured in 5% FBS medium for 3 hours. Subsequently, vehicle control (DMSO-CTL) or test drugs (AMXI-5001, Olaparib, Talazoparib, Niraparib, or Rucaparib) were added to wells and cultured for 8 days. Culture medium was changed every 3-4 days. Cells were fixed and stained with crystal violet. Wells were photographed using ProteinSimple FluorChem M. (B) For each well, the number of Crystal Violet-stained colonies was determined using ImageJ software. IC50s were determined after non-linear fit using GraphPad Prism. IC50 values were defined as the concentrations producing 50% cell viability when compared to vehicle control cells (100% cell viability). Clinical PARPis (Olaparib, Talazoparib, Niraparib, Rucaparib) were used as controls.

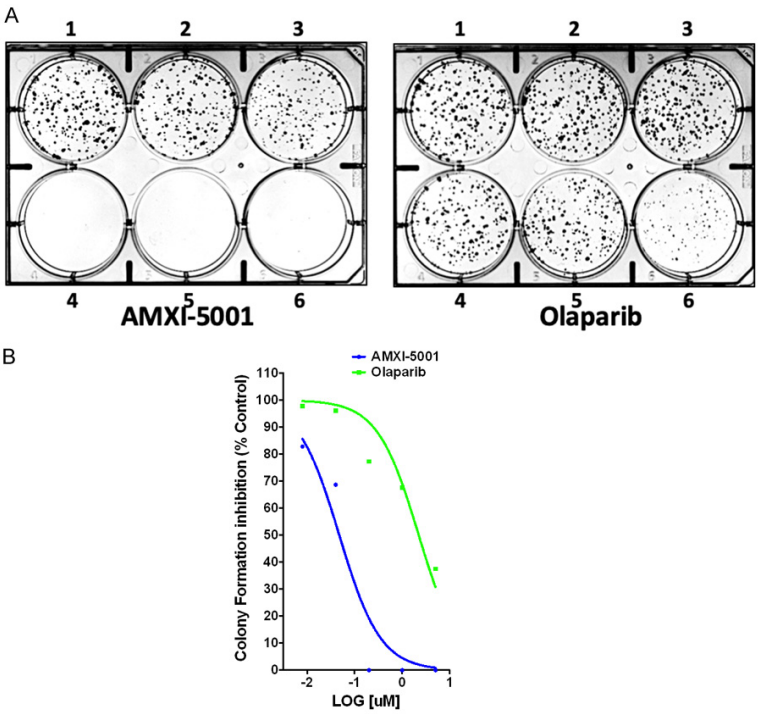

Figure S20. Clonogenic assay in Prostate Cancer line (DU145): (A) 500 cells were seeded to 6-well plates and cultured in 5% FBS medium for 3 hours. Subsequently, vehicle control (DMSO-CTL) or test drugs (AMXI-5001, Olaparib) were added to wells and cultured for 8 days. Culture medium was changed every 3-4 days. Cells were fixed and stained with crystal violet. Wells were photographed using ProteinSimple FluorChem M. (B) For each well, the number of Crystal Violet-stained colonies was determined using ImageJ software. IC50s were determined after non-linear fit using GraphPad Prism. IC50 values were defined as the concentrations producing 50% cell viability when compared to vehicle control cells (100% cell viability). Clinical PARPi (Olaparib) was used as control.

Table S13. Clonogenic assay in Ovarian cancer line (OVCAR8)

	AMXI-5001	Carboplatin	Olaparib	Talazoparib
IC50 (μM)	0.010	1.062	2.272	0.053

The effect of each test compound on cell viability was assessed using colony formation assay in an ovarian cancer cell (OVCAR8). The number of Crystal Violet-stained colonies in each well was determined using ImageJ software. IC50s were determined after non-linear fit using GraphPad Prism. IC50 values were defined as the concentrations producing 50% cell viability when compared to vehicle control cells (100% cell viability). Clinical PARPis (Olaparib, Talazoparib) and Carboplatin were used as controls.

Table S14. Clonogenic assay in Non-Small Lung Cancer line (A549)

	AMXI-5001	Olaparib	Talazoparib	Niraparib	Rucaparib
IC50 (μM)	0.0163	6.467	0.134	3.968	3.376

The effect of each test compound on cell viability was assessed using colony formation assay in a Non-Small Lung Cancer Cell (A549). The number of Crystal Violet-stained colonies in each well was determined using ImageJ software. IC50s were determined after non-linear fit using GraphPad Prism. IC50 values were defined as the concentrations producing 50% cell viability when compared to vehicle control cells (100% cell viability). Clinical PARPis (Olaparib, Talazoparib, Niraparib, Rucaparib) were used as controls.

Table S15. Clonogenic assay in Prostate Cancer line (DU145)

	AMXI-5001	Olaparib
IC50 (μM)	0.048	2.231

The effect of each test compound on cell viability was assessed using colony formation assay in a Prostate Cancer Cell (DU145). The number of Crystal Violet-stained colonies in each well was determined using ImageJ software. IC50s were determined after non-linear fit using GraphPad Prism. IC50 values were defined as the concentrations producing 50% cell viability when compared to vehicle control cells (100% cell viability). Clinical PARPi (Olaparib) was used as control.

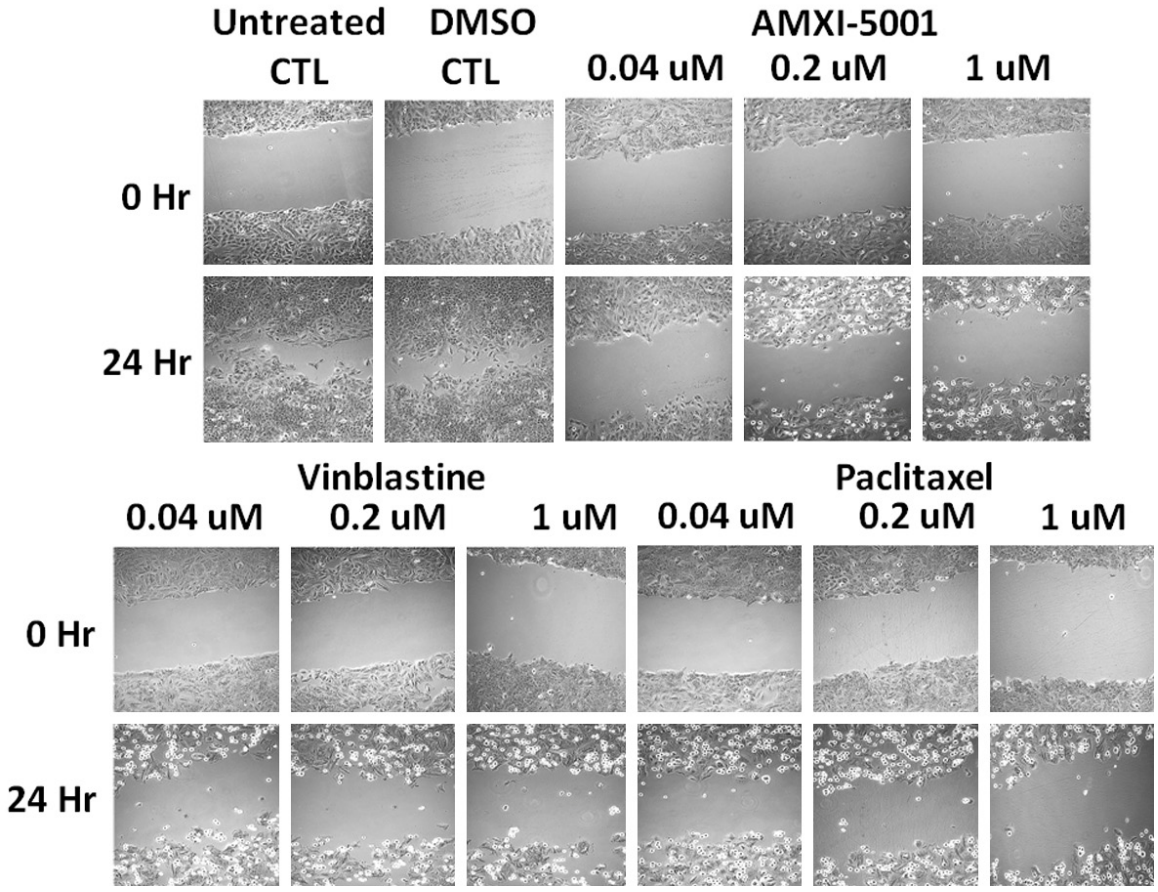

Figure S21. Scratch Wound Assays in Lung Cancer line (A549): Inhibition of Cancer Cell Migration by AMXI-5001. A549 lung cancer cells were seeded onto 12-well plates. Wounds were generated after cells reached confluence. Wounded cultures were incubated for 24 Hr in culture medium alone (Untreated control), or medium containing 0.1% (v/v) DMSO (DMSO control) or 0.04, 0.2, 1 μM of AMXI-5001, or clinical PARPis (Olaparib and Talazoparib) or clinical MTAs (Paclitaxel and Vinblastine). Random fields (40 Å~) from each scratch wound were picked and visualized by microscopy to assess cell migration ability.

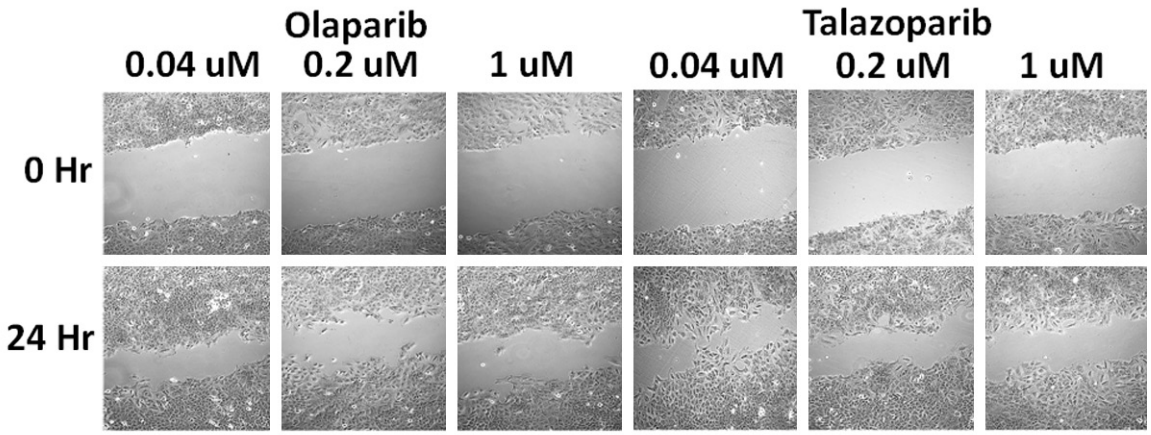

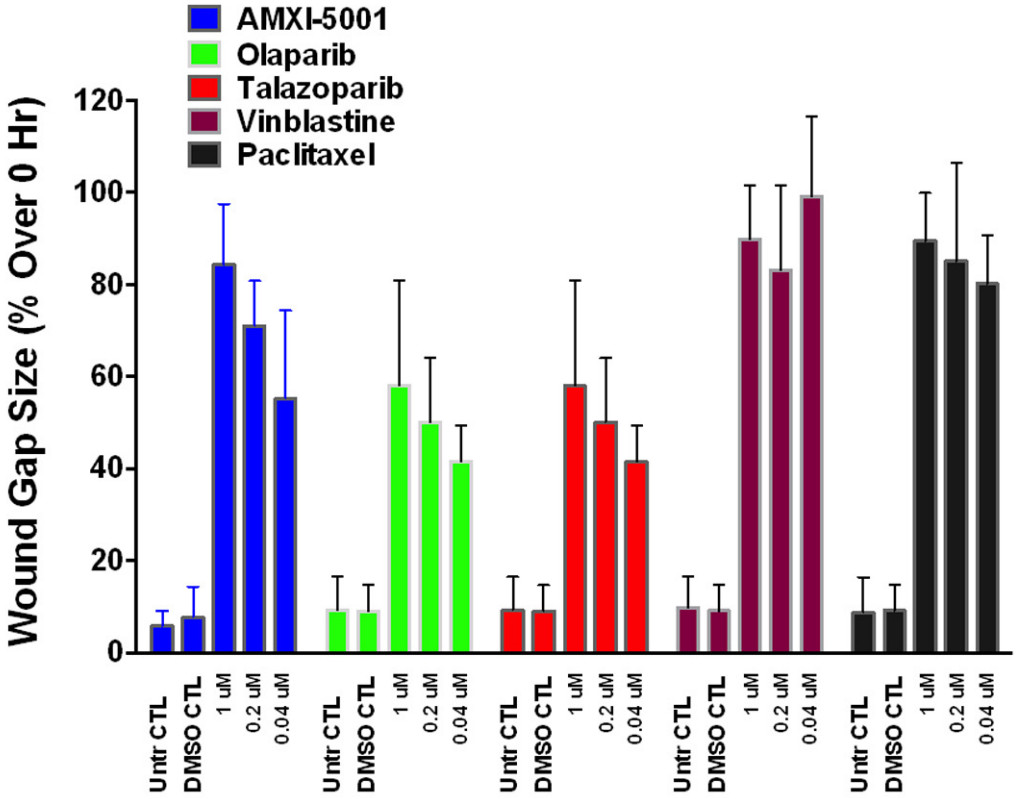

Figure S22. Scratch Wound Assays in Lung Cancer line (A549): Inhibition of Cancer Cell Migration by AMXI-5001. A549 lung cancer cells were seeded onto 12-well plates. Wounds were generated after cells reached confluence. Wounded cultures were incubated for 24 Hr in culture medium alone (Untreated control), or medium containing 0.1% (v/v) DMSO (DMSO control) or 0.04, 0.2, 1 μM of AMXI-5001, or clinical PARPis (Olaparib and Talazoparib) or clinical MTAs (Paclitaxel and Vinblastine). Random fields (40 Å~) from each scratch wound were picked and visualized by microscopy to assess cell migration ability. Images were analyzed using ImageJ analysis software to determine wound gap size in each well at 0 hr and 24 hr. treatment. Data are presented as percent of the average wound gap size at 24 hr over the average wound gap size at 0 hr treatment, ± SD (N = 9 measurements).

MDA-MB-436 (Breast)

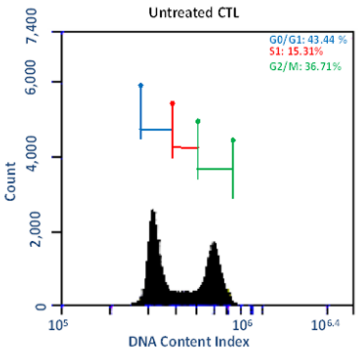

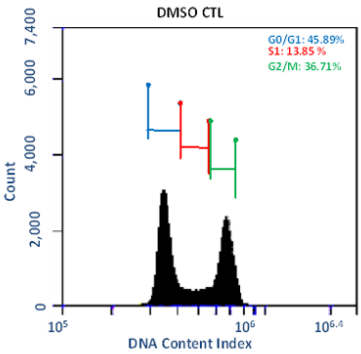

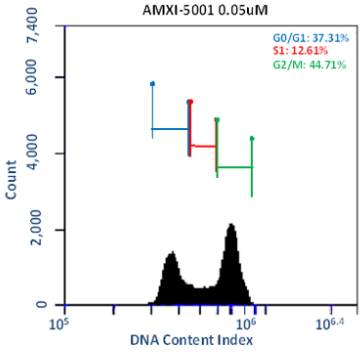

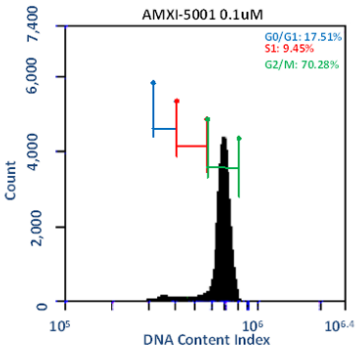

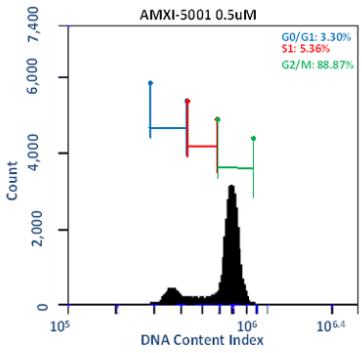

OVCAR8 (Ovarian)

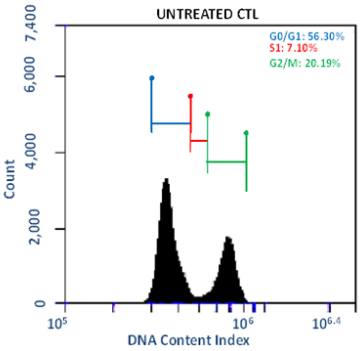

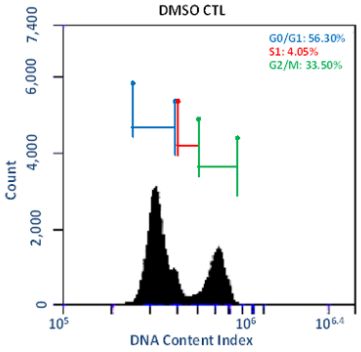

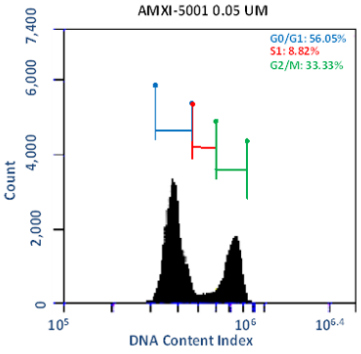

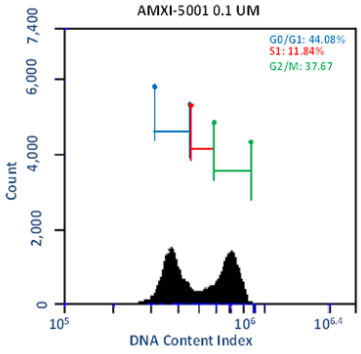

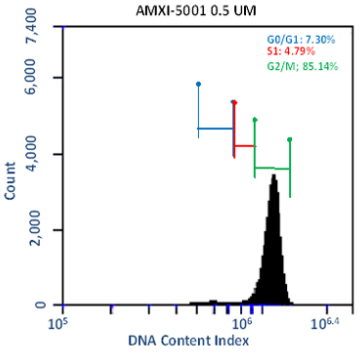

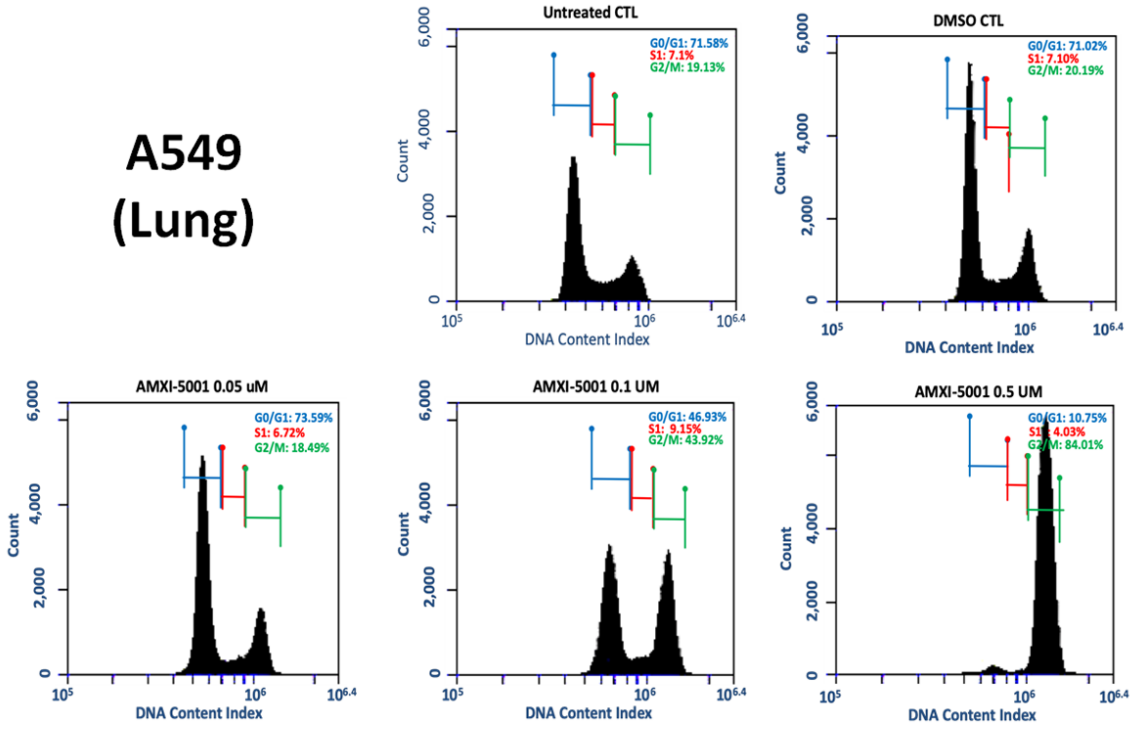

Figure S23. Cell cycle analysis. Cell cycle analysis after treatment with medium alone (Untreated CTL), or medium containing DMSO (DMOS CTRL) or increasing concentrations of AMXI-5001 in MDA-MB-436, OVCAR8, and A549 cells for 24 hr. C, Cells were harvested and DNA content was analyzed by flow cytometry. The average percentages of cells in G0/G1, S, or G2/M phase were determined and are indicated for all treatments.

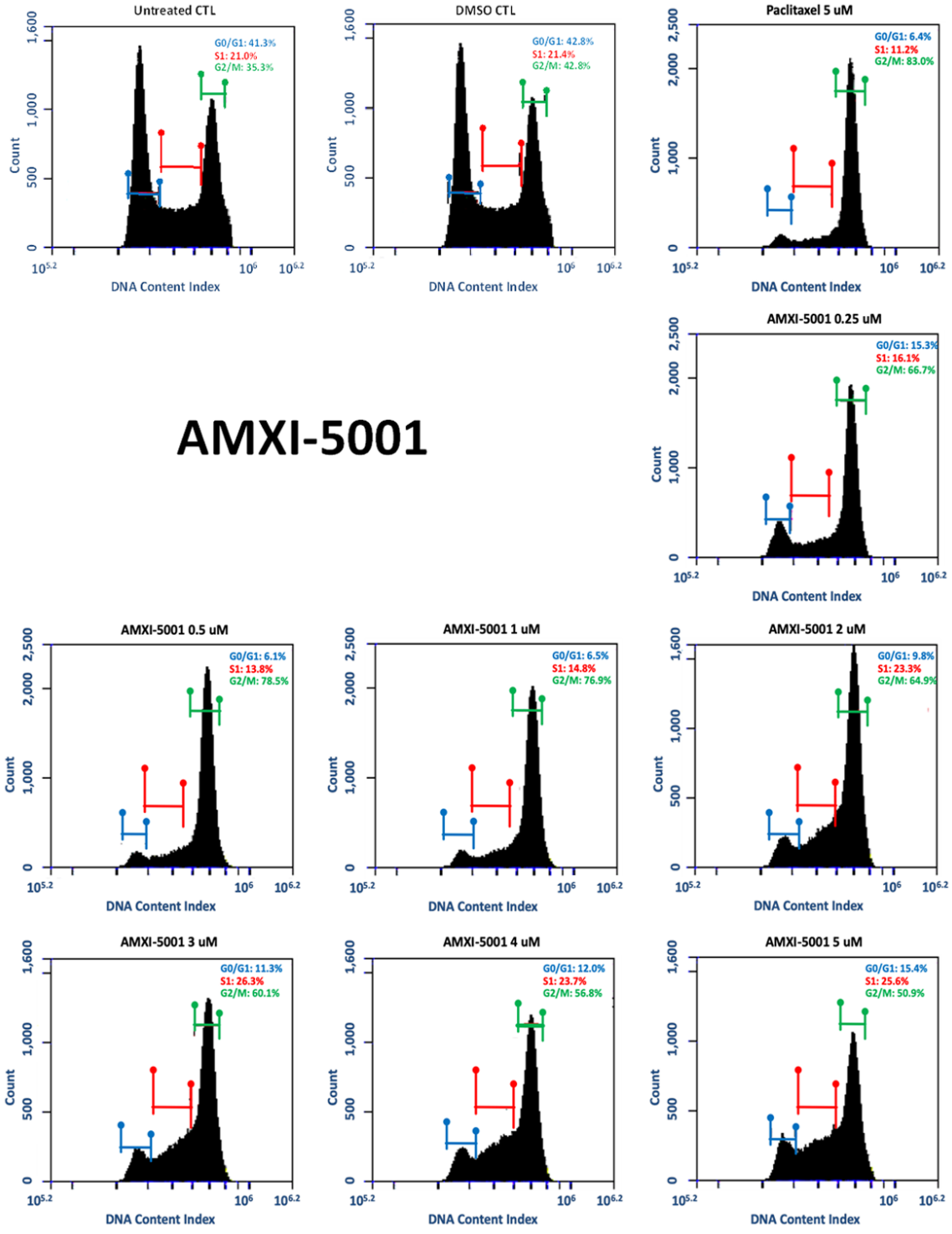
AMXI-5001
Untreated CTL
G0/G1: 41.3%
S1: 21.0%
G2/M: 35.3%
DMSO CTL
G0/G1: 42.8%
S1: 21.4%
G2/M: 42.8%
Paclitaxel 5 uM
G0/G1: 6.4%
S1: 11.2%
G2/M: 83.0%
AMXI-5001 0.25 uM
G0/G1: 15.3%
S1: 16.1%
G2/M: 66.7%
AMXI-5001 0.5 uM
G0/G1: 6.1%
S1: 13.8%
G2/M: 78.5%
AMXI-5001 1 uM
G0/G1: 6.5%
S1: 14.8%
G2/M: 76.9%
AMXI-5001 2 uM
G0/G1: 9.8%
S1: 23.3%
G2/M: 64.9%
AMXI-5001 3 uM
G0/G1: 11.3%
S1: 26.3%
G2/M: 60.1%
AMXI-5001 4 uM
G0/G1: 12.0%
S1: 23.7%
G2/M: 56.8%
AMXI-5001 5 uM
G0/G1: 15.4%
S1: 25.6%
G2/M: 50.9%
Count
DNA Content Index

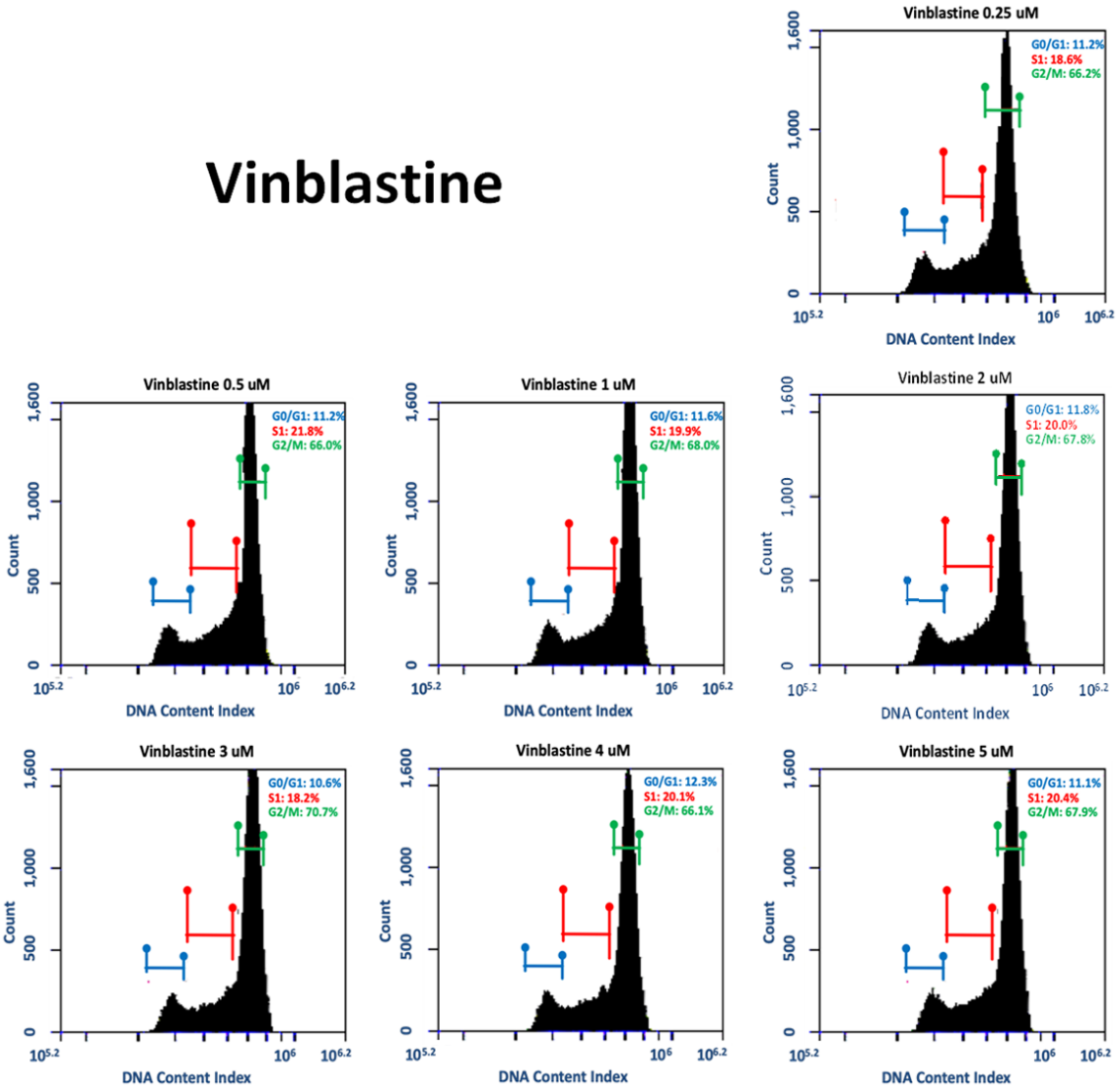

Figure S24. Cell cycle analysis. Cell cycle analysis after treatment with medium alone (Untreated CTL), or medium containing DMSO (DMOS CTRL) or increasing concentrations of AMXI-5001 or Vinblastine, or 5 μM Paclitaxel, in MDA-MB-436 cells for 24 hr. C, Cells was harvested and DNA content was analyzed by flow cytometry. The average percentages of cells in G0/G1, S, or G2/M phase were determined and are indicated for all treatments.

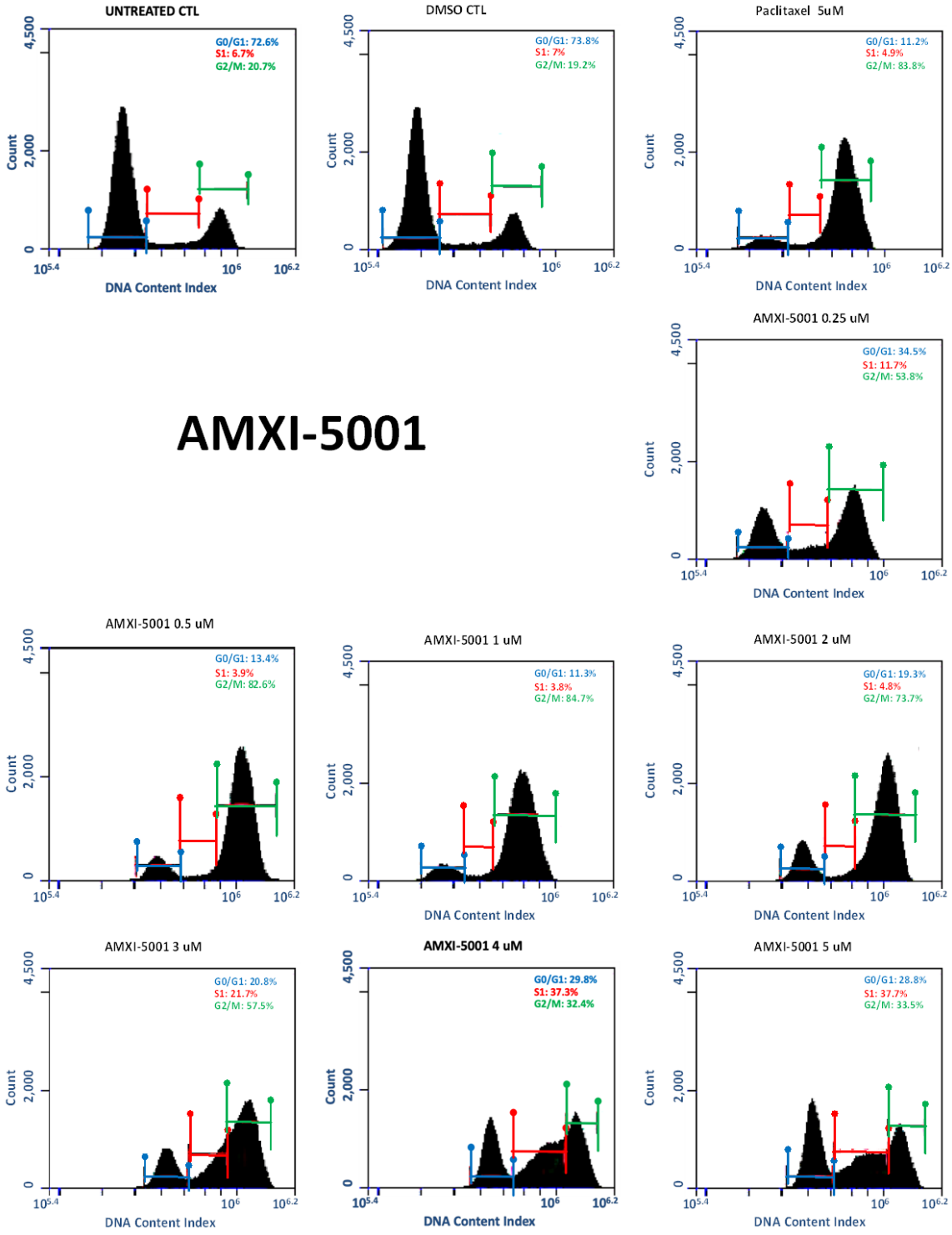
UNTREATED CTL
G0/G1: 72.6%
S1: 6.7%
G2/M: 20.7%
DMSO CTL
G0/G1: 73.8%
S1: 7%
G2/M: 19.2%
Paclitaxel 5uM
G0/G1: 11.2%
S1: 4.9%
G2/M: 83.8%
AMXI-5001
AMXI-5001 0.25 uM
G0/G1: 34.5%
S1: 11.7%
G2/M: 53.8%
AMXI-5001 0.5 uM
G0/G1: 13.4%
S1: 3.9%
G2/M: 82.6%
AMXI-5001 1 uM
G0/G1: 11.3%
S1: 3.8%
G2/M: 84.7%
AMXI-5001 2 uM
G0/G1: 19.3%
S1: 4.8%
G2/M: 73.7%
AMXI-5001 3 uM
G0/G1: 20.8%
S1: 21.7%
G2/M: 57.5%
AMXI-5001 4 uM
G0/G1: 29.8%
S1: 37.3%
G2/M: 32.4%
AMXI-5001 5 uM
G0/G1: 28.8%
S1: 37.7%
G2/M: 33.5%
Count
DNA Content Index

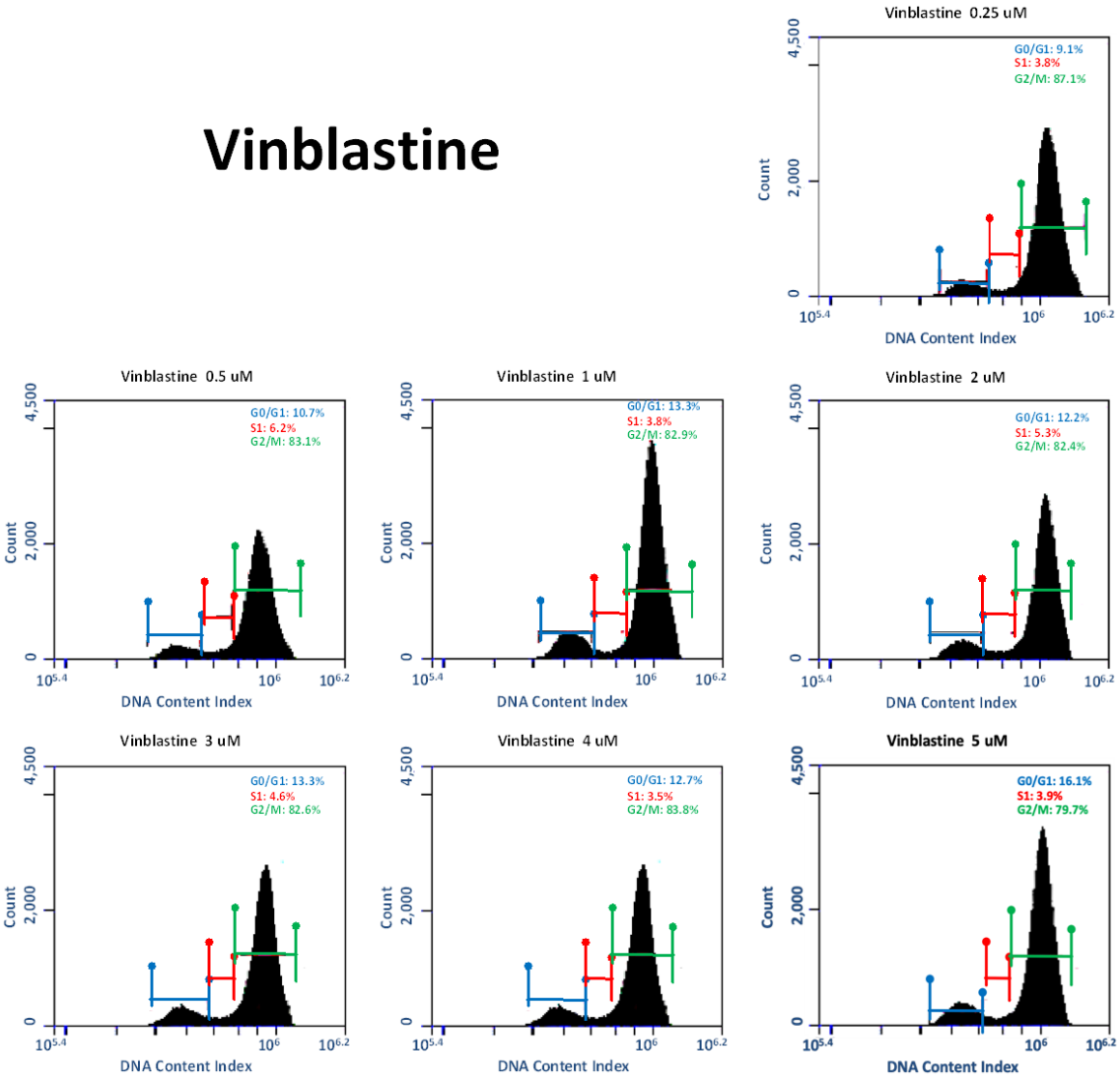

Figure S25. Cell cycle analysis. Cell cycle analysis after treatment with medium alone (Untreated CTL), or medium containing DMSO (DMOS CTRL) or increasing concentrations of AMXI-5001 or Vinblastine, or 5 μM Paclitaxel, in A549 cells for 24 hr. C, Cells were harvested and DNA content was analyzed by flow cytometry. The average percentages of cells in G0/G1, S, or G2/M phase were determined and are indicated for all treatments.

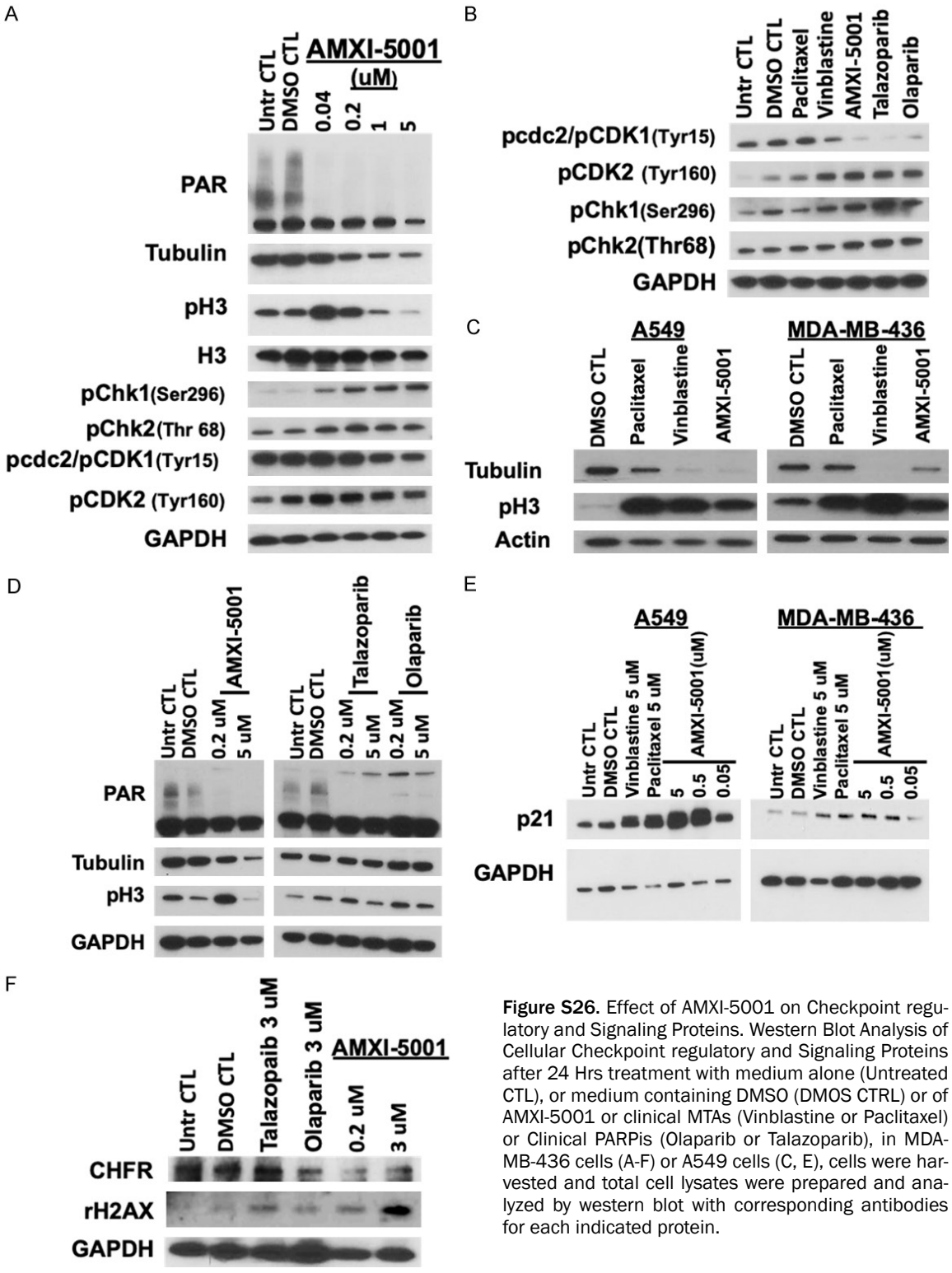

Figure S26. Effect of AMXI-5001 on Checkpoint regulatory and Signaling Proteins. Western Blot Analysis of Cellular Checkpoint regulatory and Signaling Proteins after 24 Hrs treatment with medium alone (Untreated CTL), or medium containing DMSO (DMOS CTRL) or of AMXI-5001 or clinical MTAs (Vinblastine or Paclitaxel) or Clinical PARPis (Olaparib or Talazoparib), in MDA-MB-436 cells (A-F) or A549 cells (C, E), cells were harvested and total cell lysates were prepared and analyzed by western blot with corresponding antibodies for each indicated protein.

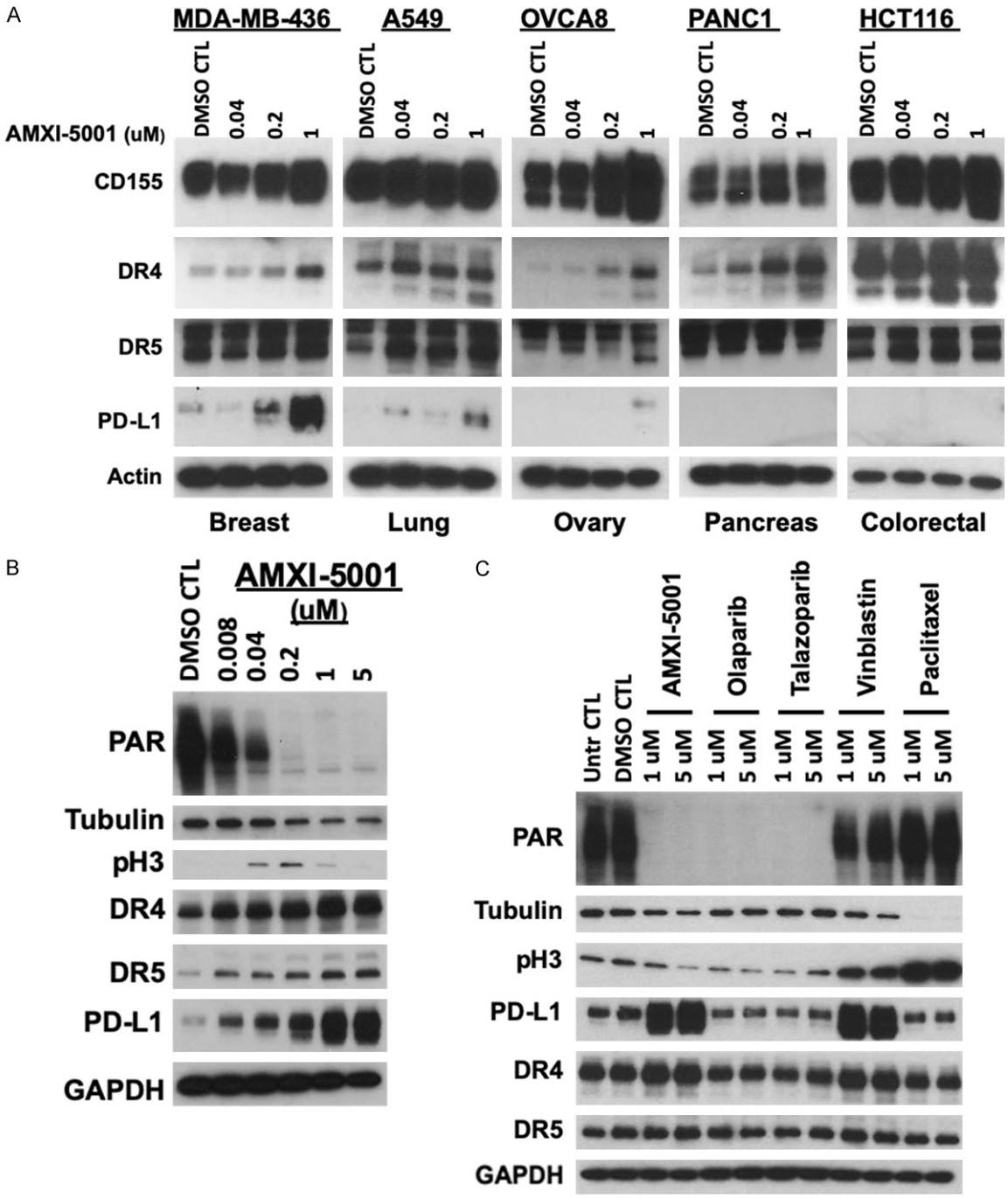

Figure S27. Western Blot Analysis of the expression of immunomodulatory antigens. After 24 hr treatment with medium alone (Untreated CTL), or medium containing DMSO (DMOS CTRL) or of AMXI-5001 or clinical MTAs (Vinblastine or Paclitaxel) or Clinical PARPis (Olaparib or Talazoparib), in various cancer cell lines (MDA-MB-436, A549, OVCAR8, PANC1, HCT116) (A) or MDA-MB-436 cells (B, C), cells were harvested and total cell lysates were prepared and analyzed by western blot with corresponding antibodies for each indicated protein.

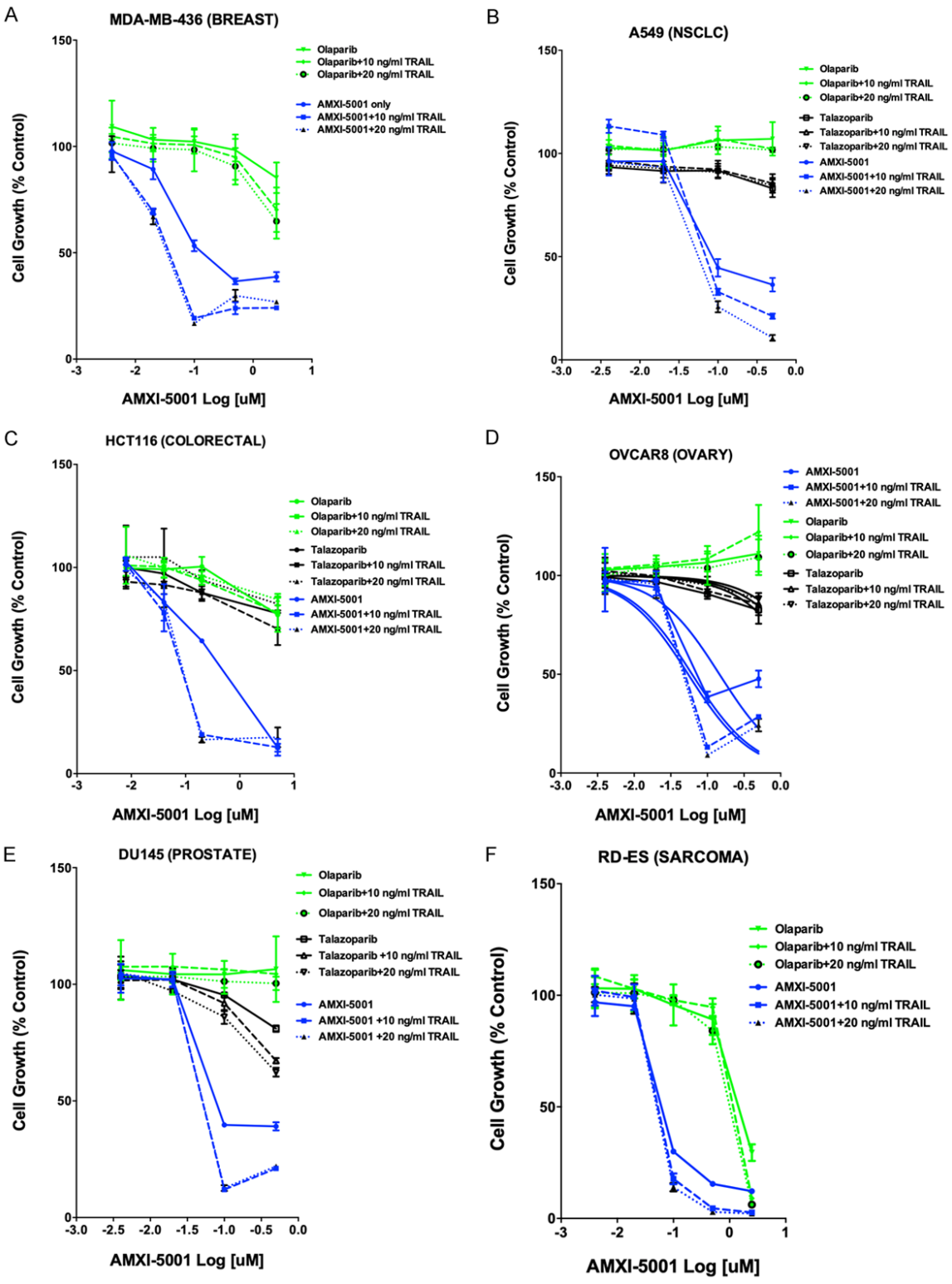

Figure S28. Effect of the combination of AMXI-5001 or Clinical PARPis with TRAIL on Cell Viability in a Panel of Human Cancer Cell Lines. The effect on cell viability of AMXI-5001 or clinical PARPis (Olaparib, Talazoparib) alone or in combination with TRAIL was assessed using Cell Titer Glo assay in a panel of cancer cell (MDA-MB-436, A549, HCT116, OVCAR8, DU145 or RD-ES). Proliferation was assessed after cells were exposed for 3 days with increasing doses of AMXI-5001, Olaparib or Talazoparib alone or in combination with trail at 10 ng/ml or 20 ng/ml. The concentration required to inhibit cell growth by 50% (IC50) was determined after non-linear fit using GraphPad Prism. DMSO treated cells were used as a vehicle control.

Table S16. Effect of the combination of AMXI-5001 or Clinical PARPis with TRAIL on Cell Viability in a Panel of Human Cancer Cell Lines

Cell Line Name	AMXI-5001 IC50 (μM)	AMXI-5001 + TRAIL (10 ng/ml) IC50 (μM)	AMXI-5001 + TRAIL (20 ng/ml) IC50 (μM)	Olaparib (μM)	Olaparib + TRAIL (10 ng/ml) IC50 (μM)	Olaparib + TRAIL (20 ng/ml) IC50 (μM)	Talazoparib (μM)	Talazoparib (10 ng/ml) IC50 (μM)	Talazoparib (20 ng/ml) IC50 (μM)
MDA-MB-436	0.222	0.043	0.040	NR	NR	NR			
A549	0.141	0.104	0.064	NR	NR	NR	NR	NR	NR
HCT116	0.352	0.092	0.096	NR	NR	NR	NR	NR	NR
OVCAR8	0.146	0.062	0.055	NR	NR	NR	NR	NR	NR
DU145	0.143	0.063	0.064	NR	NR	NR	NR	NR	NR
RD-ES	0.076	0.059	0.054	1.634	1.231	0.996			

The effect on cell viability of AMXI-5001 or clinical PARPis (Olaparib, Talazoparib) alone or in combination with TRAIL was assessed using Cell Titer Glo assay in a panel of cancer cell (MDA-MB-436, A549, HCT116, OVCAR8, DU145 or RD-ES). Proliferation was assessed after cells were exposed for 3 days with increasing doses of AMXI-5001, Olaparib or Talazoparib alone or in combination with trail at 10 ng/ml or 20 ng/ml. The concentration required to inhibit cell growth by 50% (IC50) was determined after non-linear fit using GraphPad Prism. DMSO treated cells were used as a vehicle control. NR = Non-Responsive.

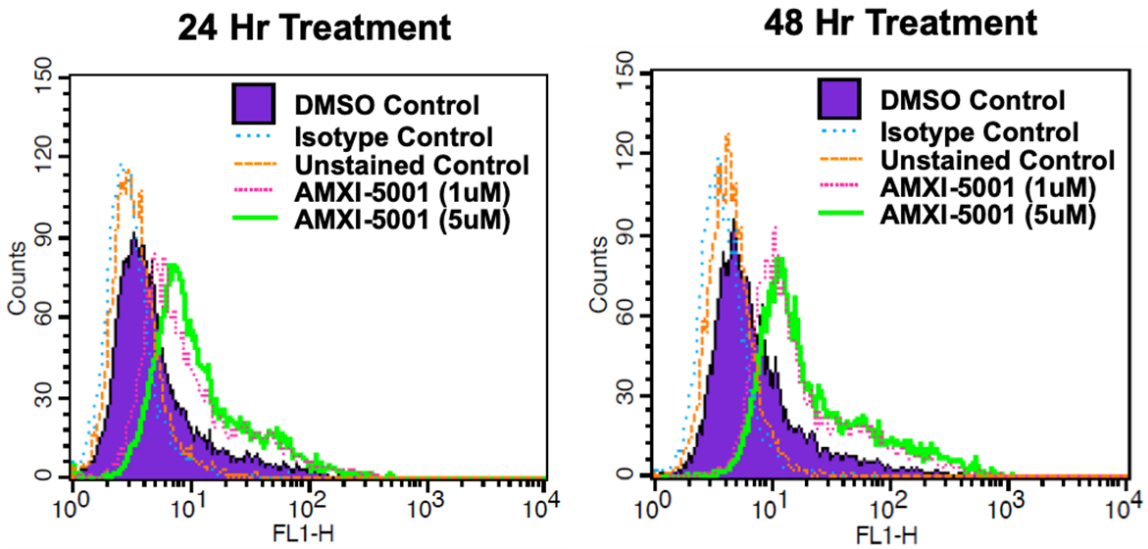

Figure S29. Flow cytometry analysis of PD-L1 cells surface expression. A549 Cell were seeded to 100 mm dishes and cultured overnight then serum starved with (0.5% FBS medium) overnight. Subsequently, cells were treated for 24 or 48 hours with medium containing DMSO control or AMXI-5001 (0, 1 or 5 μM) in 1% FBS medium. Subsequently, cells were harvested by trypsinization and stained for cell surface PD-L1 (Alexa-488 conjugated Ab) and analyzed by flow cytometry.

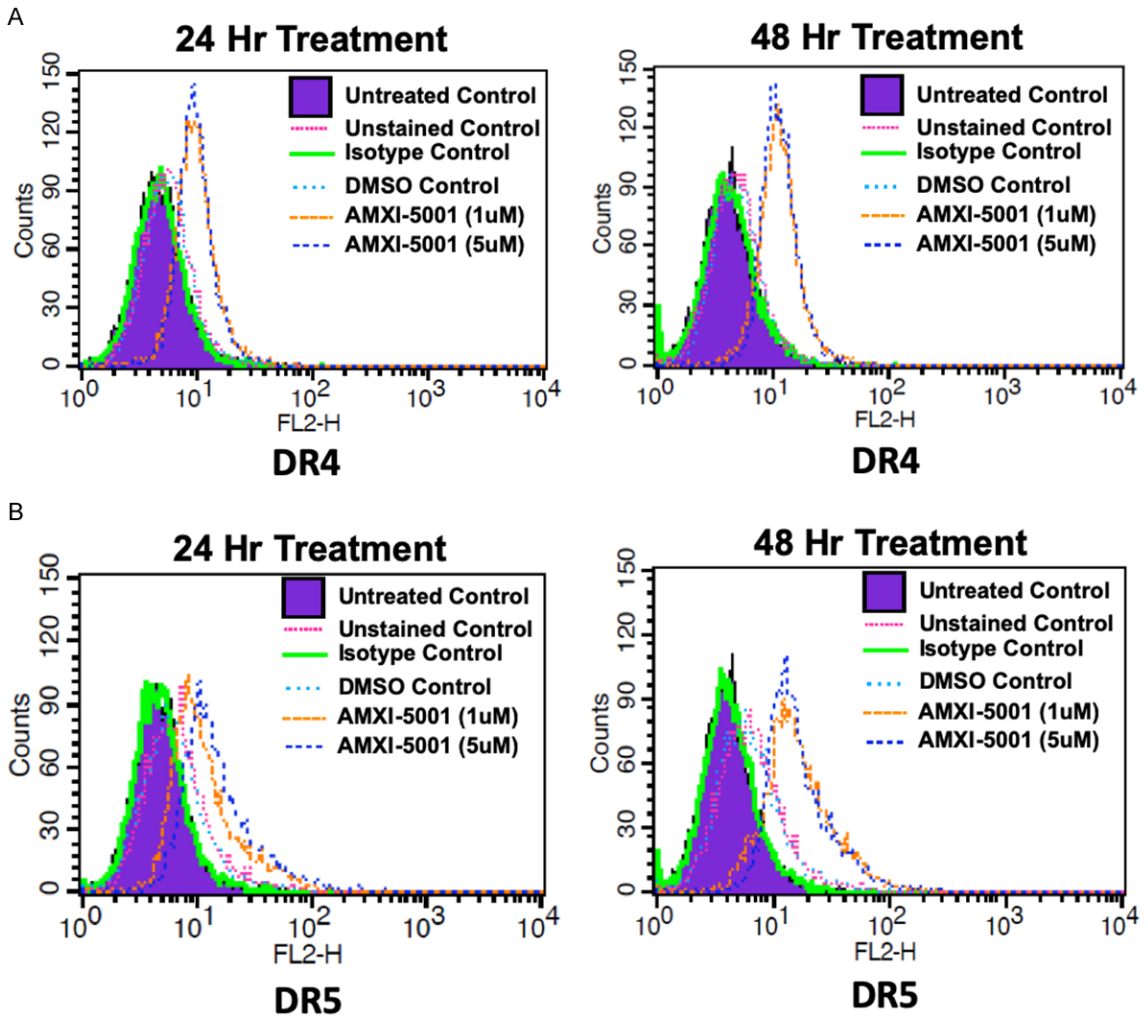

Figure S30. Flow cytometry analysis of cells surface expression of death receptors (DR4 and DR5). A549 Cell were seeded to 100 mm dishes and cultured overnight then serum starved with (0.5% FBS medium) overnight. Subsequently, cells were treated for 24 or 48 hours with medium containing DMSO control or AMXI-5001 (0, 1 or 5 μM) (Batch #19-26) in 1% FBS medium. Subsequently, cells were harvested by trypsinization and stained for cell surface DR4 and DR5 (Alexa-488 conjugated Ab) and analyzed by flow cytometry.

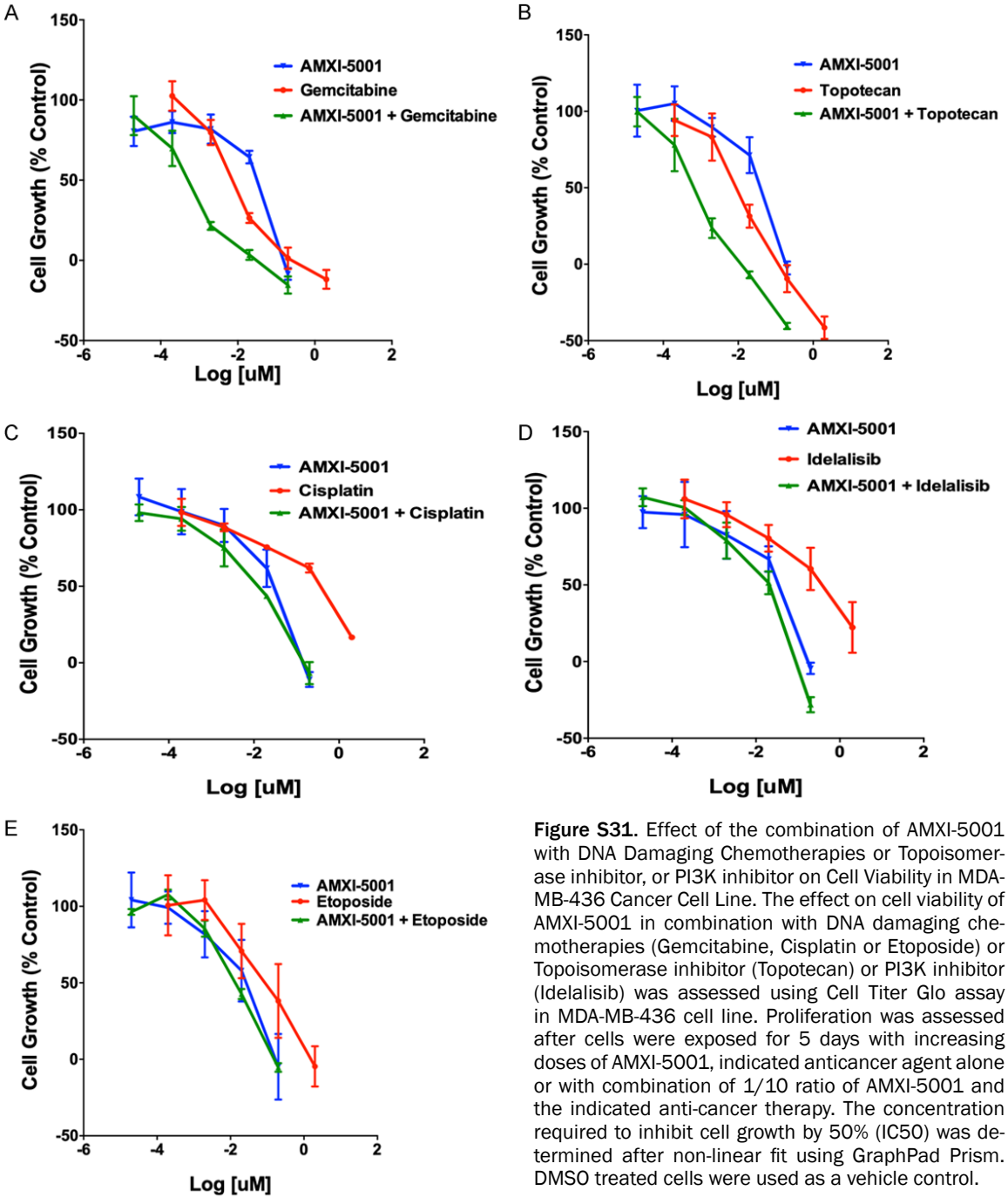

Figure S31. Effect of the combination of AMXI-5001 with DNA Damaging Chemotherapies or Topoisomerase inhibitor, or PI3K inhibitor on Cell Viability in MDA-MB-436 Cancer Cell Line. The effect on cell viability of AMXI-5001 in combination with DNA damaging chemotherapies (Gemcitabine, Cisplatin or Etoposide) or Topoisomerase inhibitor (Topotecan) or PI3K inhibitor (Idelalisib) was assessed using Cell Titer Glo assay in MDA-MB-436 cell line. Proliferation was assessed after cells were exposed for 5 days with increasing doses of AMXI-5001, indicated anticancer agent alone or with combination of 1/10 ratio of AMXI-5001 and the indicated anti-cancer therapy. The concentration required to inhibit cell growth by 50% (IC50) was determined after non-linear fit using GraphPad Prism. DMSO treated cells were used as a vehicle control.

Table S17. Effect of the combination of AMXI-5001 with DNA Damaging Chemotherapies or Topoisomerase inhibitor, or PI3K inhibitor on Cell Viability in MDA-MB-436 Cancer Cell Line

	AMXI-5001	Gemcitabine	AMXI-5001 + Gemcitabine
IC50 (μM)	0.023	0.008	0.0005
	AMXI-5001	Topotecan	AMXI-5001 + Topotecan
IC50 (μM)	0.033	0.008	0.0006
	AMXI-5001	Cisplatin	AMXI-5001 + Cisplatin
IC50 (μM)	0.023	0.287	0.0109
	AMXI-5001	Idelalisib	AMXI-5001 + Idelalisib
IC50 (μM)	0.027	0.319	0.0131
	AMXI-5001	Etoposide	AMXI-5001 + Etoposide
IC50 (μM)	0.020	0.085	0.0132

The effect on cell viability of AMXI-5001 in combination with DNA damaging chemotherapies (Gemcitabine, Cisplatin or Etoposide) or Topoisomerase inhibitor (Topotecan) or PI3K inhibitor (Idelalisib) was assessed using Cell Titer Glo assay in MDA-MB-436 cell line. Proliferation was assessed after cells were exposed for 5 days with increasing doses of AMXI-5001, indicated anticancer agent alone or with combination of 1/10 ratio of AMXI-5001 and the indicated anti-cancer therapy. The concentration required to inhibit cell growth by 50% (IC50) was determined after non-linear fit using GraphPad Prism. DMSO treated cells were used as a vehicle control.

Table S18. Summary of PK Parameters Following Administration of a Single Oral Dose of AMXI-5001 in BALB/C Mice

Parameter	Unit	AMXI-5001 FB (50 mg/kg)	AMXI5001 FB (100 mg/kg)	AMXI5001 HCl salt (50 mg/kg)
T1/2	h	3.74	4.29	3.28
Tmax	h	1	1	1
Cmax	ng/ml	5670	12233	7180
AUC 0-t	ng/ml*h	18207	87591	28333
AUC 0-inf_obs	ng/ml*h	18527	89678	28577

Summary of PK parameters following administration of a single oral dose of AMXI-5001 in BALB/C mice. AMXI-5001 FB and HCl salt forms were formulated either as NMP/CMC suspension or in 10% TPGS suspension, respectively and administered orally to female Balb/c mice. The bioavailability for AMXI-5001 FB form was assessed following a single oral dose administration at either 50 mg/kg. or 100 mg/kg per mouse. The bioavailability for AMXI-5001 HCl salt form was assessed following a single oral dose administration of 50 mg/kg. The PK parameters were determined based on a Non-Compartmental PK model Analysis of Plasma Data after Extravascular Input.

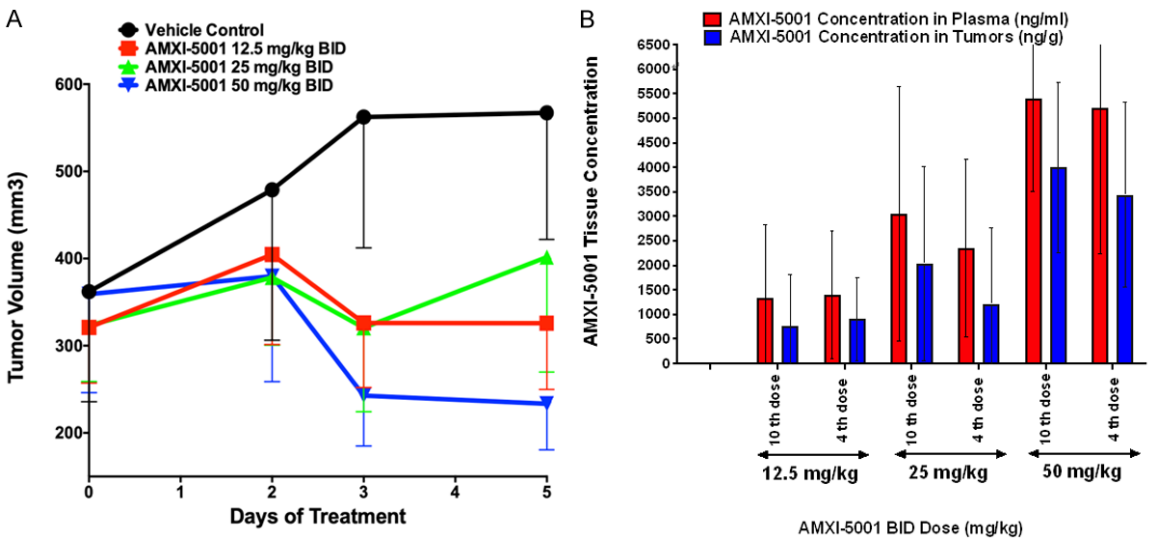

Figure S32. A. Relationship between Dose and Inhibition of MDA-MB-436 Triple Negative Breast Xenograft Tumor Growth in Mice by AMXI-5001 (5-Day BID Oral Dosing). B. AMXI-5001 Dose Relationship Between Plasma and Tumor Concentrations in MDA-MB-436 Xenograft Tumors In Vivo, following Oral BID Dosing (12.5, 25 mg/kg) BID for 2 Days (4th dose) or 5 Days (10th dose). Blood and Tumors tissues were harvested 3 h post 4th and 10th dose.

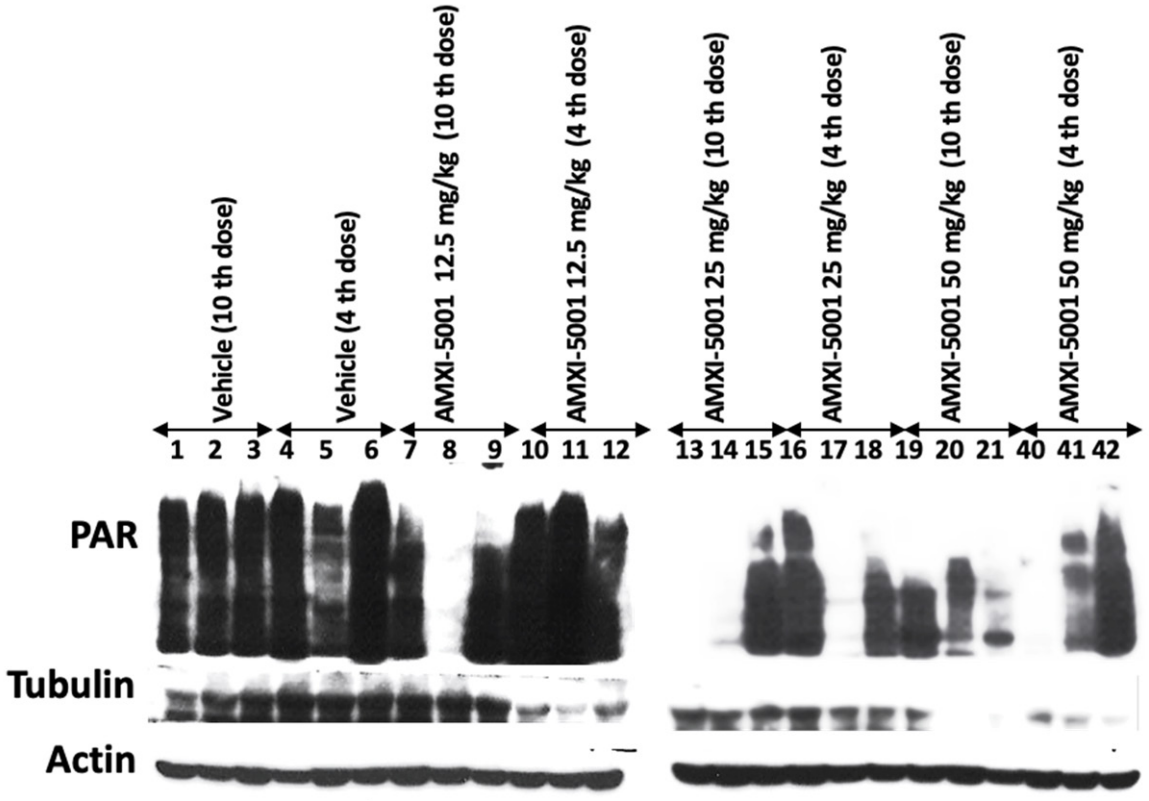

Figure S33. Dose-Response Relationship for Inhibition of PAR and Total Tubulin Expression by AMXI-5001 in MDA-MB-436 Xenograft Tumors in vivo Following Oral BID Dosing for 2 Days (4th dose) or 5 Days (10th dose) with AMXI-5001.

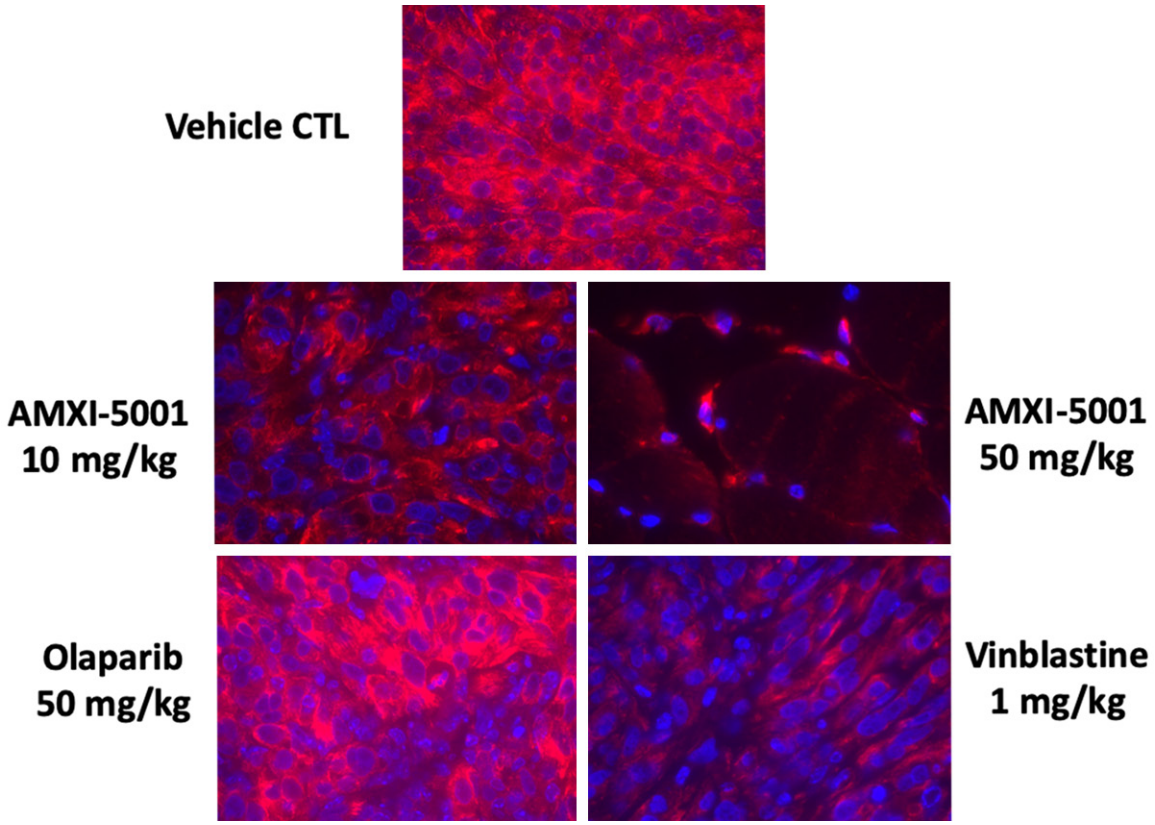

Figure S34. Immunohistochemical Analysis of the in vivo Treatment Related Effect on Microtubule Network Organization Inside the MDA-MB-436-Derived Xenograft Tumor Cells. Tumors harvested at the end of the dosing period revealed potent, dose-dependent decreases of microtubule filament. Sections from paraffin embedded tumors were stained with an antibody specific to for alpha/beta-tubulin (red), and visualized by fluorescent microscopy using Zeiss AxioImager 2 microscope; 63x objective. Cell nuclei were stained with DAPI (blue). Repeat oral dose of AMXI-5001 at either 10 mg/kg or 50 mg/kg BID resulted in a striking dose dependent inhibition of microtubule filament formation in MDA-MB-436 cells derived tumors. Vinblastine treatment (1 mg/kg once a week) also induced a marked inhibition of microtubule filament in MDA-MB-436 tumors. Olaparib(50 mg/kg BID) showed no effect on tumor cells microtubule filaments formation as compared to the effect of vehicle control (CTL) treatment.

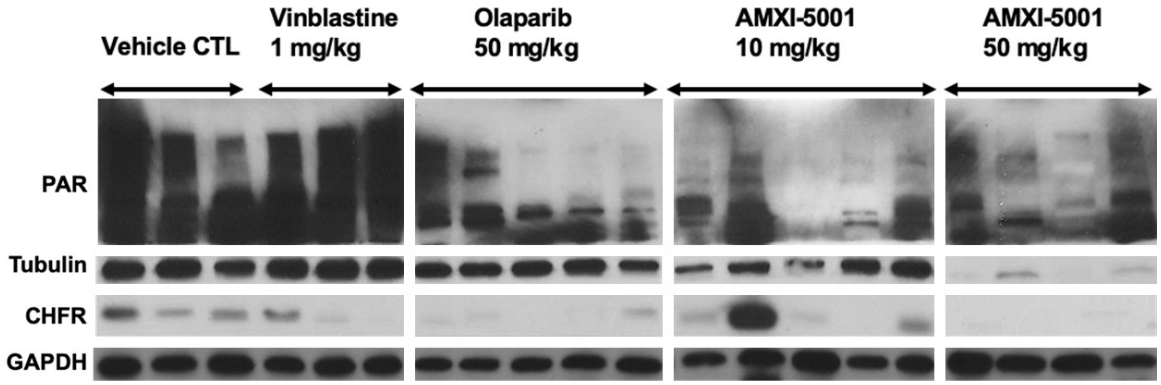

Figure S35. Western Blot Analysis of the in vivo Treatment-related Effect on PAR Total Tubulin and CHFR Expression in Lysates from MDA-MB-436-derived Xenograft Tumor Cells. Tumors were harvested and snap frozen at the end of the dosing period. Tumor lysates were prepared and analyzed by standard Western Blot assay with antibodies specific to PAR, alpha/beta-tubulin, or cell cycle checkpoint protein CHFR. Repeat oral dose of AMXI-5001 at either 10 mg/kg or 50 mg/kg BID resulted in a striking dose dependent inhibition of total tubulin and CHFR protein. PAR expression in tumor cells was also strongly inhibited by AMXI-5001 with both 10 mg/kg or 50 mg/kg dosing. Vinblastine treatment (1 mg/kg once a week) showed no significant effect on PAR or tubulin expression but demonstrated inconsistent CHFR protein expression inhibition. Olaparib (50 mg/kg BID) showed no effect on effect on tubulin expression but induced a marked PAR and CHFR protein expression inhibition.